Simulation of Unstable Two-phase Flows in Long Risers

Andreas Holm Akselsen

NTNU

Norges teknisk-
naturvitenskapelige universitet
NTNU

Institutt for energi- og prosessteknikk

MASTEROPPGAVE

for

Stud.techn. Andreas Akselsen

Våren 2012

Simulering av ustabil tofasestrøm i lange stigerør

Simulation of unstable two phase flows in long risers

Bakgrunn

Oljeselskap erfarer at gass-væske strøm i lange brønner og i stigerør kan gi ustabil produksjon, med alternerende gass og væskestrøm. Det er i hovedsak kompressibiliteten til gassen som kan gi opphav til ustabil strøm.

En form for ustabil strøm skyldes ekspansjon av gassen når den transporteres opp i et langt stigerør. Dersom gass akkumuleres før et bend kan ekspansjonen i stigerøret føre til en akselerasjon som tar resten av gassen med seg. Ny akkumulering starter etter utblåsningen og gir periodisk og ustabil strøm, selv med små akkumulerte gassmengder. Det er identifisert felttilfeller der dette kan være en aktuell situasjon, der gass kan samles ved en et vertikalt rørbend ved foten av stigerøret. Simuleringer med den kommersielle strømningssimulatoren OLGA har ikke gjenskapt denne ustabiliteten. Oppgaven går ut på å studere dette tilfelle med en slugfølgemodell under utvikling ved EPT.

Mål

Det skal utføres numeriske simuleringer som viser ekspansjonsdrevet ustabil strøm. Simuleringene skal utføres med tilgjengelige versjoner av en slug følge modell ved EPT.

Oppgaven bearbeides ut fra følgende punkter

1.   Kort oversikt over problemstillingen

2.   Kort beskrivelse av tre versjoner av slugfølgemodellen ved EPT

3.   Tilpassning av modeller og forsøk med simulering av et representativt dypvannstilfelle

4.   Rapportering med anbefaling om videre arbeid

Senest 14 dager etter utlevering av oppgaven skal kandidaten levere/sende instituttet en detaljert fremdrift- og eventuelt forsøksplan for oppgaven til evaluering og eventuelt diskusjon med faglig ansvarlig/veiledere. Detaljer ved eventuell utførelse av dataprogrammer skal avtales nærmere i samråd med faglig ansvarlig.

Besvarelsen redigeres mest mulig som en forskningsrapport med et sammendrag både på norsk og engelsk, konklusjon, litteraturliste, innholdsfortegnelse etc. Ved utarbeidelsen av teksten skal kandidaten legge vekt på å gjøre teksten oversiktlig og velskrevet. Med henblikk på lesning av besvarelsen er det viktig at de nødvendige henvisninger for korresponderende steder i tekst, tabeller og figurer anføres på begge steder. Ved bedømmelsen legges det stor vekt på at resultatene er grundig bearbeidet, at de oppstilles tabellarisk og/eller grafisk på en oversiktlig måte, og at de er diskutert utførlig.

Alle benyttede kilder, også muntlige opplysninger, skal oppgis på fullstendig måte. For tidsskrifter og bøker oppgis forfatter, tittel, årgang, sidetall og eventuelt figurnummer.
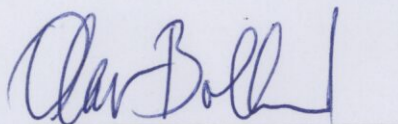
Det forutsettes at kandidaten tar initiativ til og holder nødvendig kontakt med faglærer og veileder(e). Kandidaten skal rette seg etter de reglementer og retningslinjer som gjelder ved alle (andre) fagmiljøer som kandidaten har kontakt med gjennom sin utførelse av oppgaven, samt etter eventuelle pålegg fra Institutt for energi- og prosessteknikk.

Risikovurdering av kandidatens arbeid skal gjennomføres i henhold til instituttets prosedyrer. Risikovurderingen skal dokumenteres og inngå som del av besvarelsen. Hendelser relatert til kandidatens arbeid med uheldig innvirkning på helse, miljø eller sikkerhet, skal dokumenteres og inngå som en del av besvarelsen.
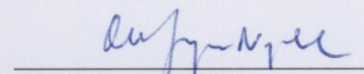
I henhold til "Utfyllende regler til studieforskriften for teknologistudiet/sivilingeniørstudiet" ved NTNU § 20, forbeholder instituttet seg retten til å benytte alle resultater og data til undervisnings- og forskningsformål, samt til fremtidige publikasjoner.

Besvarelsen leveres digitalt i DAIM. Et faglig sammendrag med oppgavens tittel, kandidatens navn, veileders navn, årstall, instituttnavn, og NTNUs logo og navn, leveres til instituttet som en separat pdf-fil. Etter avtale leveres besvarelse og evt. annet materiale til veileder i digitalt format.

NTNU, Institutt for energi- og prosessteknikk, 16. januar 2012

Olav Bolland
Instituttleder

Ole Jørgen Nydal
Faglig ansvarlig/veileder

Medveileder(e)   Tor Kjeldby, PhD EPT

NTNU – Trondheim
Norwegian University of Science and Technology

Simulation of Unstable Two-phase Flows in Long Risers

MASTER THESIS

Author:
Andreas H. AKSELSEN

Supervisor:
Prof. Ole Jørgen NYDAL

Co-supervisor:
Tor K. KJELDBY

June 13, 2012

Abstract

The principles of the object oriented slug tracking schemes at EPT (Department of Energy and Process Engineering, NTNU) have been developed and discussed in some detail. Simple bench-mark testing revealed that the LASSI code suffers form a pipe inclination-dependant lack of mass conservation, the cause of which is presently unidentified. Comparing simplified and non-simplified SLUGGIT simulations with experimental data published by Taitel *et al.* [41] mostly indicate a reasonable correspondence, though the precision is somewhat imprecise. In particular, obtaining stable riser flow (free of significant pressure oscillations) at low liquid flow rates was not managed without excessive gas rates. This is possibly a consequence of the method's intrinsic slug flow approximation to dispersed regimes, but further investigation showed that the methods stability response altered with recent code versions in which alterations to management procedures was identified as the main differences, indicating that the SLUGGIT method's riser stability properties are quite sensitive to intuition-based section management routines. Further developing the models to better accommodate vertical flow regimes is advised.

Supplementary testing was afforded through the development of a steady-state unit-cell type model for phase fractions in the riser. Excellent accordance with simulation data was found, confirming that the SLUGGIT model is capable of reproducing stable, expanding bubble flow. Coarse resolution served to disturb this process as bubbles becomes longer and are affected by riser entrance and exit effects. It was also found that pressure oscillations caused by such entrance and exit effects display the typical characteristics of terrain slugging and may be mistaken as such.

With basis in the P50 Girassol pipeline, a systematic investigation into operational instability phenomena has been carried out using the available boundary conditions. Instabilities rooted in gas accumulation in jumpers, possibly also influenced by the U-bend, were found when studying the fixed pressure open inlet condition. The character of these instabilities were of a frequency and intermittency uncongenial to the field data. Most instability phenomena captured in these simulations were sensitive to changes in geometry, inlet condition and management parameters.

Severe slugging was initially found to dominate the flow picture with a fixed flow closed inlet condition. Also this type of operational instability had too high a frequency to be a match with the field data. Nor does the well-know 'shark fin' pressure profile of the terrain slugging liquid build-up and blow-out precesses match the sinusoidal character of the field data.

It was recently found that the supplied field data needed adjustment for phase transition at the inlet state, amounting to a considerable reduction in gas flow. This produced predictions of more stable production compatible with those generated by external participant, though significant pressure fluctuations were still observed. These fluctuations were found to originate from slugging in the U-bend and entrance effects as large Taylor bubbles formed through coalescence and penetrated into the riser. This latter cause is believed to be a feature of the limited, non-dispersed flow objects available in the EPT models.

A production index type boundary condition was implemented to better accommodate the well production response. Even so, the conditions under which the Girassol field instability data was recorded could not be recreated satisfactorily without gas lift and PVT support implemented. Simulations including the productivity index inlet indicated, for the most part, that without the presence of a gas lift system, the pipeline is likely to come to a complete stand-still; unless the liquid in riser and well are strongly aerated at all times, the well head will not be sufficient to overcome the total system liquid column weight.

Sammendrag

Prinsippene bak de objektorienterte slugfølgemodellene ved EPT (institurtt for Energi og Prosessteknikk, NTNU) blir utledet og diskutert på detaljnivå. Enkel testing viser at LASSI-koden lider av en helningsavhenging og foreløpig uidentifisert feil som fører til at masse ikke blir bevart. Sammenlikning av SLUGGIT-data med eksperimentell data fra Taitel *et al.* [41] indikerer stort sett en akseptabel overenstemmelse, dog noe upresis. Særlig ved lav væskestrømningsrate viste det seg vanskelig å oppnå stabil riserstrømning uten overdrevent gassinnskudd. Modellenes slugtilnærming til dispersjoner kan ha skyld i dette. Videre undersøkelse viser at forskjellige, forholdvis nye versjoner av SLUGGIT-koden predikerer forskjellige stabilitetsdomener for risersystemet. Forskjellen blant versjonene ligger hovedsakelig i prosedyrene tilknyttet objekthåndtering, hvilket indikerer at modellenes riserstabilitet er følsom for denne intuisjonbaserte delen av simuleringsrutinen. Videre modellutvikling med hensyn på vertikalstrømning anbefales.

Videre testing ble gjennomført ved utleding av en stasjonær 'unit-call' riser-fasefraksjonsmodell. Utmerket overensstemmelse med data fra simuleringer ble observert, hvilket underbygger SLUGGITmodellens evne til å gjenskape stabil, ekspanderende riserstrømning. Grov oppløsning forstyrret derimot denne prosessen ettersom bobleseksjoner ble lengre, hvilket førte til trykkendringer forbundet med seksjonenes med inn- og uttreden av riseren. Disse forstyrrelsene i trykk var av en karakter lik det sett ved terrengslugging.

Med utgangspunkt i P50-rørledninged ved Girassol-feltet ble mulige former for produksjonsustabilitet undersøkt ved bruk av alle tilgjengelige innløpsbetingelser. Ustabilitet med opphav i gassakumulering i jumpere, samt en mulig U-rørinnvirkning, ble oppdaget under studier med konstant trykk på innløpet. Disse formene for ustabilitet viste seg derimot å ha for høy frekvens og for skarpt utfall til å samsvare med feltdata. De fleste av disse simuleringene viste seg å være følsom til endringer i rørkonfigurasjon og simuleringsparametere.

Terrengslugging type I dominerte strømningbildet hvor konstante massekilder ble benyttet som innløpsbetingelse. Også denne typen ustabilitet viste seg å gi oscillasjoner med overdreven frekvens. Heller ikke den typiske 'haifinne'-trykkprofilen assosiert med væskeopphopning og utblåsning står i samsvar med den sinusformede trykkprofilen registrert i feltdataen.

Nylig ble det oppdaget at oppgitt innløpsdata trenger korrigering for faseovergang til innløpstilstanden. Dette endrer gassraten betydelig. Resulterende simuleringer var mer stabile og dermed mer lik de gjennomført av eksterne deltakere. Allikevel var trykkprofilen preget av en anselig forstyrrelse. Denne forstyrrelsen viste seg å ha opphav i terrengslugging i U-røret, så vel trykendringer forbundet med at lange Taylor bobler, formet ved koalesens i horisontalrøret, penetrer inn i riseren. Sistnevnte kan være et resultat av mangel på dispergerte strømningsobjekter i slugfølgemodellene.

For bedre å tilpasse produksjonsresponsen til brønnen ved innløpet ble produktivitetsindeks implementert som grensebetingelse. Omstendighetene tilknyttet Girassolfeltets ustabilitet kunne likevel ikke bli tilfredsstillende gjenskapt, primært grunnet mangelen på gassløft og PVT-tilstandsberegning i kodene. Simuleringer med produktivitetsindeks på innløpet indikerte hovedsakelig at systemet ville stanse fullstendig opp uten gassløft tilstede; hvis ikke riser og brønn til enhver tid et godt utluftet vil ikke brønntrykket være tilstrekkelig til å overvinne tyngden av den totale veskesøylen.

Contents

Nomenclature

Latin symbols

$\underline{e}$	Unit vector	–
$\underline{n}$	Normal vector of control volume	–
$\dot{M}^s$	Mass rate source term	kg/s
Q	Volumetric flow rate	m^3/s
A	Pipe area, perpendicular to flow direction	m^2
c	Speed of sound	m/s
D	Pipe diameter	m
D_h	Hydraulic diameter	m
Fr	Froude number $= u/\sqrt{gD}$	–
g	Gravitational acceleration	m/s^2
GOR	Gas-Oil Ratio $= U_{g,i}^{S,ST}/U_{l,i}^{S,ST}$	–
H	Riser height	m
h	Phase height	m
IFM	Interphase Friction Multiplier	–
K	Productivity index	$\text{Sm}^3/(\text{bar} \cdot \text{day})$
k	Wavenumber	1/m
L	Pipeline length	m
M	Control volume mass	kg
m	Pipe specific mass (extensive)	kg/m^3
N	Total number of samples	–
p	Pressure	Pa
P_{well}	Well pressure	bar
Q	'Extensive volumetric flux' – see (4.3)	m^3/s
R	Gas constant	$\text{J/(kg} \cdot \text{K)}$

r	Pipe radius	m
Re	Reynolds number	–
S	Wetted perimeter	m
s_χ	Sample standard deviation	unit of χ
T	Temperature	K
u	Phase velocity	m/s
V	Volume of section	m^3
v	Border velocity	m/s
$V_{\int \mathrm{d}z}$	Total phase volume in system, computed using (5.1a)	m^3
V_{io}	Total phase volume in system, computed using (5.1b)	m^3
wc	water cut = $U^{S,ST}_{\mathrm{H_2O},i}/U^{S,ST}_{\mathrm{l},i}$	–
y	Vertical axis in pipe cross-section. Origin at pipe bottom	m
z	Position downstream the pipe	m
`MAX_BUB_COEF`	SLUGGIT simulation parameter; maximum allowed bubble length measured in diameter multiples.	–

Greek Symbols

α	Section volume fraction (hold-up)	–
χ	Representation of a property	various
Δ	Difference (macroscopic)	–
δ	Difference (differential approximation)	–
ℓ	Control volume streamwise length	m
κ	Balance of Bernoulli suction and hydrostatic head gradient (see Eq. (4.28))	m^2/s^2
λ	Darcy friction coefficient	–
λ_f	Film thickness	m
μ	Dynamic viscosity	kg/(m$\cdot$s)
Ω	Control volume domain	m^3

ω	Pulsation	1/s
$\partial\Omega$	Boundary of control volume	m^2
Φ	Total average riser phase fraction	–
ϕ	Pipe inclination angle	(deg)
ψ	Pressure error	m^3/s
ρ	Density	kg/m^3
σ	Surface tension	N/m
τ	Shear stress	N/m^2
Θ	Total phase fraction in horizontal pipeline upstream riser	–

Subscripts

κ	Fluid type: $\kappa \in \{l, g\}$
Σ	Control volume cell: $\Sigma \in \{W, E\}$
σ	Control volume border: $\sigma \in \{w, e\}$
b	'bubble'
$crit$	'critical' (criteria limit)
E	Eastern (right) control volume cell
e	Eastern (right) control volume border
f	Liquid film (around bubble)
i	'inlet'
int	'interfacial' (surface)
j	Position index along the entire pipe
n	'nose'
o	'outlet'
P	Present control volume cell
$pipe$	pipe (interior surface)
s	'slug'

8

t	'tail'
W	Western (left) control volume cell
w	Western (left) control volume border

Superscripts

gl	'gas lift'
n	Present time step
$n + 1$	Next time step
S	Superficial property (*e.g.* $u_\kappa^S = \alpha_\kappa u_\kappa$)
s	Source
ST	(At) standard conditions

Encasements

$\dot{(\cdot)}$	(dot) Rate of property
$\frac{\mathrm{d}(\cdot)}{\mathrm{d}\chi}$	Total derivative
$\frac{\mathrm{D}(\cdot)}{\mathrm{D}z}$	$= \frac{\partial(\cdot)}{\partial t} + u\frac{\partial(\cdot)}{\partial z}$ Material/particle/substantial etc. derivative
$\frac{\partial(\cdot)}{\partial\chi}$	$= \partial_\chi(\cdot)$ Partial derivative
$\langle(\cdot)\rangle$	Temporal average
$\tilde{(\cdot)}$	(tilde) Local property in space (not a cross-section average)
$\underline{(\cdot)}$	(underline) Vector
$\underline{\underline{(\cdot)}}$	(double underline) Tensor
$\lvert(\cdot)\rvert$	Absolute value

Abbreviations

CFL	Courant Friedrich Levy (criterion)
DNS	Direct Numerical Simulation
EOS	Equation Of State

EPT   Department of Energy and Process Engineering, NTNU

FVM   Finite Volume Method

GOR   Gas-to-Oil Ratio

IKH   Invicid Kelvin-Helmholtz stability criteria

LHS   Left Hand Side

NTNU   Norwegian University of Technology and Science

RHS   Right Hand Side

SSB   Slug Stability criterion using the Bendiksen bubble-nose velocity

VKH   Viscous Kelvin-Helmholtz stability criteria

Glossary

Gas lift Production technique for reducing the static head and stabilizing the flow by means of pumping gas into the pipeline.

Hold-up local (liquid) volume fraction. 'Gas hold-up' is also sometimes found in the literature.

Horizontal (noun) Part of the P50 pipeline geometry – a 3.5 km segment between well and riser

Manifold Pipeline intersection unit. In the Girassol P50 production line, one is found the the inlet of the long horizontal.

Production Flow (of a specified phase) through the pipeline outlet.

Riser Long, vertical pipe segment, transporting fluid from seabed to surface.

Stability See Section 2.

1 Introduction

1.1 Multiphase flow

1.1.1 Flow regimes

Multiphase pipe flow is characterised by a wide variety of flow patterns, or regimes, each characterised by different pressure, shear stress, velocity and phase fraction properties as a result of the flow patterns being topologically different. In near horizontal pipelines the flow patterns will be separated at low phase velocities, and all gas and liquid will be separated by a single, relatively flat interface. This is called a *stratified* flow regime. Increasing the gas flow rate causes waves to appear on the liquid interfacial surface due to interfacial friction. At high enough relative velocities these small interface disturbances will grow due to the effects of reduced local pressure at the wave location caused by heightened gas velocities due to a narrowing of gas side cross-section area. Interfacial friction will also act unevenly on the interface, increasing wave formation. If the weight in hydrostatic height potential is not great enough to dampen the wave formation, then the stratified flow will be *hydrodynamically unstable.* This results in the liquid phase at locations spanning the entire cross section area (possibly with gas bubbles entrapped within). A new flow pattern, *slugging flow*, is now established. This flow pattern is characterised by intermitted flow of sequential liquid slugs followed elongated (*Taylor*) bubbles surrounded by a thin liquid film.

Should the gas rate be increased even further the gas will begin to occupy most of the pipe centre, pushing the liquid out towards the pipe walls. This flow pattern is known as *annular* flow. The converse situation, in which the amount of liquid far exceeds the amount of gas, a fully dispersed *bubble flow* regime appears. Here, small bubbles propagate through a continuous liquid phase. From here, *void waves* of high bubble concentration may form causing bubble coalescence, returning the flow to a slugging pattern. Similarly, rolling waves may accumulate liquid and span the cross-section, manifesting regime transition from the stratified regime [10]. Figure 1.1 presents a schematic of the different flow regime in horizontal pipes and Figure 1.2 portray schematically the corresponding regime flow map. In vertical pipes, slugging and annular flow will replace the stratified. 'Chunk flow' is a term also sometimes used to characterise some vertical flow patterns. A combined term for the annular and stratified patterns is *separated flow.*

Slugs and rolling waves form a particular challenge as these have sharp fronts and constitutes near discontinuities in cross-section phase fraction. They also form jumps in pressure and velocity. Modelling these slugs on Eulerian grids tend to demand fine gridding to avoid numerical diffusion of the slug fronts. Slugs may also be treated in a statistical manner using, for instance, unit-cell approaches. Alternatively, slug or wave tracking methodology may be adopted in order retain exact information of where the slug front discontinuity is positioned, and condition the scheme thereafter. The methods considered in this work apply a Lagrangian slug tracking strategy where dynamic grid manipulation if achieved by means of object oriented programming.

In the case of waves, an interesting strategy is to tackling the Riemann problem in a way similar to the Rusanow method [30]. Dynamic grids in stratified regions may be utilised to promote a control volume which follows the wave front in space and time. This strategy is applied in LASSI [37] and will be discussed in later. Bernoulli suction becomes an important mechanism as the waves grow – difference in gas and wave velocities account for a relative flow past waves and therefore across regions of changing cross-sectional area. The local alteration in gas velocity this causes produce a pressure gradient normal to the stratified interface, producing a suction force which may overpower the gravitational weight and cause slug formation. Capturing of these phenomenon directly is fully possible [13, 7], but, for the foreseeable future, too computationally costly for large engineering purposes in which the diameter-to-pipe length ratio is large. Applying some subgrid model to determine a hydrodynamic slug initiation criteria is a natural alternative. Several models for slug initiation representing this phenomenon have been proposed during recent years [3, 25], some of
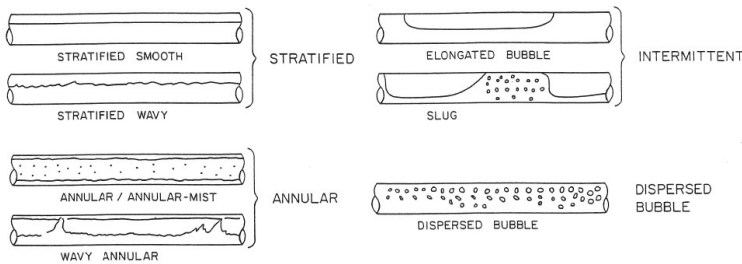
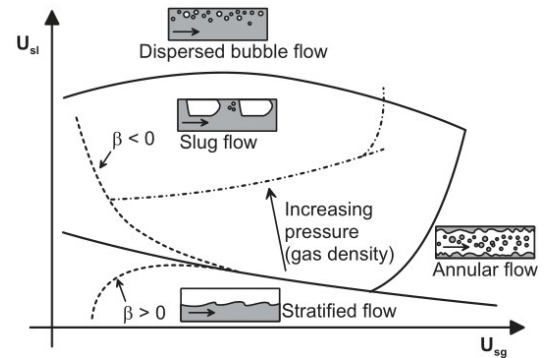Figure 1.1: Flow patterns in horizontal flow. Source: [16]

Figure 1.2: Flow map for horizontal pipes. β is here the pipe inclination. Source: [25]

which will be presented and tested within this text.

1.1.2 Industrial importance

Instabilities in multiphase pipe systems are natural phenomena which during the recent decades have posed challenges to the industry. These instabilities produce highly transient flow behaviour with large, undesired, fluctuations in pressure, velocity and flow pattern. For offshore oil and gas production, these unsteady flow patterns are associated with loss of production and additional strain and material fatigue on equipment and production facility. Safety also quickly becomes an issue, as it always does whenever equipment is place under strains exceeding their design purpose.

In the Nuclear industry the need for accurate prediction of fast pressure transients in thermal multiphase cooling systems have been apparent ever since the Three Mile Island accident in 1979. The *pressuriser* in pressurised cooling reactors is an important component for controlling the the pressure in the primary cooling system, and it provides a surge volume for coolant expansion and contraction. [9]

Multiphase flow stability is also an issue for renewable energy systems, for example in thermal solar systems and heat and refrigeration pumps..

Means with which unstable flow patterns can be avoided is therefore immensely valuable to the all industry operating with multiphase pipe flow systems. Common stabilisation methods in oil fields today inclued *e.g.*, back pressure control systems, dynamic choking, and intermitted or continuous gas injection

techniques [20, 38, 40, 14].

The mechanisms which cause the transition to slugging flow are often divided into two main categories: hydrodynamic slugging, as described earlier, and terrain slugging.

1.1.3 Limitation of exact simulation

In single phase flows analytical solutions only exist in a few, very simple, laminar flow situation. As soon at the Reynolds number increases beyond the laminar regime the governing equations take on an infinite number of possible solutions, rendering true predictions impossible [35, 42]. Direct and modelled simulation of the governing equations can reproduce statistical characteristics of both single and multiphase flow patterns, but often at great computational expense. Direct numerical simulation (DNS) techniques such as immersed boundary methods in the framework of a Navier Stokes solver [48] or multiphase lattice-Boltzmann codes are examples of methods [39] are examples of approaches aiming to reproduce the dynamic behaviour of the flow by capturing the physics in as an exact a manner as possible. Though results from quite small, moderate Reynolds number case studies are quite invaluable as an experimental arena, their computational cost makes DNS inadequate for any appropriate engineering purpose. There seem to be little hope of computers obtaining the required capacity anywhere in the foreseeable future, with the steady development in performance

seen to date.[1] Indeed, although Moore's law of long term trends in computer development may still be said to be valid, the limitation of single processors have long since been reached. For the near future then, DNS to have purely experimental, or laboratorial, use as it's main application.

Therefore, in attempting purely mechanistic simulations to large problems, fine scale physics require modelling and colsure relations in order to reduce the computational cost. The mechanistic ideal is still the same; in capturing enough of the physical mechanisms governing the dynamic behaviour of the flow, a general-purpose method will be obtained capable of responding adequately to each scenario. Again, large problems force coarser grids, demanding more modelling, which in turn generally corrupt the general purpose ideal.

1.1.4 Common methodology in simulation of multiphase pipe flow

It has always been an ideal to provide a single 'grand unified' model with which *all* flow situations can be simulated. Particularly when dealing with multiphase flows there seem to be little hope of achieving such an ideal, except on the tiny DNS-realm. The reason for this was seen in Section 1.1.1; creating a model which intrinsically incorporates all vastly different flow pattern characteristics without capturing the fine-scale mechanics which are source to the differences is simply not done. Instead, the more widely adopted strategy is to group flow patterns and adopt different bespoke models for each flow regime. However, this begs the question *which regime to simulate? A priori* knowledge of the state of the flow becomes required, though this information is often a part of the motivation for doing the simulation in the first place. For many years this has been a motivation for creating flow maps such as that in Figure 1.2. Unfortunately, these two-dimensional maps have proven to be of limited applicability, particularly in terms of changing geometries. Also, many of the phenomena causing phase transitions are transient in nature, and

reversing the circumstances which caused transition from one state to the other may not necessarily return the flow back to its original state. There is also the problem of the pattern grouping itself; the process of transition is also be associated with changes in flow characteristics. The introduction of transient dynamic models around the 1980's provided an improvement to this condition. Criteria for determining flow pattern could now be based on local, dynamic *events* rather than the flow state. Still, flow map strategies are still in use.

An alternative to mechanistic strategy is a phenomenological modelling. Here, the nature mimicking ideal is abandoned in favour of a response-oriented approach. Rather than aiming at capturing the underlying physics well enough to obtain the appropriate dynamic system behaviour, the phenomena and dynamic response involved therein directly become the subject of modelling. The slug tracking scheme studied in this work are indeed based upon such a strategy, the object oriented framework being ideal for the purpose of tailoring dynamic response. Admittedly, such procedures can be said to be incapable of handling scenarios involving phenomena not explicitly included in the model framework. However, the same has already been said about many of the mechanistic models as they are usually heavily dependant on their empirically determined closure relations [35]. The main goal is usually not to retrieve exact details, but a wider picture of the overall dynamical system behaviour.

1.1.5 Commercial codes

Most commercially successful codes available today are in some degree based on phenomenological modelling, though some more than others. When considering multiphase industrial pipe flow, length-to-diameter ratios will often be so large as to render any form of three or two dimensional simulation unfeasible in terms of computational expense. Rather, attention is given to one-dimensional models which treat properties which are statistically averaged over

---

[1]By assuming that the smallest scales of turbulence are independent of the larger scales and only dependant on dissipation as viscosity, while also assuming that the mean energy transfer through the scales is steady, it is easily shown that $\eta/D \sim Re^{-3/4}$, η being the smallest scale to resolve. In three dimensions, including the cost of time step refinement, one finds that the computational cost increases proportional to Re^{-3}

the pipe cross-section. In the mid 1970's, headway was made in physical understanding of two-phase flows, leading to development of numerous mechanistic models being developed. Most of these were initially steady-state models, seeking to provide statistical information on flow rates, phase distribution, pressure and temperature. In contrast to empirical models, which on their own tend to have a validity limited to the pipelines and states at which they are calibrated, mechanistic models show far greater potential for being applicable in a wide range of flow situations.

Among the most popular early steady-state codes available are PIPESIM from Baker Jardine, PROSPER GAP from Petroleum Express, PIPEPHASE from SimSci, PEPTITE and WELLSIM Total, and TUPPF developed within the Tunisia university fluid flow projects [11, 35]. In recent years these steady-state models are being replaced by more advanced mechanistic and phenomenological transient models less dependant upon traditional empirical correlations. These models usually first identify the flow regime and then solves regime-dependant mass and momentum equations supplied with empirical closure laws. The energy equation may also be included.

Steady-state models are not able to predict the transition form one flow pattern to another, nor necessarily all phenomena occurring in a pipe [13]. The nuclear industry was amongst the first to create dynamic multiphase simulation codes, such as TRAC, RELAP_5 and CATHARE [5]. These codes were mainly motivated by safety protocols in reactor cooling systems, and focused on capturing the quick pressure transients, *i.e.,* smaller systems during shorter time intervals. The petroleum industry quickly followed, focusing on the slow transients associated with mass transfer.

OLGA and TACTILE are perhaps the most commercially successful of these codes. The former has been developed in a joint research programme between the Institute for Energy and Technology (IFE) and SINTEF which applies a unit-cell model. In such models, empirical criteria are used to determine the flow regime. The dynamics inside a 'cell', at the scale of the pipeline diameter, is treated statistically in a steady-state manner as the control volume frame of reference follows the flow. Flow pattern depen-

dant empirism plays a large role in how the content of each cell is treated in order to derive phase-specific properties (slip, bubble nose velocity, interfacial mass transfer, friction factors, etc.) from the mixture properties and close the model. These mixture values for the slower transient, large scale dynamics are found by solving mechanistic consecration equations in the system of linked cells. Based on the two-fluid principle, OLGA solves three continuity equations (gas, liquid bulk and droplets) together with two momentum equations (liquid film and gas-droplet mixture). [5, 13]

The TACTILE model, which is based on a drift-flux formulation, differentiates between two types of flow patterns: separated and dispersed. Intermitted flow is treated as a treated as a combination of the two using a *fraction of separation* variable to combine them. This variable is then also included in the flow regime transition criteria.

A survey preformed in [11] judged the transient models OLGA and TACTILE to be superior to the steady-state models as these were found to be applicable to a wide range of flow situations. This survey also found TACTILA to perform better than OLGA.

TRIOMPF is another code which also ought be mentioned. This code is a directly finite volume discretisation of the two-fluid model, which consists of a pair of one-dimensional momentum and energy equations, one for each phase, applicable to stratified flow. TRIOMPF solves the differential system in a 'brute force' manner, applying finite volume upwind discretisation, very fine griddling and iteration at each time step to solve non-linearities with precision. It was used by Issa and Kempf [13] to demonstrate that is it possible to automatically capture hydrodynamic slug formation since the mechanism which causes this phenomenon is present in the two-fluid model (see Section 4.11.) This strategy (applying enough computational effort to capture the mechanisms causing flow phenomena, rather than modelling them) bears resemblance, but should not be confused with, DNS simulation techniques.

1.2   Present work

1.2.1   The Girassol oilfield

Girassol is a deep-water oilfield located 150 km Northwest of the coast of Luanda in Algeria. The seabed depth of the Girassol field is situated approximately 1 300 meters, while the reservoir is relatively shallow (1 200 meters) [47]. Though the seabed pipeline is located at high pressures, the relatively shallow well depth means that the well pressure itself is not sufficient to drive a steady production. Artificial gas injection, known as *gas lift*, has therefore been applied to the riser base. Gas lifts are commonplace in such fields an their purpose is to reduce the hydrostatic riser head by increasing the total riser void fraction. Gas injection proves stabilising to production and is often preferable to increasing upstream pressure by means of mixture pumping stations. Some forms of operational instabilities, commonly called 'headings', are associated with the riser itself (see Section 3.)

From May 12th to 15th 2004 single-well riser stability tests were carried out on the P50 pipeline, while multi-well tests were performed on the P10 pipeline from May 29th to June 3rd, 2004. Gas lift injection rates were stepwise reduced from 190 $^{kSm^3}/_d$ to 70 $^{kSm^3}/_d$ through the stages $Q_g^{gl} \in$ {190, 150, 100, 70} $^{kSm^3}/_d$, producing for several hours at each stage. As the gas lift was reduced to 100 $^{kSm^3}/_d$, the oscillations form the system disturbance surpassed 5 bars in amplitude and the oscillation damping was slow. When reduced to 70 $^{kSm^3}/_d$ gas lift the riser became unstable, showing increasing fluctuating amplitudes reaching $\Delta p = 30$ bar before the gas lift was again increased to prevent production system damage. Pressure, temperature and flow rate data were collected form manifolds and riser valves. Figure 1.3 show the pressure and gas lift rate history at the well manifold. The data was supplied by TOTAL [43].
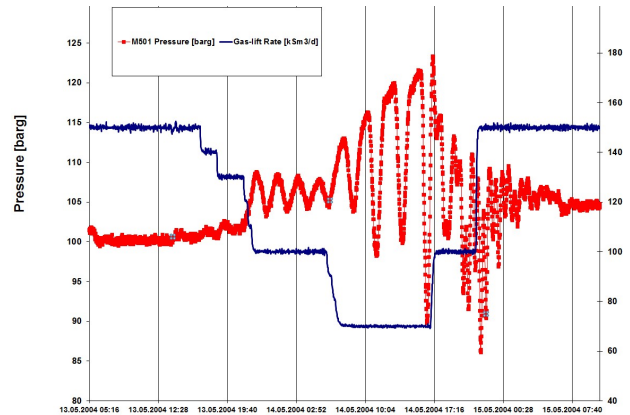

Figure 1.3: P50 Girassol pipeline stability field tests. Source: [43]

Another challenge typical of deep water oil fields is low temperatures. Although the fields are situated at deep waters, the wells themselves are shallow, making the fluid cool. The temperature measured at the manifold of the P50 pipeline is about 64 °C on average, but lower well temperatures are also found in this field. Even though insulated against the 4 °C surroundings, there is a distinct temperature reduction associated with transporting the fluid up the riser, as internal energy in the fluid is abstracted into potential energy. A lift of 1 300 meters entails a temperature reduction of about 5 °C [35]. As wax deposition becomes problematic around 40 °C, retaining the liquid enthalpy quickly becomes an issue. Expensive and energy consuming electric pipeline hearing may then become a necessary measure.

1.2.2   Suspected causes of case instability

The P50 pipeline offers many possibilities for the cause of operational instability seen in Figure 1.3. At the seabed, the pipeline stretches horizontally for about 4.5 km. It is possible that hydrodynamically initiated slugging in this region will affect the overall system dynamic. Also, this horizontal has a light downward inclination ($\phi \approx 0.8$ deg on average,) making it susceptible to terrain slugging (see Section 3.3)

'Jumpers' (small upwards-pointing bends to allow for slight thermal expansion/contraction of the pipeline) are positioned along the horizontal part of the pipeline. Eldar Khabibullin [18] showed that gas accumulation is these jumpers may cause periodic gas releases in the form of void waves, promoting

15

system oscillation.

The total length of the pipeline, form well bore to separator, is approximately 7.7 km long. Because the production from the well will be dependant upon local pressure gradient, and this in turn will be dependant upon the liquid fraction in the riser at the other end of the pipeline, there exist the potential for a void, density or surge wave type instability [38, 26]. Such types of instabilities are seen as promising candidates for the operational instability seen at the P50 Girassol pipeline as the long spatial stretches covered by such well-to-riser wave communication would involve long periods of oscillation. Oscillation period of the data in Figure 1.3 is three hours.

Instability driven by gas expansion in the riser is also likely due to the large change in hydrostatic pressure across the riser. A gross steady state calculation assuming ideal gas, no phase transfer, and a riser completely filled with liquid reveals that a bubble released at the inlet of a filled riser will expand to about 3.5 times its original volume. In fact, gas expansion in the riser is fount to play an important role in most of the operational instability mechanisms discussed in this work.

This topic will be further discussed in Section 3

1.2.3 Aims

The foremost aim of this thesis work is to acquire insight an knowledge about the slug tracking methods available at EPT, as well as becoming familiar with the dynamics of multiphase pipe flow and instability mechanisms active therein. In achieving these goals a case study will be undertaken to set a concrete physical setting for the investigation. The Girassol field described in Section 1.2.1 is chosen for this purpose Consequently, the methods abilities to simulate riser flow will take centre stage in this evaluation. The P50 pipeline is chosen. This line become production unstable as the gas lift injection rates are reduced below $70\,\mathrm{kSm^3/d}$. Attempts at reproducing this instability in simulation using OLGA and SINTEF's LedaFlow have not proven successful; both these codes predict stable flow [47, 18]. Achieving instability, and possibly gaining an understanding of which type(s) of instability mechanisms are active in this pipeline, is therefore an additional exciting challenge. Through collaboration with Eldar Khabibullin

at Kongsberg Oil & Gas Technologies and TOTAL, we seek to understand the field instability better and highlight differences and similarities in the predictions form the LedaFlow and SLUGGIT codes.

1.2.4 Phenomenological slug tracking models at EPT

As a counterpart to the TRIOMPF code, which sought to reproduce dynamic phenomena by capturing the mechanisms through sufficiently detailed mechanistic modelling, the initial SLUGGIT code [34] sought instead to model the phenomena in themselves. Such phenomenological strategies constitutes a philosophy different form capturing schemes, focusing on response rather than recreation.

The first SLUGGIT code, and the code descending from this, utilises object oriented programming to construct a framework within which dynamic behaviour can be hand tailored in compliance with experimental observations. Such a strategy provides direct control of model behaviour and arena for extending behavioural capability limited only by the detail of information at which the model operates. Simplicity is a central ideal. In abandoning the prospect of phenomena capturing, there is a unique opportunity to push the limits of simplification and investigate which factors are dominating the macro scale system dynamics. Pushing the limitations of simplicity also implies pushing the boundaries of application as cases of larger scales become manageable at less computational expense. The great challenge lies of course in determining where the limit at which simplification seems to be justifiable and what boundaries may be pushed without damaging the main system dynamic.

Four codes of varying complexity are available at EPT. These are

- The code implemented by Pascal Klebert [23, 24], in this work referred to as 'SLUGGIT v.1'.

- The code implemented by Jørn Kjølaas [21, 22], here referred to as 'SLUGGIT v.2'.

- A simplified version of Jørn's scheme implemented in the same code by Tor Kjelby, referred to as 'SLUGGIT v.2s'.

16

- A Lagrangian Approximate Scheme for Slug Initiation ('LASSI') code [36, 37] by Fabien Renault.

These codes are described in some detail in Section 4.

2   Definitions and terminology

Unfortunately, in the literature researched during this thesis work a large portion of the terminology encountered is found to be rather ambiguous depending on the author and topic. Therefore, it is fount helpful and clearly define a few of the most commonly confused terms and concepts.

Flow patterns

Some ambiguity in the characteristic features of individual flow patterns are also present in the literature, in particular with the 'slug', 'plug' and 'chunk' patterns. 'Plugs' here refer to solid blockage, as by a pig or hydrate formation. the terminology applied in Figure 1.1 will be adopted here. Due to the limitations of the slug tracking methods, smooth stratified flow and slug flow (mostly without gas entrainment) will be the most widely discussed patterns.

'Stability'

Model stability To be understood in terms of the stability of a model composed of discrete or differential equations (such as Lyapunov stability.) In quasi-technical terms, a small disturbance to a steady system should have finite influence on the solution as time progresses towards infinity. Model stability is usually analysed by finding the criteria for which there exist a diverging Fourier mode.

(Physical) flow stability The conditions for which a specified flow pattern can physically be sustained. Examples of instability mechanisms in horizontal and vertical pipes may be Kelvin-Helmholtz instability (see Annex E) and Rayleigh-Taylor instability [8], respectively. These are characteristics of the *fluid dynamics* – even though models such as the two-fluid model are used to analyse such phenomena, they should not be confused with model stability. If, however, teh model captures the physics perfectly, they terms are equivalent.

Numerical stability The ability of a system of discrete equations to converge towards (close to) a finite solution not dependant on the discretisations itself (asymptotic convergence). A method spoken of as *robust* is a method which remains numerically stable for a large verity of parameter combinations.

Operational stability Sable flow in this context is flow which retains steady properties in time and space. Operational instabilities are typically termed 'headings' in the petroleum industry. This kind of stability will be the main focus of the present work. As mentioned in Section 1.1.2, operational stability is a hot topic in industry. Unfortunately, the author has not yet come across any clear definition of a criterion for when a flow situation may be deemed unstable. Most industrial pipe flows processes operate in a turbulent regime, which is intrinsically unstable and chaotic on a microscopic level. Industrial processes usually include dynamic and transient features where small call oscillations or noise is present. Both the frequency and amplitude of disturbance may be included in a possible definition and could, *e.g.*, represent fluctuations of any flow or fluid property in the same order of magnitude as those bulk.

Though throwing the terms 'stable' and 'unstable' about without definition is not unusual, Zakarian and Larrey applies the usefully, yet arbitrary, '5-bar fluctuation' stability criterion on the pressure upstream

17

the riser in [47] for the Girassol oilfield. In lack good of alternatives, a similar convention is applied here. However, because risers of different dimensions will be analysed, a slightly more general formulation is decided upon, namely that the fluctuation peak amplitudes be less than 5% of the unaerated static riser head. This is about equivalent in the case of the Girassol field.

In the literature, terminological ambiguity concerning this type stability is a nuisance, and no commonly agreed upon term has been found by the author. The term operational stability has been coined herein.

'Riser stability' Whether a small, disturbing gas penetration into the riser will cause a blow-out event – see Section 3.3

well-posedness The property of a model to have a unique solution continuously dependent upon the initial conditions.

Steady-state

By steady-state it is in this text meant a state in which all flow variables are constant in time.

Types of operational instability

Many types of operational instability are possible within the flow regimes of even a simple pipeline-riser system. This will become apparent in Section 3, where a few of the most important types of operational instability is discussed. As far as the this author can understand, some ambiguity in the terminology used to describe these instability phenomena is present in the literature, validating the need to for a definitions. The descriptions given in Sections 3.2 and 3.1 should suffice in defining the terms 'void wave-' and 'expansion driven instability', respectively. When it comes to terrain slugging choices will have to be made.

In this work the term *terrain slugging* it used for all terrain induced slugging, *i.e.* changes in pipeline elevation causing slug initiation. Slugging due to a pipeline 'obstacle', such as a jumper, also falls into this category.

The term 'severe slugging' is by many authors used synonymous with the term 'terrain slugging'. Other authors use it to characterise all terrain slugging events in which full blockage of the bend oc-

curs at some point, *e.g.*, Cycle C and Cycle D [33, 35, 20, 40, 41]. Yet another take on the term is a cycle in which the vigorous blow-out event takes place, including cycles like Cycle E (but not Cycle D) [17]. According to Jansen *et al.*, the term *severe* is by definition reserved for terrain slugging events in which full blockage occur and the slug length is longer or equal the riser height [14].

Presently, to avoid contusion, the term 'severe slugging' will be reserved for this latter extreme event. 'Terrain slugging type I' will be used for all terrain slugging cycles in which the low-point becomes completely blocked (Cycle C and Cycle D, enclosed by the Bøe criterion envelope in Figure 3.3), while 'Terrain slugging type II' is used for cycles where gas continuously enters the riser (Cycle E, marked 'unstable oscillations' in Figure 3.3), as in [20, 33]. Further specification (with fall-back, blow-out event) is given when necessary.

Terms like 'quasi-steady' and similar, arbitrarily scattered around in many pieces of literature, are a nuisance and will be avoided within this text.

3   Operational instabilities in vertical risers

Numerous instability mechanisms for operational instability have been documented from industrial, experimental and theoretical investigations. In the petroleum industry, many such instabilities are found in connection with gas-lift systems. Quickly summarise, instability types usually associated with gas-lift systems are:

- Casing heading

- Formation heading

- Tuning heading

- Pipeline heading

Casing head may occur in gas-lift systems where the gas flow through into the tubing is subsonic, allowing pressure information from the tubing to propagate into the annulus between tub and casing. The flow in the tubing may then be subject to compression of the gas in the annulus. This phenomenon is similar to oscillations caused by the compressibility of trapped pockets of gas, which will be visited later.

Formation heading is similar to casing heady, except that the accumulation takes place in the formation.

Tubing heading is a density wave phenomenon which may occur also when the gas injection is supersonic.

Pipeline heading is associated with the upstream pipeline and terrain slugging.
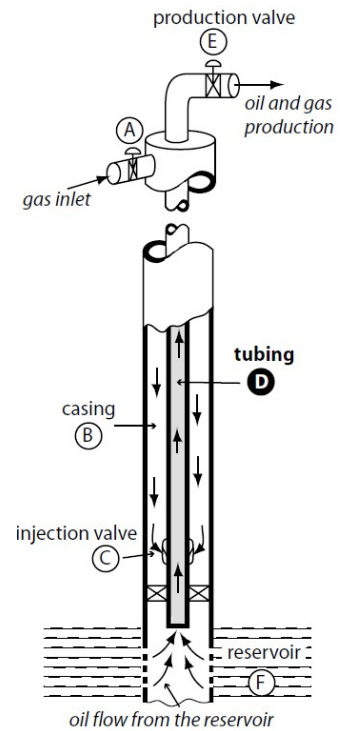
Figure 3.1: Gas-lift well. Source: [38]

Rather than using this terminology, the more general instability mechanism terms will be adopted, namely

- Expansion driven instability

- Density wave (void wave) instability

- Buoyancy driven instability

- Terrain slugging instability

3.1 Extension driven instability

Expansion driven instability is a term not commonly found in literature. In this work, the term is used to describe the cyclic entrapment and expulsion of gas in 'pocket volumes' upstream the riser in a production pipeline.

Cycle A. *Expansion driven operational instability*

A.1 After a gas pocket – in this case a pipeline jumper – has been filled with gas, an increased gas amount will pass by the pocket and propagating into the riser in the form of a void wave.

A.2 The gas surplus travels up the riser and expands, reducing the riser static head and accelerating the liquid ahead of it.

A.3 Expansion of the gas trapped in the upstream pocket and/or the acceleration of the system fluid contribute to further release more of the trapped gas into the main flow and riser base. Consequently, the gas pocket is drained of gas.

19

A.4 The expended gas surplus exits the riser, the system slows down. The total void fraction in the riser is reduced as gas form the well is now entrapped in the now flooded gas pocket. As the pocket fills, the cycle repeats itself.

3.2   Density wave instability

The mechanism of density wave instability in riser systems is, like expansion driven instability, is related to changes in upstream static head afforded by a variation of the total liquid present in the riser. This phenomenon is categorised as a dynamic form of instability in that it has a negative-feedback (self regulating) nature where the driving force of cyclic oscillatory behaviour is a delay in the liquid production response to alterations in upstream pressure. This delay is associated with the limited propagation velocity of a density changes through the pipeline. Propagation, or drift, of changes in mixture density is known as a *density*, *consentration* or *void wave*. The steps of a wave cycle may be described as follows:

Cycle B. Density wave operational instability

B.1 An alteration phase fraction enters the riser base and propagates up the riser. As it propagates upwards and an altered amount of gas expands, the total void in the riser changes.

B.2 As the total amount of liquid in the riser alters, so does the static pressure upstream the riser. A density waves of increased liquid hold-up (concentration waves) would cause increased pressure while the opposite is true for waves of decreased hold-up (void waves). This is the riser-to-well communication channel – pressure changes, and this information propagates at the mixture speed of sound.[2]

B.3 The well responds to a drop in static head by increasing the well flow rate, and oppositely of pressure increases (self-regulation or negative feedback). This well responds propagate down the system at the concentration wave velocity.

B.4 The density wave reaches the riser and the total liquid amount of liquid in the riser changes. Because of the delay in time from the well responds to pressure changes till the density wave reaches the riser, the well will over-compensate. This over-compensateion in turn reverses the pressure situation and, through delay, causes the well to over-compensate in the opposite manner. The cycle continues.

In pipeline a gas lift system is applied a smaller fraction of the total riser void will originate from the well. Consequently, the expansion of a gas surplus originating form the well will have a smaller impact on the total riser void fraction Φ_g, as seen in Section 5.3. Gas lifts therefore has a stabilising effect on the flow, as well as helping production by compensating for low well pressure.

It is further interesting to note that decreasing the injection rate in the gas lift will produce a 'jolt' in riser liquid fraction which would upset the production-pressure balance and initiate this cycle. Also, fraction of riser gas originating from the gas lift will directly influence whether this cycle will converge towards stable production or diverge towards operation instability.

Finally, the delayed response feature of this cycle makes places it amongst the few operation instability phenomena discussed here which would exhibit a sinusoidal pressure disturbance similar to that seen in the field data Figure 1.3.

Sinègre and Petit [38] produced a simple model for the pressure change due to changes in production. The well was treated as a boundary condition with linear delay accounting for the transport time of the density wave. Laplace transformations were applied and an analysis of the underlying characteristic equation performed using control engineering theory. Is was fount that the critical parameter was

---

[2]Though significantly less than the single-phase speeds of sound [16], it is reasonably quick.

the gas injection rate and a simple control strategy of linear feedback to the gas lift from the well pressure, a P-regulator, was shown by OLGA simulation to stabilize the the system.

Apazidis [2] attacks the same problem. Rather than using a delay model for the reaction to the well response, a more complete model based on mass and momentum balances of each phase was developed. A particular air lift pump is considered, and an empirical relation is used for bubble rise velocity. A linear stability analysis is performed on this model using Fourier transformation. Instability for intermediate injection rates were observed which were put down to the density wave mechanism. The size of the bubbles form the injection valve was shown to be significant for the stability domain.

The characteristics of void wave propagation have been studied further in detail by *e.g.*, Lahey [26], who performed both linear and nonlinear analysis of the void-wave phenomena on the two-fluid model (4.26). Different types of void wave profiles are found and the conditions necessary for sustaining them. Smooth, time-invariant void wave profiles (solitons) were shown to be possible only with relatively large void fractions. It was also found that void wave propagation data can be a powerful tool for assessing interracial momentum transfer laws applied in the two-fluid model.

3.3 Terrain slugging instability

Terrain slugging is caused by liquid accumulating at local low-points in the pipeline. If the accumulation become sufficient for liquid to block the entire pipe cross section, a slug if formed. As long as this slug occupies the low-point position it will accumulate more liquid and grow in length. A requirement for this is that the jump in pressure across the slug is not sufficient to move the slug from the low-point up the pipeline. Should the pressure difference across the slug be great enough to move it as soon as the slug is formed, then this terrain slugging will initiate the transition to slugging flow, but not necessarily operational instability, merely a terrain induced slug flow pattern.

Should however the opposite be true then gas will be prevented form flowing passed the low-point. Gas may then accumulate upstream the low-point blockage, gradually increasing the pressure difference across the slug. Simultaneously, new liquid will be fed to the slug, lengthening it and increasing the required pressure difference needed in order to move it. One of two things may happen: Either the pressure resistance provided by the slug and the rest of the pipeline becomes higher than what can be supplied from the inlet, and the system comes to a stand-still. Alternatively, the accumulated pressure will at some point be sufficient to move the entire slug passed the low-point. This may either be because the pressure accumulation happens faster than slug pressure resistance grows due to new liquid supply, or because the upstream end of the slug has reached piping with reduced inclination or the outlet ('proper' *severe* slugging). The result is a rapid acceleration of the slug down the pipeline followed by a high-pressure gas front. In expelling the slug the upstream gas volume is abruptly increased causing a sharp, sudden pressure decrease. It is this abrupt, large-scale variation in velocity and pressure which characterizes of terrain slugging as unstable in a operational stability sense. After expulsion, a new liquid accumulation may take place at the low-point and the cycle is repeated. In short:

Cycle C. *Terrain slugging operational instability*

C.1 Cross section blockage at low-point dip.

C.2 Compression of gas upstream the blockage, increasing the upstream pressure.

C.3 Eventual slug expulsion (blow-out), releasing the gas and plummeting the pressure.

C.4 Possible liquid fall back. New liquid accumulation at low-point and eventual blockage.

A visual example of this cycle can be seen in Figure B.3 in Appendix B.

The 'severity' of the terrain slugging (*i.e.*, the length of the liquid slug at the time of blow-out) is strongly dependent upon the upstream pipeline volume. During slug build-up there is a race between the increasing slug column height (liquid supply) and the pipeline pressure increase (gas supply). A larger upstream gas volume means slower pressure build-up and increased severity/reduced frequency of the slugging. The 'severity' of the terrain slugging can therefore be said to be proportional to the ratio of upstream compressible volume to gas injection rate ($AL\Theta_g/\dot{M}_g$). Notice that this ratio takes the units

$$\frac{AL\Theta_g}{\dot{M}_g} = \left[\frac{m^3}{kg/s}\right] = \left[\frac{s}{kg/m^3}\right] \sim \frac{\mathcal{T}}{\varrho}$$

i.e., slugging frequency versus upstream gas density (or multiple of specific volume).

Figure 3.2 show a typical terrain slugging geometry. The low-point bend (downward pipeline inclination) is a requirement. Figure 3.3 present a flow map of stability regimes, including the riser stability criteria developed by Taitel *et al.* [40, 41]. Some elaboration of the cyclic modes of operation instability represented within this flow map is worth including – both because it is informative in light of the dynamics active in riser systems without gas lifts, but also because similar cyclic instability patterns will be encountered later on.

The Bør criterion (marked 'Boe criterion') is here included as a heavy, solid line. This well-known criterion gives a necessary condition for gas blockages to occur, and it amounts to a simple balance marking the limit for when the read ends of the slug cannot penetrate back into the pipeline due to the high relative gas velocity (monotonically increasing part of curve). At sufficiently high liquid flow rates the pipeline void fraction approaches zero and the criterion bends off to a horizontal line. The original Bøe assumption – that inside this criterion envelope slugging flow will prevail – is today acknowledged as inaccurate (see [32] for an alternative criterion.). The

Bøe criterion has the form [14]

$$\text{Type I slugging} \;\Rightarrow\; U_{l,i}^S \geq \frac{\rho_{g,o}RT}{\rho_l g \alpha_l H} U_{g,o}^S \qquad (3.1)$$

where the notation is consistent with that used throughout this work – see the nomenclature.

The solid, horizontal line mark the divide for *riser stability* in the case of a riser completely filled with liquid. Again a new take on the *stability* term; riser stability is the limit at which, when a small gas amount protrude into the riser, the static head reduction due to increased riser void is balanced by the reduction in upstream pipeline pressure due to the expansion in gas volume. During steady operation the riser will contain a constant, total riser liquid fraction Φ_l. A steady state riser stability model is presented in the broken line marked 'steady state stability criterion'. This is given by [40]

$$\text{(riser) stable} \;\Leftrightarrow\; P_o > \Phi_l\left[\left(\Theta_g/\alpha_g'\right)L - H\right]\rho_l g \quad (3.2)$$

Θ_g its the spatially average void fraction in the pipeline affront the riser. α_g' is the void fraction of the bubble nose entering the riser, being of the order 0.9 [41].
In [40] Taitel assumed that flow in the stability region of this criterion (above the line) will produce steady production. A correction to this is presented in [41] and is show in Figure 3.3 as the region marked 'cyclic no fall-back'. Here, 'fall-back' indicates whether the top, or surface interface, of the liquid column is re-established at the riser outlet or falls back to a level below the outlet after the penetrated gas has left the riser. Although blow-out does not take place in this region due to riser stability, oscillatory behaviour happens which may result in cyclic slugging similar to the terrain slugging described in Cycle C. The mechanism causing these oscillations are, and the flow pattern itself, is very similar to that of the expansion drive instability, Cycle A, and consists of the following steps:

Cycle D. *Cyclic terrain slugging with blockage but no blow-out*

D.1 Cross section blockage at low-point bend.

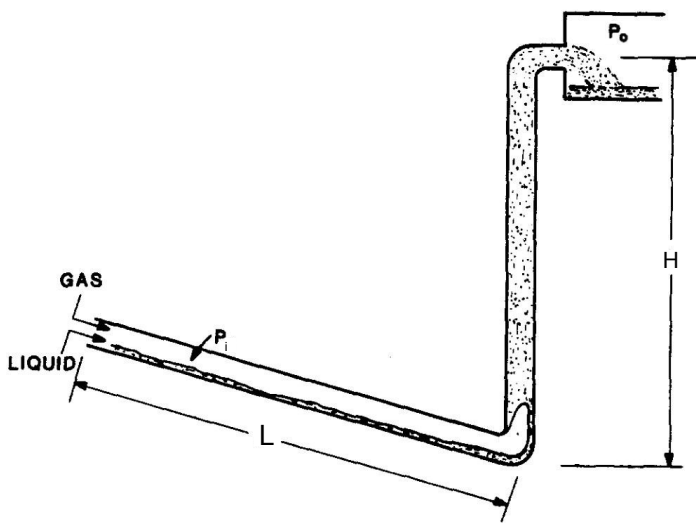D.2 Increasing gas pressure forces gas to penetrate into the riser.

Figure 3.2: Geometry subject to terrain slugging. Moment of blow-out event or transition to steady of oscillatory cycle. Source: [40]
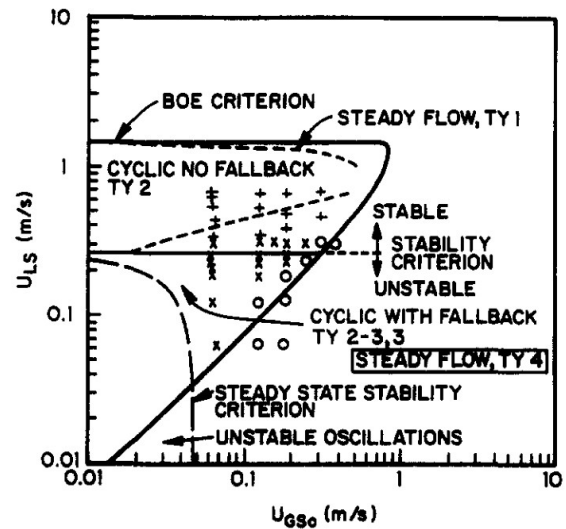
Figure 3.3: Terrain slugging flow map example. Source: [41]

D.3 The riser is stable in the sense that the liquid flow rate is too great for blow-out to occur. Bubbly flow initiates at the riser base.

D.4 As new gas fills the riser and expands, the riser void in increased and upstream static head reduced.

D.5 Consequently, the pipeline gas expands, increasing the rate at which gas penetrates into the riser.

D.6 At some point the riser may become sufficiently aerated so that the reduction in static head is not sufficient to make up for the reduction in upstream gas density. This causes the flow rate into the riser to decrease.

D.7 If the gas flow rate at any point becomes negative doe to this deceleration, the rear liquid front will again penetrate into the pipeline and cause gas blockage. Gas remaining in the riser exits through the outlet, reducing the void fraction and increasing static head. At the same time pressure builds up as gas density increases. At some point (possibly before the riser is gas-free) new gas penetration occurs and the cycle is repeated.

If, however, the gas flow rate in Step D.6 does not become negative, then Step D.7 will not take place. Rather, the (expansion driven) oscillations will be sufficiently dampened to bring the flow to a steady state.

A final region of the flow map in Figure 3.3 worth some attention is that marked 'unstable oscillations'. According to the Bøe criterion, this a region of steady flow. However, it is also in the region of 'steady state instability', and the liquid velocity is much too low to prevent liquid fall-back after blow-out. The net result is a cyclic slugging process taking place even though the flow is inherently steady state (a liquid front will not penetrate back into the riser.) The cycle takes events are the following:

**Cycle E.** *Cyclic terrain slugging with blow-out but no blockage*

E.1 Temporarely stable bubbly flow passes through the liquid column. Because the height of the liquid column is less than the riser outlet, no liquid is produced.

E.2 As new liquid enter the riser base, and as gas expands when the bubbles propagate towards the liquid column top, the liquid column height is increasesd.

E.3 At some point, the liquid column reaches the riser outlet. Because of the inherit lack of stability at this gas flow rate, a blow-out of the fully aerated liquid will occur rather than obtaining a steady liquid production.

E.4 Fallback takes place and the system returns to its initial state. The cycle repeats itself.

This region of the flow map is a transition region between steady flow and terrain slugging.

Figure 3.4: Stability map example, function of *GOR* and riser height. Source: [35]
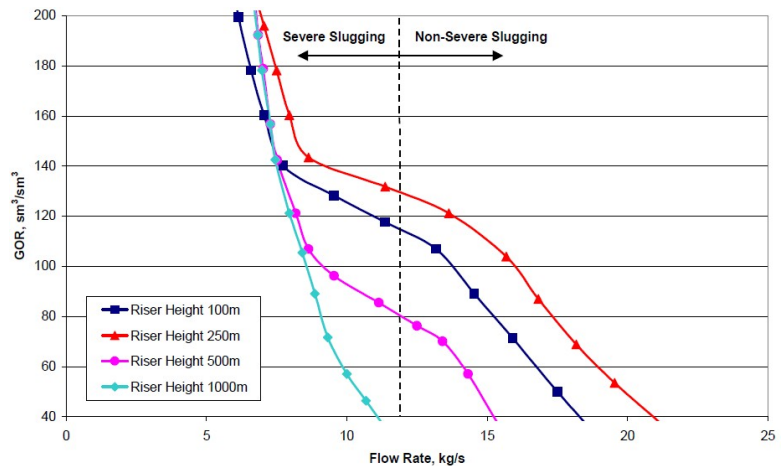
Taken from [35], Figure 3.4 shows a stability map similar to that in Figure 3.3, here as a function of *GOR* and liquid flow rate, plotting the stability limit for different riser heights. To the left of the stability lies, cyclic terrain slugging dominates. In the region enclosed to the left of the stability lines, but to the right of the broken line, oscillation without blow-out (Cycle D) dominates. In [35] and Figure 3.4, the terminology 'severe slugging' and 'non-severe slugging' was applied, which is not adopted in this work. It is evident form the figure that increasing the *GOR* has a stabilising effect on the flow. Increasing the riser height can however be both stabilising and destabilising. The two competing effects influenced by increasing riser height are the increased gravitational riser pressure drop, promoting blockage and destabilisation, and increased pipeline operating pressure, stabilising the system.
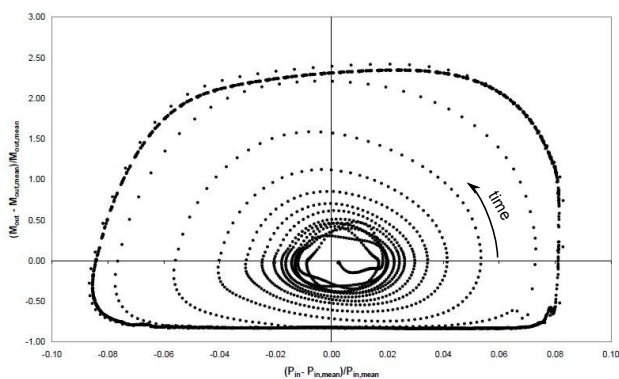
(a) With blow-out and fall-back
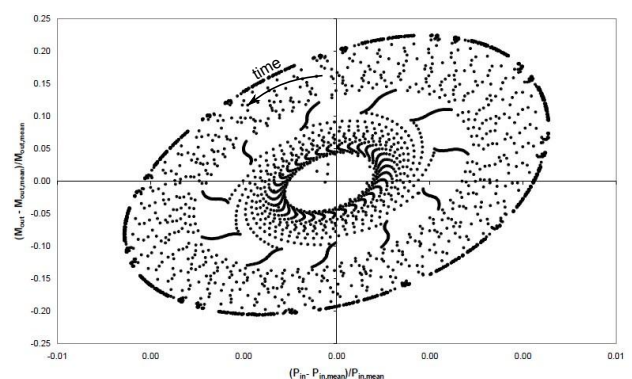
(b) Without blow-out and fall-back

Figure 3.5: Phase portrait examples, terrain slugging. Source: [35]

Another informative visualisation technique is given by the *phase portraits*, as shown if Figures 3.5. Here, the normalised mass fluxes leaving the riser are plotted against the normalised inlet pressure. The state is marked at each time step of the slugging simulation. From the initial, unstable condition, the operation state spirals outwards counter-clockwise until a fixed slugging cycle is established. In Figure 3.5a slugging takes place at a state to the left of the broken line in Figure 3.4 and the system diverges to a cyclic state in which the liquid production is intermitted, giving the phase portrait the 'flat bottom' characteristic of classical severe slugging (Cycle C.) Figure 3.5b show the phase portrait for a situation in which the system is at a state to the right of the broken line in Figure 3.4 (above the horizontal line of Figure 3.3.) Here, no fall-back takes place and there is a continuous, though oscillating, liquid production (Cycle D), giving the portrait a circular shape.

Jensen *et al.* [14] takes the analysis of Taitel [40, 41] further by also including gas lift into the analysis, including the chock from [40]. It is shown that chocking the riser outlet can bring an unstable, slugging system to stable, steady production. The gas lift was also shown to have a stabilising effect by increasing velocities and reducing liquid hold-up.

4   Details of Methods

In this section the common framework of EPT models is established form finite volume analysis, together with the the empirical closure relations used in all method versions. The main development of the fundamental equations will focus primarily on the newest SLUGGIT code, though clarifying important and unique features of each individual method will also be attempted.

The disinterested reader may skip Section 4.3-4.10 without severe loss of comprehension.

During the derivation of this section the following assumptions will be made use of:

Assumptions A. *Slug tracking model assumptions*

A.1 All key features of the multiphase dynamic can be captured in the stratified or slugging flow patterns. Bubbles can be treated as closed regions of stratified flow.

A.2 No entrainment of one phase into the spatial domain of the other takes place – each phase κ in a control volume domain $\partial\Omega$ is fully contained within a respective, closed sub-domain $\partial\Omega_\kappa$. In other words, dispersed flow topologies are not considered.

A.3 The momentum of all pipe-normal movement is neglectable compared with that in the streamwise direction.

A.4 Liquid phases are assumed incompressible.

A.5 Pipe wall normal density gradients within a phase sub-domain are neglectable.

A.6 Momentum exchange through the fluid interface can be handled analogous to wall friction.

Additional assumptions applied in this work – but which are not crucial to the methods themselves – are:

Assumptions B. *SLUGGIT, additional assumptions*

B.1 Two-phase flow is assumed.[3]

---

[3]Although SLUGGIT v.2/v.2s supports three-phase flow.

B.2 There are no exchange of mass between phases (no evaporation or condensation.) [4]

B.3 The ideal gas law is valid. [4]

B.4 Surface phenomena such as rolling waves, surface tension, etc. are not included here.[5]

B.5 The flow is assumed isothermal – the energy equation will not be touched in the present work. See *e.g.* [22] for handling of thermal issues in SLUGGIT.

Similar for all models discussed is that only two types of flow objects are considered: separated and (possible aerated) slugs. Elongated Taylor bubbles are treated as enclosed regions of stratified flow, and in SLUGGIT v.2 and LASSI forms of the two-fluid model are used to describe these.

4.1 Method structure

Central to the dynamic behaviour of the SLUGGIT and LASSI programmes is the dynamic, object oriented programming techniques used in their structure. The fundamental benefit of a completely object oriented programming structure is the way in which dynamic behaviour is implemented on a local level; rather than operating from the level of the entire flow system, responses and interactions are given each individual fluid object, allowing for tailor-made local dynamic responses to local bubble-scale events. The dynamic behaviour seen from a flow system level is thereby the result of the combined interactions of all objects which individually live and respond according to individual characteristics.
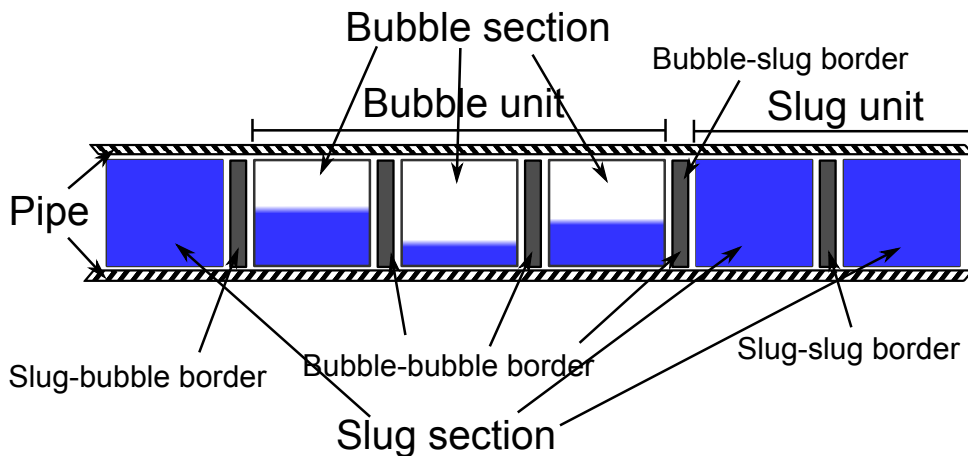

Figure 4.1: Main object classes

Details on the object oriented code structure will not be given here – see *e.g.* [22] for this purpose. Some description is however deemed necessary as differences in programme versions are strongly connected with the object oriented structure. These objects are continuously and dynamically moved, destroyed, created and transformed during the simulation. Figure 4.1 illustrates the fundamentals of object structure; objects of the ancestor class `Section` hold masses and have spatial extent. Those objects of the ancestor class `Border` divide the `Section` objects at a spatial position. The movements of these borders govern the movement of the fluid objects and change in section lengths. Pipe properties, such as diam-

---

[4]This assumption may be influential in deep-water case simulations.

[5]These topics are however approached and take a central place in the LASSI scheme [37] (Section 4.11) and indirectly in the topic of hydrodynamic instability and the Kelvin-Helmholtz criterion (Annex E). Rolling wave functionality has been implemented in the SLUGGIT v.2 framework, though this will not be approached or activated during the present work (see *e.g.* De Leebeeck [10])

eter, roughness and inclination, are extracted from the `Pipe`. `Section` objects retrieve pipe information from the `Pipe` object spanning the spatial length which the section in question occupies. Unit classes (`Unit_slug` and `Unit_bubble`) are ancestors of `Section` classes, collecting all sequentially similar `Section` objects into one. It could be said that sections are 'subgrids' of 'unit grids', but in order to underline the strongly object oriented nature of these programmes the term 'grid' will be avoided. A 'grid' suggests something static rather than the a dynamic, self-sustaining environment wherein the number and nature of objects change continuously. Perhaps the most important dynamic feature in this respect is that the pipeline is automatically divided into compressible (bubble) and incompressible (slug, plug) units, generating regions wherein the system solved may be compressible or incompressible. Thus, the problem of having a universal scheme for both compressible and incompressible flow is elegantly avoided. It becomes possible to control the level at which each of the governing equations are solved. In particular, mass and momentum equations may be solved at

section level in bubbles while the same equations are treated at unit level in slugs, making it possible to connect single equations to whole slugs.

4.2 SLUGGIT scheme versions

The method derived in Section 4.3 is based on the implementation [21] by Jørn Kjølaas [22], referred to as 'SLUGGIT v.2'. This implementation was further developed by Tor Kjelby and Angela De Leebeeck, and adjusted further by the present author during this thesis work. Alternative implementations of similar, yet simpler implementations are also available at EPT; previous to Kjølaas' version, Pascal Klebert implemented a code [23], documented in [24], closer to the original model of Nydal and Banerjee [34]. This code is in the present work referred to as SLUGGIT v.1. In addition to these versions, Kjelby has implemented an alternative, simplified procedure in the framework of SLUGGIT v.2, with the purpose of merging the different procedures into a single framework.[6] Here, this simplified version is termed 'SLUGGIT v.2s'

Here will follow short version descriptions to underline the main differences between versions.

SLUGGIT v.1: In form of implementation, this version has benefited for far less time in development and debugging than v.2. It makes use of template function structures rather than class inheritance which is widely adopted in v.2. In terms of the model, uniform pressure (and gas density) throughout every bubble unit (Taylor bubble and stratified region) is assumed. As a consequence, a slug or pig object is needed to generate a change in pressure. The benefit of this assumption is that only a single pressure equation is solved for each bubble unit. Because checker board solutions become impossible with this scheme, non-staggered grids have been employed – see Figure 4.7a and 4.6a. The mass flux and convection terms are neglected in the pressure and momentum equations. Gas entrainment in slugs is also included in the v.1 implementation, promoting a mixture formulation of the slug mass and momentum equations. No sources, endothermal behaviour or boundary conditions other than fixed inlet flows are presently supported.

SLUGGIT v.2: Motivated by the need to capture quick transients reactions for sudden pig and plug discharges in pipelines, SLUGGIT v.2. was implemented with individual pressures for each section of a bubble unit. In order to avoid unphysical checker board solutions, a staggered grids must then be used (Figure 4.7b.) The momentum balance, including all terms, is solved for slug units and both phases in all bubble sections, except those neighbouring a slug unit where the empirical border velocity relations of Section 4.8 dominate – see Figure 4.6b. Gas entrainment in slugs ('void in slugs') is not supported in this version, though thermal behaviour (solving the energy equation), support for rolling wave phenomena [10] and a wider range of inlet conditions are available. Implicitness is imposed as presented in Section 4.3. Also,

---

[6]A great misfortune of the codes at EPS is that they have been developed separately in individual frameworks, see section 6

automatic time step length based on the CFL condition is implemented, optimising the computation time while ensuring numerical stability.[7]

SLUGGIT v.2s: This simplified version can be considered a cross between SLUGGIT v.1 and v.2. It is implemented in the v.2 framework, allowing it to benefit form all the work invested into the v.2 implementation in terms of making the code more robust. Additionally, all extra management and parameter options are available, such as the automatic time step regulation, possibility of simulation restart and hydrodynamic slug initiation mechanisms. The assumption of a uniform bubble pressure is employed also here, and convection terms in the pressure and momentum equations are neglected. The slug momentum and bubble unit pressure equations are coupled and solved implicitly (see Figure 4.6a). For the liquid phase in bubbles, an explicit momentum balance is solved at the sections (non-staggered,) while the border velocities sat to the mean of that in neighbouring sections. The gas velocities are not determined by the momentum equation at all, but form an explicit mass balance at the borders. Here, the velocities are governed by the fact that gas velocity equal border velocity at bubble unit borders. As the gas density, due to the pressure, is uniform throughout the bubble unit, this determines the gas velocity as inversely dependant on the void fraction of the cross section area α_g. Neighbour means are used for the gas section velocities. Mass equations are treated as in v.2. Void in slugs is presently not supported. Suggested documentation: [24, 34, 33].

4.3 SLUGGIT – Fundamental Equations

In this section the the basis for the SLUGGIT model is derived and presented in some detail. The aim here is to present the model in details fine enough to establish an overview of the fundamental ideas and differences between the models. This is done by first deriving the general balances used in the methods and then examining the way in which the grids are defined and quantities approximated within the different frameworks. In order to obtain new insight, for both reader and writer into the methods, the present section seeks to establish the undamental equation applying control volumes directly to the *discrete* scheme and derive the numerics from there. In contrast, [16, 22, 37, 24] proceed by deriving or presenting the continuous two fluid model (4.26) and simplify and discretise from there. The notation used presently is chosen to correspond reasonably to the model sources [22, 37, 34, 24, 20] and CFD conversion [45, 30]. This derivation was developed during the present work.

Notation

The following subscript conventions will be used (see Figure 4.2)

$$\sigma \in \{w, e\} \qquad \Sigma \in \{W, E\} \qquad \kappa \in \{l, g\}$$

where l and g denote 'liquid' and 'gas', respectively. W, P and E denote 'western', 'present' and 'eastern' control volume cell, while w and e denote the western and eastern control volume face values, respectively. This is in accordance with the conversion used in many CDF applications (*e.g.* [45]). 'Left' and 'right' are also standard notations, though letters denoting 'left' and 'liquid' may easily be confused. As the model to be developed is 1D, dimensional indexation is deemed superfluous and non-bold vector and tensor counterparts are streamwise components by conversion (*e.g.*, $u \triangleq u_z$, $\tau \triangleq \tau_{zz}$). All variables not marked with a tilde (˜) represents cross section averages unless otherwise stated. Some attempt is made of distinguishing the main variables stemming from the conservation equations from those of a parametric or algebraic nature by using capital symbols for the latter.

---

[7]As with the other EPS slug tracking codes, SLUGGIT v.2 has issues with robustness, but this is mainly due to the flow object management operations. Only during the present thesis work SLUGGIT v.2 has improved in stability greatly through continuous debugging and management measures.
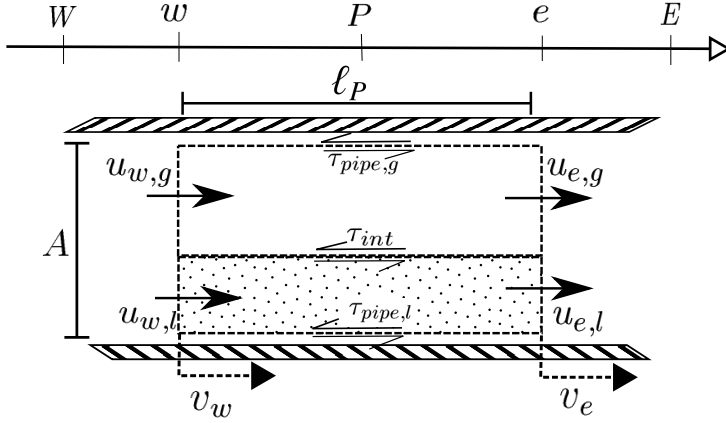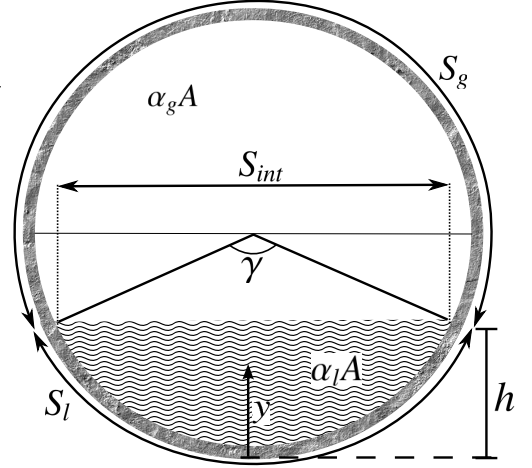
Figure 4.2: Control volume

Figure 4.3: Pipe cross section

4.3.1 Mass Balance

By applying unity as the transported property to the Reynolds transport theorem over the control volume in Figure 4.2 the continuous momentum equation takes the form

$$\frac{\mathrm{d}}{\mathrm{d}t} \oiiint_{\Omega_\kappa} \tilde{\rho}\, \mathrm{d}V + \oiint_{\partial\Omega_\kappa} \tilde{\rho}\,(\tilde{\underline{u}} - \tilde{\underline{v}}) \cdot \tilde{\underline{n}}\, \mathrm{d}A = \oiiint_{\Omega_\kappa} \dot{m}^s\, \mathrm{d}V \tag{4.1}$$

The tilde indicated that these are local variables in all dimensions of space, that is, they are continuous and their integral values will be approximated by control volume averages. Based on Assumption A.5, a key approximation used in the FVMs is:

$$\iint_{\partial\Omega_{\sigma,\kappa}} \tilde{\rho}(\tilde{\underline{u}} \cdot \tilde{\underline{n}})\, \mathrm{d}A \approx \frac{1}{(\alpha_\kappa A)_\sigma} \iint_{\partial\Omega_{\sigma,\kappa}} \tilde{\rho}\, \mathrm{d}A \cdot \iint_{\partial\Omega_{\sigma,\kappa}} (\tilde{\underline{u}} - \tilde{\underline{v}}) \cdot \tilde{\underline{n}}\, \mathrm{d}A = [n\rho_\kappa\alpha_\kappa A(u_\kappa - v)]_\sigma \tag{4.2}$$

α_κ in (4.2) is the section volume fraction of fluid κ, *i.e.* $\alpha_\kappa = V_\kappa/V$, V_κ being the volume occupied by fluid species κ. $\alpha_\kappa A$ thereby represent the mean stream-normal area occupied by fluid κ. n_σ is the z-component of the $\partial\Omega_\sigma$ surface normal; $n_e = 1$, $n_w = -1$.

In the following, the convection term is slightly reformulated in terms of *superficial* mass and flux quantities[8] m, Q; rather than expressing the flux of mass $\rho_\kappa V_\kappa$ across a border sub-area $(\alpha_\kappa A)_\sigma$, the total area A and superficial specific masses $m_\kappa = M_\kappa/V = \rho_\kappa\alpha_\kappa$ are used, M_κ and V being the *total* specie mass and control volume. Likewise, the extensive volu-

metric flux Q is defined by

$$Q_{\sigma,\kappa} = [(u_\kappa - v)A^n]_\sigma \tag{4.3}$$

The term 'extensive' is here, perhaps improperly, applied because Q is defined using the total pipe area A while retaining the intrinsic velocity averages, and so only appropriate for the flux of pipe-specific superficial quantities (m, mu). Beware that the area of Q^{n+1} is still taken from the previous time step.

m is nearly equivalent to the density, except that it is the specific mass based on total pipe area A. Also, ρ should not be confused with m in that the notation ρ will be reserved for densities derived form the equation of state (EOS), used in the pressure equation,

---

[8]The term 'superficial' is equivalent to *extensive* (as opposed to *intrinsic*) spatial averages, *e.g.*, using the notation of [16]: $\rho_\kappa = \langle\tilde{\rho}_\kappa\rangle^i$ and $m_\kappa = \langle\tilde{\rho}_\kappa\rangle = \alpha_\kappa\langle\tilde{\rho}_\kappa\rangle^i$

while M_κ (and m_κ) originate from the conservative mass equation.

The mass flux over a border in (4.2) can now be written on superficial form $(mQ)_{\sigma,\kappa}$:

$$\left[\frac{\mathrm{d}M_P}{\mathrm{d}t} + \sum_\sigma (nmQ)_\sigma = \dot{M}_P^s \right]_\kappa \qquad (4.4)$$

The implicit Euler method is used for the time discretization:

$$\left[\frac{(mV)_P^{n+1} - M_P^n}{\delta t} + \sum_\sigma \left[n(mQ)^{n+1} \right]_\sigma = \dot{M}_P^s \right]_\kappa \qquad (4.5)$$

The volumetric fluxes for the current time step Q^{n+1} is available as the phase momentum equations and pressure equation are computed prior to the phase mass conservation equations. In practice, the volume V^{n+1} is taken after the border positions are corrected with $z^{n+1} = z^n + v^n \delta t$, but before the slug border positions have been accurately adjusted with respect to the new liquid mass [21], making it only a preliminary future volume. Implicitness between the control volume masses and the velocities is lost. However, the mass continuity equation is still incorporated implicitly into the momentum equation in two ways. Firstly, the mass equation (4.5) is used to simplify the momentum equation, allowing the transient volume integral to be evaluated for velocity rather than momentum. Secondly, the pressure, which is solved implicitly with the velocity, originates from a reformulation of the continuity equation, incorporating a compressibility relation for the gas phase.

4.3.2 The pressure equation

The pressure equation is obtained directly by reformulating the mass balance (4.4) by applying the chain rule on the first transient term, assuming $\rho_g = \rho_g(p, T)$:

$$\frac{\mathrm{d}M_\kappa}{\mathrm{d}t} = V_\kappa \frac{\mathrm{d}\rho_\kappa}{\mathrm{d}t} + \rho_\kappa \frac{\mathrm{d}V_\kappa}{\mathrm{d}t} = V_\kappa \left[\frac{\partial \rho}{\partial p} \frac{\mathrm{d}p}{\mathrm{d}t} + \frac{\partial \rho}{\partial T} \frac{\mathrm{d}T}{\mathrm{d}t} \right] + \rho_\kappa \frac{\mathrm{d}V_\kappa}{\mathrm{d}t}$$

Since the main contributions to the absolute hydrostatic pressure is found from streamwise pressure gradients, and only pressure gradients have a fine scale impact on the momentum equation, there is no ambiguity is placing this EOS pressure p at the fluid interface. As the liquid phase is assumed incompressible (Assumption A.4) this equation only becomes informative for the gas phase. Still, a combined phase control volume formulation (overall continuity) allows for the simplest form:

$$\sum_\kappa \frac{V_{P,\kappa}^n}{\rho_{P,\kappa}^n} \left[\left(\frac{\partial \rho}{\partial p} \right)_T \frac{p_P^{n+1} - p_P^n}{\delta t} + \frac{\partial \rho}{\partial T} \frac{\mathrm{d}T}{\mathrm{d}t} \right]_P + \sum_\kappa \sum_\sigma \frac{n_\sigma}{\rho_{P,\kappa}^n} \left[m^n Q^{n+1} \right]_{\sigma,\kappa} + \sum_\sigma (nv^n)_\sigma A_P = \sum_\kappa \left(\frac{\dot{M}^s}{\rho_P^n} \right)_\kappa + \psi_{s,P}^n \qquad (4.6)$$

Dividing by the respective density serves to balance the equation with respect to the fluid densities. Doing otherwise would cause the liquid phase to dominate the equation, possibly leading to convergence problems [13]. In this work only isothermal systems will be considered (Assumption B.5). Because of this the temperature term in (4.6) is disregarded and no energy equation will be solved. Equation (4.6) is Laplacean in nature, meaning that it governs the streamwise *change* in pressure as a function of the *change* in mass. Such a formulation is useful as it is the pressure gradient which appears in the momentum equation. However, absolute pressure is also important as pressure must be in agreement with gas density in upholding the Equation Of State (EOS), which in this case is the ideal gas law. Because simplifications and non-conservative inaccuracies occur in this non-conservative mass formulation, the *absolute* pressure will eventually diverge from that pressure which is consistent with the EOS and densities from the conservative mass equation (4.5). The final term ψ is a countermeasure for this; a correction source term accounting for the discrepancy between EOS pressure as found form the conservative masses, and the pressure change from the non-conservative pressure equation 4.6. This 'trick' of enforcing mass conservation by explicitly supplementing the pressure with the error from the previous time step allows

for consistency to remain between pressure and gas mass. The volume error takes the form:

$$\psi_s = \frac{V}{\delta t} \left[\left(\sum_\kappa \frac{m_\kappa}{\rho_\kappa} \right) - 1 \right] \tag{4.7}$$

By including this error correction source term the error sustained during one time iteration is removed in the iteration which follows. Thus, pressure-density discrepancy in the momentum equation can originate only from the present time iteration.

The SLUGGIT v.2 scheme uses a staggered grid in order to avoid the notorious checker-board pressure solution. An uniform interface pressures across entire bubble units is assumed in SLUGGIT v.1. Accordingly, SLUGGIT v.1 solved (4.6) at bubble unit level, while SLUGGIT v.1 solves it at section level.

4.3.3 Momentum Balance

By applying the momentum to the Reynolds transport theorem (*e.g.*, [16, 46, 45]) over the control volume in Figure 4.2 the continuous momentum equation takes the form

$$\frac{\mathrm{d}}{\mathrm{d}t} \iiint_{\Omega_\kappa} \tilde{\rho}\tilde{\underline{u}} \, \mathrm{d}V + \oiint_{\partial\Omega_\kappa} \tilde{\rho}\tilde{\underline{u}} \left(\tilde{\underline{u}} - \tilde{\underline{v}}_b \right) \cdot \underline{n} \, \mathrm{d}A = \oiint_{\partial\Omega_\kappa} \left(\tilde{\underline{\underline{\tau}}} \cdot \underline{n} - \tilde{p}\underline{n} \right) \mathrm{d}A + \iiint_{\Omega_\kappa} \left(\tilde{\rho}\underline{g} + \dot{m}^s \tilde{\underline{u}}^s \right) \mathrm{d}V \tag{4.8}$$

Here $\underline{g} \cdot \underline{n} = -g \sin\phi$.

The pressure integral require some extra attention. It evaluates as a surface integral of local pressure $\tilde{p}$, but only the pressure p at the gas-liquid interface generated from (4.6) is available. Transverse pressure gradients must also be included. Because there may be streamwise gradients in the liquid height h_l, transverse pressure consideration will affect the pressure acting in the streamwise momentum balance also. The two-fluid model, applies a hydrostatic approximation to include the gradients in fluid height. In fact, the two fluid model, on which this derivation is based, becomes ill-posed if this hydrostatic pressure contribution is neglected (the 'constant pressure model') [16].
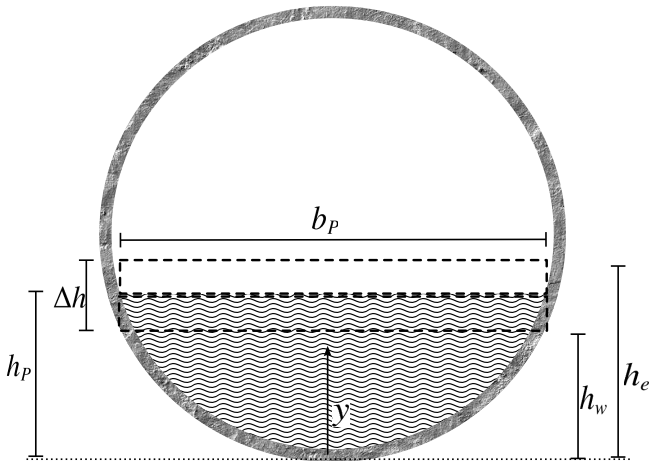
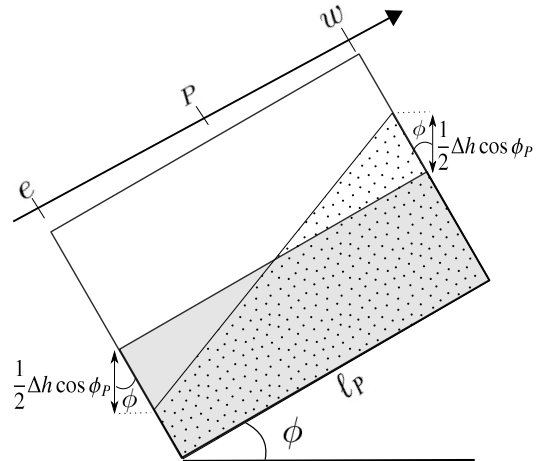

Figure 4.4: Pipe cross section

Figure 4.5: Hydrostatic approximation of liquid height gradient influence

The pressure integral in (4.8) may be evaluated hydrostatically, formulating the western and eastern inte-

grals around the centre hight h_P:

$$\underline{e}_z \cdot \oiint_{\partial\Omega_\kappa} -\tilde{p}\underline{n} \, \mathrm{d}A = -\sum_\sigma n_\sigma \iint_{\partial\Omega_{\sigma,\kappa}} \left[p(z) + (h(z) - y)\rho_l\underline{e}_z \cdot \underline{g} \right] \, \mathrm{d}A$$

$$= \sum_\sigma (n\alpha_\kappa p)_\sigma A + \underbrace{\left[\sum_\sigma h_\sigma \iint_{\partial\Omega_{\sigma,\kappa}} \mathrm{d}A - \int_{h_w}^{h_e} y \, \tilde{b}(y) \, \mathrm{d}y \right]}_{V_h} \rho_l g \cos\phi_P \tag{4.9}$$

where $\tilde{b}(y)$ is the pipe breadth orthogonal to the flow plain (see Figure 4.4) and p is the pressure *at the interface* found from the pressure equation (4.6). V_h (the term inside the square brackets) require some extra attention. In a differential formulation its value would follow from integration using Leibnitz' theorem. Here one must trod carefully

$$V_h \cong (h\alpha_\kappa A)_e - (h\alpha_\kappa A)_w - \tfrac{1}{2}\tilde{b}(h_P) \cdot \underbrace{\left(h_e^2 - h_w^2 \right)}_{(h_e + h_w)(h_e - h_w)} = h_e \left[(\alpha_\kappa A)_P + \tfrac{1}{2}\Delta h \tilde{b}_P \right] - h_w \left[(\alpha_\kappa A)_P - \tfrac{1}{2}\Delta h \tilde{b}_P \right] - h_P \tilde{b}_P \Delta h$$

where $\Delta h = h_e - h_w$. The western and eastern areas have been expressed as deviations around $A_{P,\kappa}$ — see the schematic of Figure 4.5. $\Delta h \ll d$ has here been assumed, allowing the pipe breadth $\tilde{b}(y)$ to be approximated constant equal to $\tilde{b}(h_P)$ within the narrow integral region. Rearranging yields

$$V_h \cong A_{P,\kappa}\Delta h + \tilde{b}_P \underbrace{\tfrac{1}{2}(h_e + h_w)}_{h_P}\Delta h - \tilde{b}_P h_P \Delta h = A_{P,\kappa}\Delta h$$

accordingly, the hydrostatic non-constant pressure model (4.9) evaluates as

$$\underline{e}_z \cdot \oiint_{\partial\Omega_\kappa} -\tilde{p}\underline{n} \, \mathrm{d}A = -\sum_\sigma (n\alpha_\kappa)_\sigma A_\kappa \left[p_\sigma + h_\sigma \rho_l g \cos\phi_P \right] \tag{4.10}$$

The result is easily understood from Figure 4.5 as a correction to the gravity term for the liquid height gradient. There $h_e > h_w$ have arbitrarily been assumed, which does not affect the result. Expression (4.10) was derived with the liquid phase in focus ($\sigma \to l$), though it also holds for the gas phase ($\sigma \to g$).[9] It is however only in quite special cases that the contribution of the gas weight will be important.

In the final paper of [37] a simplified transverse momentum balance is developed as an alternative to hydrostatic approximation.

The convection integral ('momentum flux') is now sat in focus. Again, the base assumptions of the finite volume method is that integrated properties can be approximated by a uniform control volume average. Also applying Assumption A.5 of neglectable

wall normal density gradients within the phase sub-domains, the fluxes may be assumed averaged and the final simplification with regard to the convection term is

$$\iint_{\partial\Omega_{\sigma,\kappa}} \tilde{\rho}\tilde{u} \left(\underline{\tilde{u}} - \underline{\tilde{v}} \right) \cdot \underline{\tilde{n}} \, \mathrm{d}A$$

$$\approx \frac{1}{(\alpha_\kappa A)_\sigma} \iint_{\partial\Omega_{\sigma,\kappa}} \tilde{\rho}\tilde{u} \, \mathrm{d}A \cdot \iint_{\partial\Omega_{\sigma,\kappa}} \left(\underline{\tilde{u}} - \underline{\tilde{v}} \right) \cdot \underline{\tilde{n}} \, \mathrm{d}A$$

$$= (\rho u Q)_{\sigma,\kappa}$$

The shear force integral in (4.8) evaluates as:

$$\underline{e}_z \cdot \oiint_{\partial\Omega_\kappa} \underline{\tilde{\tau}} \cdot \tilde{n} \, \mathrm{d}A = \left[(\tau A)_{pipe,k} + (\tau A)_{int} \right]_P \tag{4.11}$$

where the subscripts *pipe* and *int* respectively indicate the pipe wall and fluid interface control volume

[9] In the gas region, both $y \geq h$ and $\tilde{p}(y) \leq p$, changing the signs twice and producing the same result.

32

surfaces. The shear forces τ must be evaluated from the local strain across these surfaces. Simple Darcy friction factor relations will be used to approximate these, and so they will be linearised functions of the relative difference in kinetic energy across radial surfaces.

$$\tau = \frac{1}{8}\lambda\rho|u|u \qquad (4.12)$$

Many different friction correlations are have been developed throughout the years. Issa *et al.* proved these to be of some influence in their slug capturing scheme [13]. Here, the Darcy friction coefficient λ is determined form the explicit Haaland correlation:

$$\frac{1}{\sqrt{\lambda_\kappa}} = -1.8\log\left[\frac{6.9}{Re_\kappa} + \left(\frac{\varepsilon}{3.7D_{h,\kappa}}\right)^{1.11}\right] \qquad (4.13)$$

where ε is the pipe wall roughness and the phase Reynolds number Re_κ is computed using the hydraulic diameter $Re_\kappa = \rho_\kappa D_{h,k} u_\kappa / v_\kappa$. The D_h is the hydraulic diameter – the length scale analogous to a pipe diameter evaluated from the surface periphery and cross section area. Momentum exchange between phases across the interface is strongly simplified and use the same kind of friction factor, which is equivalent to approximating the phases as solid surfaces in relation to each other (Assumption A.6). Possibility for including some linear deviation from this assumption is supplied by adding an *Interphase*

Friction Multiplier (IFM) to the friction factor. The friction forces used are computed from the gas phase

$$\tau_{int} = \frac{1}{8} \cdot IFM \cdot \lambda_g \rho_g \left|u_g - u_l\right|\left(u_g - u_l\right)$$

and so the interface perimeter is included in the gas hydraulic diameter

$$D_{h,g} = \frac{\pi D^2}{S_g + S_l}, \qquad D_{h,l} = \frac{\pi D^2}{S_l} \qquad (4.14)$$

Since the convection term of the momentum equation introduces non-linearities (momentum is transported by means of fluid motion,) the convective flux terms are evaluated using velocities from the previous times step Q^n. The same non-linearity is found in the friction factor definition (4.12) and also here the squared velocity is approximated as the product of the velocity form the precious time iteration and the present velocity for which the system is being solved $- u^{n+1}|u^n|$. An iterative approach is also possible here. This would require expensive re-evaluation of the pressure-momentum system in each times step and has for this reason not been implemented. The possible benefits in terms of accuracy are small in light of the overall model simplifications As before, the first order Euler method is used for the time derivative. Collecting all the above methods of evaluation, (4.8) takes the form:

$$\left[\frac{(Mu)^{n+1} - (Mu)^n}{\delta t}\right]_{P,\kappa} = \begin{cases} -\sum_\sigma n_\sigma \left[\left(m^n Q^n u^{n+1}\right)_{\sigma,\kappa} + \left(\alpha_\kappa^n A p^{n+1}\right)_\sigma\right] \\ -\frac{1}{8}(S_\kappa L \lambda_\kappa \rho_\kappa)_P^n \left|u_{P,\kappa}^n\right| u_{P,\kappa}^{n+1} \\ -\frac{1}{8} \cdot IFM \cdot (S_{int} L \lambda_g \rho_g)_P^n \left|u_{P,\kappa}^n - u_{P,\uparrow\kappa\downarrow}^n\right|\left(u_{P,\kappa}^{n+1} - u_{P,\uparrow\kappa\downarrow}^{n+1}\right) \\ -g M_{P,\kappa}^n \left[\sin\phi + \frac{h_{l,e}^n - h_{l,w}^n}{\ell_P^n}\cos\phi\right] \\ +\left(\dot{M}u\right)_{P,\kappa}^s \end{cases} \qquad (4.15)$$

where the subscript $\uparrow\kappa\downarrow$ indicates a property of *the other* phase. The last source term is usually of little relevance as mass source inn and outflows are in most cases orthogonal to the main stream.

In multiplying the discrete mass balance (4.5) with the velocity at the computed time step u_P^{n+1} and subtract-

ing this from (4.15) the momentum balance simplifies to[10]

$$
\left[M^n \frac{u^{n+1} - u^n}{\delta t} \right]_{P,\kappa} =
\begin{cases}
+ \sum_{\sigma} n_{\sigma} \left[(mQ)^n_{\sigma,\kappa} (u_P - u_{\sigma})^{n+1}_{\kappa} - \left(\alpha^n_{\kappa} A p^{n+1} \right)_{\sigma} \right] \\[2ex]
- \frac{1}{8} (S_{\kappa} L \lambda_{\kappa} \rho_{\kappa})^n_P \left| u^n_{P,\kappa} \right| u^{n+1}_{P,\kappa} \\[2ex]
- \frac{1}{8} \cdot IFM \cdot (S_{int} L \lambda_g \rho_g)^n_P \left| u^n_{P,\kappa} - u^n_{P,\text{⇅}} \right| \left(u^{n+1}_{P,\kappa} - u^{n+1}_{P,\text{⇅}} \right) \\[2ex]
- g M^n_{P,\kappa} \left[\sin\phi + \frac{h^n_{l,e} - h^n_{l,w}}{\ell^n_P} \cos\phi \right] \\[2ex]
+ \left[\dot{M}^s \left(u^s - u^{n+1} \right) \right]_{P,\kappa}
\end{cases}
\tag{4.16}
$$

In slugs, Equation 4.16 is solved for the liquid phase only ($k = l$), meaning that the interfacial friction term (3rd term on RHS) vanishes. If gas entrainment is included in the scheme (SLUGGIT v.1,) then gas propagation is determined by a slip relation. [7, 24, 10].

The complete system of Equations (4.5), (4.6) and (4.16) is first order accurate in both time and space.

4.4 Implicitness and time regulation

A purely explicit scheme may appear attractive is terms of simplicity of implementation. However, for stability reasons explicit procedures are impractical for the purpose of simulating slow transients. Traditionally, most nuclear reactor safety codes would be implemented explicitly as these were designed to simulate small time inervals [5].

However,the Courant Friedrich Levy (CFL) criterion for explicit time iteration imposes a time step restriction of $\delta t \leq \min_{j,\kappa} \ell_j / \left| u_{j,\kappa} \pm c_{j,\kappa} \right|$ where $c_{j,\kappa}$ is the speed of sound for fluid κ at position z_j.[11] This reflects the non-relative propagation of information in the system of hyperbolic Euler equations. For implicit procedures however, only the dynamic mass-transport criterion applies:

$$
\delta t \leq \min_{j,\kappa} \frac{\ell_j}{\left| u_{j,\kappa} \right|}
$$

which basically is the assurance that the advection will not be able to pass entirely through, or bypass, a cell within a single time step. In practice, the Courant number chosen to determine the time step is less than unity

$$
C_{\max} = \max_{j,\kappa} \frac{\left| u_{j,\kappa} \right| \delta t}{\ell_j} < 1
$$

For accuracy reasons, choosing $C_{\min}$ in the range of 0.1 to 0.01 is appropriate for large cases using SLUG-GIT. For the TRIOMPF slug capturing code Bonizzi *et al.* operated with $C_{\max} = 0.5$ [7], which for that code is acceptable as accuracy is ensured through iteration at each time step.

4.5 Computational expense

Let $\Delta \mathcal{T}$ be the (real) time the SLUGGIT programme needs perform a simulation of the time interval Δt of a pipeline of length L. The length of a computational time step δt will, due to the CFL criterion, be linearly dependant on the smallest bubble section length:

$$
\delta t \propto \min_j \ell_j, \qquad j \in [1, N]
$$

Because the system is one dimensional, forming tri- and heptadiagonal band systems, the physical computation time $\delta \mathcal{T}$ needed to compute a single simulation time step δt will be proportional to the number

---

[10]As a sidenote, applying the same procedure to the differential formulation of mass and momentum equations produce a convection term on the form $\rho (u - v) \partial_z u$ for each phase. The upwind discretisation of $u^{n+1}_{\sigma,\kappa}$ in (4.16) will then, in a finite difference formulation, be equivalent to moving the differential $\partial_z u$ upwind.

[11]The speed of sound originate from the eigenvalues of the Euler equations and the CFL criterion can either be understood by decoupling this equation system through transforming it to eigenvalue variables and performing a von Neumann stability analysis, or simply by realizing that for the information required at time $n + 1$ to be available from neighbouring cells at time n, the time step must be small enough so that cells beyond neighbouring cells cannot be reached along the system characteristics in a single iteration [45, 30].

fluid sections:

$$\delta\mathcal{T} \sim N \cdot \delta\tau \approx \frac{L}{\overline{\ell}} \cdot \delta\tau$$

where $\delta\tau$ is the physical computation time needed per section per simulation time step and $\overline{\delta z}$ the average section length. The total physical computation time becomes

$$\Delta\mathcal{T} = \frac{\delta\mathcal{T}}{\delta t}\Delta t \approx \frac{\delta\tau \,^{L/\overline{\ell}}}{\min_j \ell_j}\Delta t$$

By assuming that the average and minimum section lengths are proportional it is found that

$$\Delta\mathcal{T} \propto \ell^{-2} \tag{4.17}$$

4.6 Non-locally defined properties

Some properties included in the control volume equations are not defined at all locations where they art needed. As a consequence,approximations these quantities at other locations are needed.

All slug tracking schemes discussed here uses the upwind scheme to evaluate the advection terms and central averaging for the flux terms. The benefit with using an upwind approach is that it is both simple and numerically robust. The most prominent drawbacks are that it is only first order accurate and subject to severe numerical diffusion. The same goes for the first order Euler discretisation in time. Numerical diffusion would be especially damaging to the solution had the model been purely Eulerian, which is standard in most unit-cell and capturing codes. Often Eulerian schemes compansate by enforcing a higher order spatial discretisation or solving with a high resolution in space. However, the Lagrangian slug tracking approach avoids diffusion at slug and wave fronts by where it would be most damaging. This is the main idea of slug tracking.

A border property χ evaluated by an upwind scheme (indicated by a 'hat') is taken from upstream the flux:

$$\widehat{\chi_w} = \begin{cases} \chi_W; & Q_w \geq 0 \\ \chi_P; & Q_w < 0 \end{cases} \qquad \widehat{\chi_e} = \begin{cases} \chi_P; & Q_e \geq 0 \\ \chi_E; & Q_e < 0 \end{cases}$$

while centrally defined properties $\overline{\chi}$ are simply evaluated as

$$\overline{\chi}_\sigma = \frac{1}{2}(\chi_\Sigma + \chi_P)$$

4.7 Staggerd and non-staggered grids

Where properties are defined depends on how the scheme grid is constructed, or rather, where the control volume is placed. To avoid the notorious checker board solution, staggered grids must be applied in schemes where pressure-velocity variable pairs are to solved in each node. In SLUGGIT v.1 and v.2s this issue is avoided solving for a single bubble unit pressure rather than respective pressures for each section velocity. Accordingly, non-staggered grids are chosen. Here, all properties are defined in each section. SLUGGIT v.2 and LASSI are based on a two-fluid formulation and must apply staggered grids in which the control volumes are shifted for the velocity and pressure equations, respectively. This places implicitly computed velocities at borders in SLUGGIT v.2 while pressures are places at borders in LASSI. Figure 4.7 illustrates the difference for the momentum balance control volume. In evaluating the mass and pressure equations both versions apply the grid over the section object, similar to Figure 4.7a

Shifting the pressure rather than the velocity in a staggered scheme, as is done in LASSI, may introduce some benefits. Such schemes will have a fully defined flux term in the section. In dips, having the pressure defined at the borders may also be beneficial as pressure gradients here will be of importance for the seepage and fluid accumulation which affects terrain slugging characteristics. Also, as will be discussed later, Renault [37] found that the velocity staggered grid in conjunction with the upwind scheme tend to shift the pressure drop caused by Bernoulli suction downstream the hold-up protrusion.

Table 1 lists the variables not locally defined when using the different grid structures in a stratified area.

Figure 4.6 illustrate the schematic differences in momentum control volume systems between the simplified and non-simplified versions of SLUGGIT v.2. Key features in the simplified scheme are single unit bubble pressures and neglect of momentum convection between bubbles and slugs. This allows the momentum equation to be formulated as a system of slug control volumes only. Pressures and border velocities are formulated into the the momentum sys-

tem, making bubble units similar to control volume face values. An attempt at surmising the all evaluation situations in SLUGGIT v.2 and v.2s has been attempted in Table 2. This information has been (painstakingly) collected form the source code [21] for the purpose of familiarisation.

	Mass Eq	Pressure Eq	Momentum Eq
non-staggered	m_σ^{n+1}, u_σ^{n+1}	m_σ^n, u_σ^{n+1}	m_σ^n, u_σ^n, u_σ^{n+1}, α_σ^n, h_σ^n
Velocity-staggered (SLUGGIT v.2)	m_σ^{n+1}	m_σ^n	m_P^n, u_σ^n, u_σ^{n+1}, v_σ^{n+1}
Pressure-staggered (LASSI)	m_σ^{n+1}, u_σ^{n+1}	v_σ^{n+1}, m_P^n(in ψ^n)	m_σ^n, u_σ^n, u_σ^{n+1}, α_σ^n, h_σ^n

Table 1: Variables not locally defined

SLUGGIT version:	v.2			v.2s(VI)
Variables	Slug(I)	immersed bubble section	bubble unit border	
$(mQ)_{\sigma,l}^{n+1}$	$\rho_l\widehat{Q_{\sigma,l}^{n+1}}^{(III)}$	$\left(\widehat{\dfrac{M_{\sigma,\kappa}^{n+1}}{\ell_\sigma^{n+1}}}\right)(u_l-v)_\sigma^{n+1}$	$\left(\dfrac{M_l^n}{\ell^{n+1}}(u_l-v)^{n+1}\right)_\Sigma^{(IV)}$	Same as v.2
$(mQ)_{\sigma,g}^{n+1}$	Not solved	$\left(\widehat{\dfrac{M_{\sigma,g}^{n+1}}{\ell_\sigma^{n+1}}}\right)(u_g-v)_\sigma^{n+1}$	$0^{(I)}$	Not solved(V)

(a) Mass equation

SLUGGIT version:	v.2		v.2s(VI)
Variables	immersed bubble section	bubble unit border	
$\left(m^n Q^{n+1}\right)_{\sigma,l}$	$\left(\widehat{\dfrac{M_{\sigma,\kappa}^n}{\ell_\sigma^n}}\right)(u_l-v)_\sigma^{n+1}$	$\left(\dfrac{M_l^n}{\ell^n}(u_l-v)^{n+1}\right)_\Sigma$	$\left(\widehat{\dfrac{M_{\sigma,\kappa}^n}{\ell_\sigma^n}}\right)(u_l-v)_\sigma^{n+1}$
$\left(m^n Q^{n+1}\right)_{\sigma,g}$	$\left(\widehat{\dfrac{M_{\sigma,\kappa}^n}{\ell_\sigma^n}}\right)(u_g-v)_\sigma^{n+1}$	$0^{(I)}$	$0^{(I)}$

(b) Pressure equation

SLUGGIT version:	v.2		v.2s(VI)	
Variables	Bubble	Slug(I)	Bubble(III)	Slug(I)
$(mQ)_{\sigma,\kappa}^n$	$(\alpha_\kappa A)_\sigma^n \left(\dfrac{M_\kappa}{V}\right)_\sigma^n \left(\overline{u_\kappa}^{(II)}-\overline{v}\right)_\sigma^n$	$A_w\rho_l\left(u_{P,l}^n-v_\sigma^n\right)$	$Q_l=0$, gas not solved(VII)	0
$u_{\sigma,\kappa}^{n+1}$	$u_{\sigma,\kappa}^{n+1}$	$u_{\sigma,l}^{n+1}$	0	0
$\left(\alpha_\sigma^n A p_\sigma^{n+1}\right)_\kappa$	defined	$\frac{1}{2}(A_w^n+A_e^n)p_\sigma^{n+1}$	0	$\left(\dfrac{V}{\ell}\right)_P^n p_\sigma^{n+1}$
$M_{P,\kappa}^n$	$\overline{M_{P,\kappa}^n}$	defined	defined	defined

(c) Momentum equation

Table 2: Undefined variables

(I)   Special case of no void in slugs; no gas flux through unit border as $u_{\sigma,g}=v_\sigma$.
(II)   for the liquid phase, $u_{\sigma,\kappa}^n$ is computed from an explicit section momentum balance.
(III) Explicit computation
(IV)   Due to explicit slug treatment this term takes the old mass
(V)   Gas mass equation not solved; section gas mass computed by $M_{g,section}=M_{g,unit}\frac{V_{g,section}}{V_{g,unit}}$
(VI)   Uniform bubble pressure assumed
(VII) Bubble gas velocities are determined from mas balance assuming constant uniform density (pressure) and the the gas velocity to equal the border velocity at the slug front.

When evaluating the momentum equation of the simplified scheme v.2s in bubble units, a non-staggered

(a) Simplified scheme: SLUGGIT v.2s

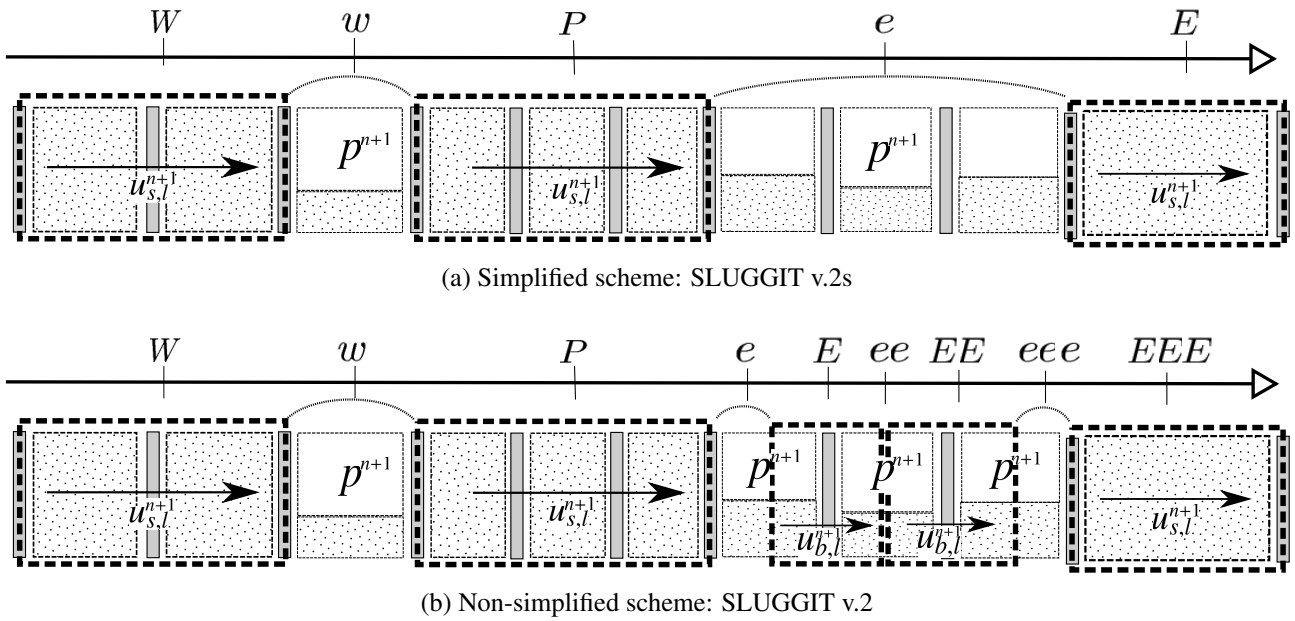(b) Non-simplified scheme: SLUGGIT v.2

Figure 4.6: Momentum equation control volumes included in implicit system momentum computation. Note that $p^{n+1} = p(u^{n+1})$ is included as the pressures in the momentum equation (4.16) are eliminated using the pressure equation (4.6)
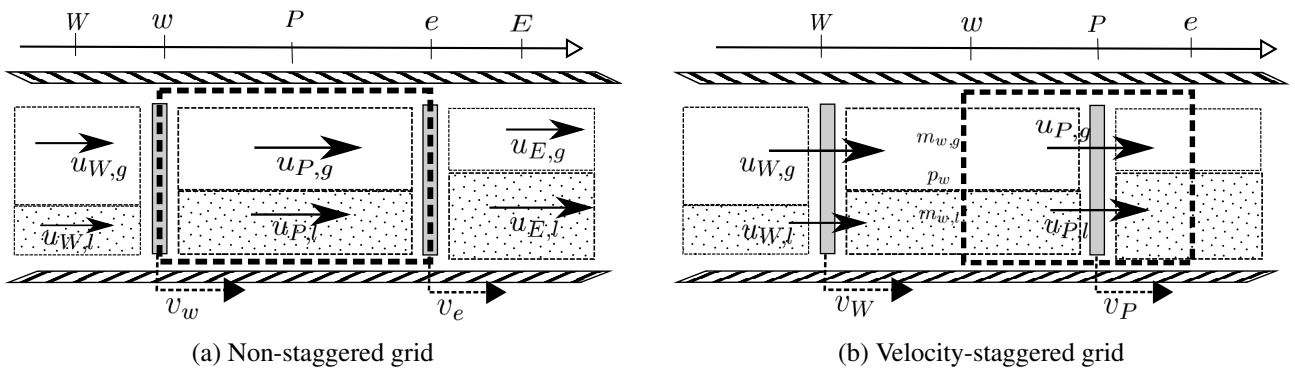

(a) Non-staggered grid

(b) Velocity-staggered grid

Figure 4.7: Momentum equation control volume

grid (Figure 4.7a) is used for the liquid phase while staggered grids (Figure 4.7b) are used for the gas phase [21]. In this way, $u_g = v$ is maintained at the bubble-slug/slug-bubble borders. Undefined border and section velocities are then later approximated by the means $\bar{u}$.

4.8 Slug border velocities

The mechanics governing the propagation of bubbles through slugs, or slugs through stratified sections, are essentially three dimensional and influenced by mixing effects, wake effects, bubble shape and surface tension. Obviously, a coarse grid, one dimensional method cannot obtain the relevant detailed information needed to capture bubble propagation warranting the need for empirically modelled closure relations for the slug and bubble unit border velocities.

Firstly, a distinctive classification is needed in order to characterise the behavioural properties of the border. Two basic types of borders are defined – bubble noses (alternatively 'slug tails') and bubble tails (alternatively 'slug fronts'). The basic characteristics behind this distinction is the physical bubble shape; a bubble front will be the 'spearhead' of bubble penetration through slugs, entrapping liquid from the slug tail. The relations imposed to model bubble propagation applied in all versions of the slug tracking schemes follows the assumption of Nicklin *et al.* that the bubble front velocity can be expressed as a linear relation from the slug mixture velocity

$$v_{b,n} = C_0 u_{s,m} + U_0 \qquad (4.18)$$

where subscripts b and s denote 'bubble' and 'slug', respectively. n denotes 'nose' while m the 'mixture' velocity, *i.e.* $u_m = \sum_\kappa \alpha_\kappa u_\kappa$. The work of Bendiksen [4] for long Taylor bubbles in inclined tubes is applied to close the model [34, 22, 20, 24, 37] [12]

$$
\begin{aligned}
&\left.\begin{array}{l}
C_0 = 1.05 + 0.15 \sin^2 \phi \\
U_0 = U_{0,v} \sin \phi + \xi_\pm U_{0,h} \cos \phi
\end{array}\right| \; Fr_{s,m} \leq \frac{3.6}{\cos \phi} \\
&\\
&\left.\begin{array}{l}
C_0 = 1.2 \\
U_0 = U_{0,v} \sin \phi
\end{array}\right| \; Fr_{s,m} > \frac{3.6}{\cos \phi}
\end{aligned}
\qquad (4.19)
$$

where $U_{0,v}$ and $U_{0,h}$ are the bubble drift velocities in stagnant liquid (neglecting surface tension) for verti-

cal and horizontal pipes, respectively [5, 4]:

$$U_{0,v} = 0.35 \sqrt{gD} \qquad U_{0,h} = 0.54 \sqrt{gD}$$

The relation's dependency on the slug Froude number $Fr_{s,m} = u_{s,m}/\sqrt{gD}$ is an effect of bubble position in the pipe cross-section. Increasing the Froude number tend to move the bubble nose centre towards the pipe cross-section centre. For Reynolds numbers in the range $Re \in \left[4 \cdot 10^4, 10^5\right]$, the centre field velocity is about 1.21 times the cross-sectional average. This supplies a limiting bubble-bulk liquid velocity ratio C_0 of about 1.2 in turbulent flows – the bubble moves faster than the surrounding liquid. In horizontal pipes, complete bubble centring takes place for $Fr > 3.5$. [4] When the slug velocity is opposite that of the bubble (sign $U_0 \neq$ sing $u_{s,m}$) the relative flow across the bubble is from nose to tail, giving a different bulk drag on the bubble. Bendiksen's experiments indicate that a C_0 value close to unity ($C_0 = 0.98$) is then appropriate [4], which is also included in the implementation.

$\xi_\pm$ in (4.19) is a variable added to indicate the sign logic influencing the horizontal drift. This logic is a bit cumbersome and depends on whether the pipe inclination is positive, negative or zero, and whether the nose is pointing to the left or the right. These features also influence – and should be seen in light of – whether a unit border is defined as a bubble nose or tail (Section 4.9). As an illustration, the logic applied for SLUGGIT v.2 and v.2s (taken form source code [21]) is

$$
\xi_\pm = \begin{cases} \text{sign } \phi & \phi \neq 0 \\ n_b & \phi = 0 \end{cases} \qquad (4.20a)
$$

$$
n_b = \begin{cases} +1 & \text{bubble-slug border} \\ -1 & \text{slug-bubble border} \end{cases} \qquad (4.20b)
$$

A similar expression may be used for the slip velocity for gas entrained in slugs. Such slip relation

---

[12] The presented drift model (4.19) is not identical in all publications [4, 34, 22, 37, 20, 24] and some alterations have been made in recent time to the source codes. For instance, smoothing functions have been implemented in SLUGGIT v.2 similar to those presented in [15], expanded to handle flow in both directions. [37] contains an error in the presentation of (4.19).

often have the form $u_{g,s} = S_d(u_{l,s} - U_0)$, S_d being the distributed slip ratio [24, 10]. A similar slip relation approach is used in the case of three-phase flow.

As slugs shed liquid at the slug tails (to the trailing bubble), they may retrieve liquid at the slug fronts (from the tail of the downstream bubble.) This happens when the slug mixture velocity is larger than the liquid film velocity around the bubble ahead of it, which will be the case for steady state bubble propagation due to continuity. Obtaining a relation for the slug front velocity from a mass balance in this case is straight forward and schematically demonstrated in Figure 4.8.
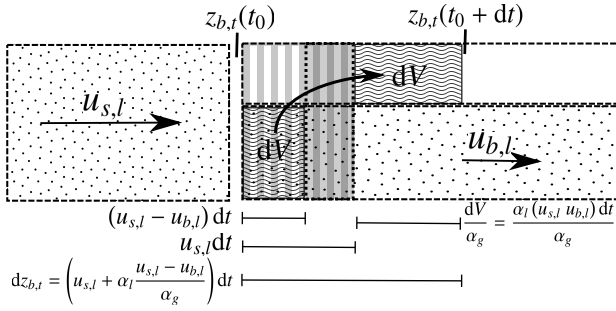
Figure 4.8: Principle used when computing slug front velocities

This reveal that

$$v_{b,t} = \frac{dz_{b,t}}{dt} = \frac{u_{s,l} - (\alpha u)_{b,l}}{\alpha_{b,g}} \qquad (4.21a)$$

or, more generally, if the slug entrains gas, the relation becomes a balance of mixture velocities:

$$v_{b,t} = \frac{(\alpha u)_{s,l} - (\alpha u)_{b,l}}{\alpha_{b,g} - \alpha_{s,g}} \qquad (4.21b)$$

subscript t denoting 'tail'. If the liquid film velocity is greater than the slug liquid velocity, the shock expression (4.21) would be entropy violating, and so (4.21) is disregarded in such cases [22, 37].

In the case of rolling wave objects, which is implemented in SLUGGIT v.2/v.2s, expression (4.21b) will also be used for wave fronts [10]. In this case,

$\alpha_{s,g}$ will be substituted with the void fraction in the wave section. Also analogous to slugs, a wave tail relation will be used similar to that of the bubble nose expression (4.19), except that the wave liquid hold-up, rather than wave section length, will be altered as a consequence of unequal liquid fluxes at tail and front. Rolling waves will not be considered in this work and accordingly disabled in all simulations.

In SLUGGIT v.2 and v.2s, the border velocities v are expressed as multiples of the gas and liquid velocities

$$v^{n+1} = C_g u_g^{n+1} + C_l u_l^{n+1} + U \qquad (4.22)$$

allowing for the border fluxes to be expressed with full implicitness in the mass and pressure equations (4.5), (4.6). The momentum equation applies the old border velocity; doing otherwise would make it non-linear.

4.9 Turning point criteria

Relation (4.19) only holds for bubble nose borders while (4.21) is only appropriate for slug fronts moving faster than the liquid film ahead. Therefore, some turning point criterion is needed in order to determine whether the border in question is a bubble nose or bubble tail. Empirical studies indicate that the sign of the pressure gradient constitutes an appropriate criterion – *i.e.* bubble fronts points the opposite direction of the pressure gradient [4, 22].

Slightly different turning point criteria are used in the different method versions. All rely on a turning a friction-gravity balance based on the general assumption is that the bubble always moves opposite of the pressure gradient [34].

$$\tfrac{1}{2}\lambda_l \rho_l U_{crit} |U_{crit}| S = \rho_l g A \sin\phi \qquad (4.23)$$

which constitutes a criterion based on the (liquid film) Froude number, as in the bubble noes model (4.19). Bendiksen [4] applied this criterion in a mostly analytical investigation and found this to be in good agreement whit experimental data.

SLUGGIT v.1 uses Nydal and Banerjee's original procedure [34] where, if the pipe is inclined upwards along the general flow direction, all bubble-slug borders are assumed to be bubble noses and all slug-bubble borders are assumed to be slug fronts. The Froude number condition (4.23) is solved iteratively.

isNose:	$\phi > 0$	$\phi < 0$
bubble-slug	true	$u_{s,m} > U_{crit}$
slug-bubble	false	$u_{s,m} < U_{crit}$

If `isNose == true` then $v = v_{b,n}$ and Bendiksen's empirical bubble nose velocity (4.19) is used. Otherwise the border is assumed to be a slug front and (4.21) is applied.

SLUGGIT v.2n and v.2s uses the Blasius friction coefficient in turbulent pipe flow to find a simplified explicit critical velocity such that no iteration is needed (see source code [21]). Applying Blasinus' friction coefficient to (4.23) yields

$$|U_{crit}| = \max \left\{ |U_0|, \left[2gD\frac{|\sin \phi|}{0.316} \left(\frac{\rho_l D}{\mu_l} \right)^{1/4} \right]^{1/1.75} \right\}$$ (4.24)

The following logic is applied for determining the boolean `isNose` [21]:

isNose:	$\phi > 0$	$\phi < 0$	$\phi = 0$
bubble-slug	$u_{s,m} > -|U_{crit}|$	$u_{s,m} > |U_{crit}|$	$u_{s,m} > -|U_{crit}|$
slug-bubble	$u_{s,m} < -|U_{crit}|$	$u_{s,m} < |U_{crit}|$	$u_{s,m} < |U_{crit}|$

or, using the logical variables (4.20)

$$\text{isNose} = n_b u_{s,m} > -n_b \xi_\pm |U_{crit}|$$ (4.25)

LASSI uses the same critical velocity (4.23), only LASSI allows for bubbles to travel towards the inlet in inclined pipes. Rather than basing the formulation on whether the Bendiksen correlation (4.19) is appropriate or not, LASSI bases the formulation on when the *slug front* formulation (4.21) is *not* appropriate, *i.e.* when the slug liquid velocity is not great enough to capture liquid from the neighbouring bubble's liquid film: $u_{s,l} < u_{b,l}$

isNose:	$u_{s,l} < u_{b,l}$	$u_{s,l} > u_{b,l}$
bubble-slug	$u_{s,m} > U_{crit}$	true
slug-bubble	true	$u_{s,m} < U_{crit}$

As with SLUGGIT v.1, an iterative approach is used for obtaining U_{crit}.

4.10 SLUGGIT v.2/v2s computational sequence

The sequence undergone at each simulation time step is the following:

1. Border velocity coefficients (4.22) are computed from bubble nose (4.18) and slug front (4.21) relations.

2. The coefficients in the combined pressure (4.6) and momentum (4.16) equation system are found from previous time step values and stored in an external matrix. Each object is connected to a row of this matrix and individually takes care of updating this row without management interference (for details, see [22] and source codes [21, 23, 36]). In the SLUGGIT v.2 scheme, this forms a linear, heptadiagonal band systems of three upper and three lower co-diagonals, along with the main diagonal. Tridiagonal band systems are formed in the case of the other two SLUGGIT versions.

3. The pressure-momentum system is solved using Gauss-elimination. u, v, z and p are updated to $n + 1$.

4. The coefficients in the mass equation for bubble sections are found from available quantities and stored in external matrices, one for each bubble unit. In the simplified scheme, this is done for the liquid phase only. If not simplified, this forms two, tri-diagonal systems (one for gas and one for liquid) for each bubble unit consisting of more than two bubble sections.

5. The mass systems are solved through Gauss-elimination without pivoting (Thomas or TDMA algorithm.) Bubble masses are updated.

6. Liquid mass equations for slugs are solved explicitly and slug lengths are updated.

7. Gas densities ρ_g are updated form the EOS and a test is preformed to see whether the volume fraction error ψ from the pressure equation (4.6) is too big. If it is, values are reset and the time step computation is re-preformed using a smaller time step.

8. Management operations are preformed. This is the only part of the routine which takes place above object level. Here, too long section objects are split in two, too small sections are merged with neighbouring objects, and the nature of objects may be converted according to initiation criteria.

9. $n := n + 1$: the cycle is repeated.

The computational sequence of the LASSI scheme is similar, but slightly different in due to less time in development and a different set of equations (Section 4.11). Mainly, the difference lies in the shallow water wave equation solving procedure forming a central component is this scheme. For details, see [37, 36].

4.11   The LASSI scheme

Although also the LASSI scheme is based on the same fundamental two-fluid equations as SLUGGIT v.2, it developers them into a rather different system of equations. LASSI can be seen as an intermediary between a fully resolved two-fluid model as that of Issa and Kempf [13], and the SLUGGIT schemes originating from [34]. Including the full model derivation also for this scheme would make the this text too extensive in terms of methodology. Rather, an abbreviated presentation is given and the interested reader may refer to the thesis source [37] for further details.

4.11.1   Abbreviated method presentation

LASSI is based on a differential formulation of the two-fluid model:

$$\frac{\partial}{\partial t}(\rho\alpha)_\kappa + \frac{\partial}{\partial x}(\rho\alpha u)_\kappa = 0 \qquad (4.26a)$$

$$\frac{\partial}{\partial t}(\rho\alpha u)_\kappa + \frac{\partial}{\partial x}\left(\rho\alpha u^2\right)_\kappa = \begin{cases} -\dfrac{(\tau S)_{pipe,\kappa}}{A} \mp_\kappa \dfrac{(\tau S)_{int}}{A} \\[2mm] -\alpha_\kappa \dfrac{\partial p}{\partial x} \\[2mm] -\rho_\kappa g\alpha_\kappa \left[\sin\phi + \cos\phi\dfrac{\partial h_\kappa}{\partial x}\right] \end{cases} \qquad (4.26b)$$

which constitutes four equations. The friction τ is defined so that $\mp_\kappa$ is (+) for the liquid phase and (−) for the gas phase. S symbolise the wetter perimeter

and $h_\kappa(\alpha_\kappa)$ the phase height (seeFigure 4.2). Further details on these variables are given later in Section 4.3

The LASSI scheme employs a few simplifying assumptions in order to decouple the gas and liquid phases in (4.26). These assumptions are

Assumptions C. *LASSI*

C.1 Assumptions A and B holds. Wave phenomena are not neglected.

C.2 In regard to the momentum equation (4.26b) for liquid, the gas phase may be considered incompressible

C.3 Derivatives of the mixture velocity can be neclecten in (4.26b) for the liquid.

C.4 Gas momentum is neglectable compared to liquid momentum (*i.e.*, $\rho_l u_l \gg \rho_g u_g$)

By eliminating the pressure in the liquid momentum equation (4.26b) through substitution with its gas equation counterpart, and then applying the assumptions, a decoupled, modified shallow water equation is produced for the liquid phase:

$$\frac{\partial}{\partial t}\alpha_l + \frac{\partial}{\partial x}(\alpha u)_l = 0 \qquad (4.27a)$$

$$\frac{\partial}{\partial t}(\alpha u)_l + \frac{\partial}{\partial x}\left[\left(\alpha u^2\right)_l + \tfrac{1}{2}\kappa\alpha_l^2\right] = \frac{\alpha_l}{\rho_l}F_V \qquad (4.27b)$$

41

where the modification appears in the form of a second spatial derivative involving κ:

$$\kappa = \frac{\rho_l - \rho_g}{\rho_l} g \left(\frac{\mathrm{d}\alpha_l}{\mathrm{d}h_l}\right)^{-1} \cos\phi - \frac{1}{\alpha_g}\frac{\rho_g}{\rho_l}(u_g - u_l)^2 \quad (4.28)$$

which is the balance between the Bernoulli suction $\frac{1}{\alpha_g}\frac{\rho_g}{\rho_l}(u_g - u_l)^2$ and hydrostatic head $\frac{\rho_l - \rho_g}{\rho_l} g \left(\frac{\mathrm{d}\alpha_l}{\mathrm{d}h_l}\right)^{-1}\cos\phi$. F_V is the volumetric forces acting on the liquid phase:

$$F_V = \sum_\kappa \mp_\kappa \left(\frac{(\tau S)_{int}}{\alpha_\kappa A} - \frac{(\tau S)_{\kappa,pipe}}{\alpha_\kappa A} - \rho_\kappa g \sin\phi\right) \quad (4.29)$$

In the LASSI scheme, (4.26) is first solved implicitly for the gas velocities and pressures along the pipe. The border velocities are then sat as described in Section 4.8. A modified Lagrangian shallow water scheme is then employed to solve (4.27) for the liquid velocities and hold-up. This shallow water scheme solves the Reimann problem at each bubble border, accurately determining wave propagation. The mobility of borders is utilized in moving bubble-bubble borders to coincide with the wave shock fronts, allowing the inherit discontinuity to be handled without much numerical diffusion (smearing) while avoiding excessively refined grids. As in the SLUGGIT schemes, an upwind spatial discretisation is applied combined with Euler discretisation in time – see [37, p. 87-89] for details on the discrete scheme.

4.11.2 Domain of well-posedness and slug capturing

A characteristic of the discrete LASSI scheme which is of some importance is that it retains nearly the same model stability domain as the original two-fluid model, converging towards the Viscous Kelvin-Helmholtz criterion (VKH). In stability analysis, the

The domain of well-posedness is determined by formulating the two fluid model as an equation system and finding its eigenvalues. For the two-fluid model, the well-posedness criterion reads [16, ch. 5]

transition to model instability takes place when there exist a disturbance wavenumber whose corresponding pulsation has a negative imaginary part (see Annex E). The continuous two-fluid model is used for such analysis. Renault went on to prove for the discrete LASSI scheme that the effect of finite border spacing ℓ on model stability is a new term proportional to that spacing, along with a 'numerical surface tension' term. In terms of model stability, the latter has no significant impact. The former increases the discrete model stability domain all over as border spacing ℓ increases. Enlarging the pipe diameter reduce this effect.

Further, a character of the continuous two-fluid model is that relative velocities leading to the system being ill-posed as a hyperbolic problem coincides with the *inviscid* Kelvin-Helmholtz (IVH) two-fluid model stability criterion [13]. [13]

This means that in the inviscid case, the transition to a non-stratified flow takes place as the eigenvalues – the slopes of the characteristics – of the two-fluid model become complex. Unique solutions continuously dependant upon the initial conditions is then no longer guaranteed. Rather, numerical solutions strongly influenced by the numerical discretisation may be found. Ill-posedness is usually manifested in a discrete model by the solutions produced therefrom failing to become independent of grid spacing as this is continuously reduced. To illustrate this, Figure 4.9 show two plots borrowed from a publication of Issa and Kampf wherein one is well-posed and and the other is ill-posed. The growth rate increases asymptotically with *decreasing* grid spacing in the ill-posed case, whereas this becomes independent of grid spacing in the well-posed case.

$$\text{well posed} \iff (u_g - u_l)^2 \le (\rho_l - \rho_g)g\left[\frac{\alpha_l}{\rho_l} + \frac{\alpha_g}{\rho_g}\right]\left(\frac{\mathrm{d}\alpha_l}{\mathrm{d}h_l}\right)^{-1}\cos\phi \qquad (4.30)$$

---

[13]Though very similar and, perhaps, both arising from the mechanism causing flow regime transition, the issue of well posedness should not be entirely confused with stability of the stratified flow regime. While the former is a mathematical property of the continuous two fluid model (4.26) the latter is physical character of the fluid dynamics, often analysed using that same model.
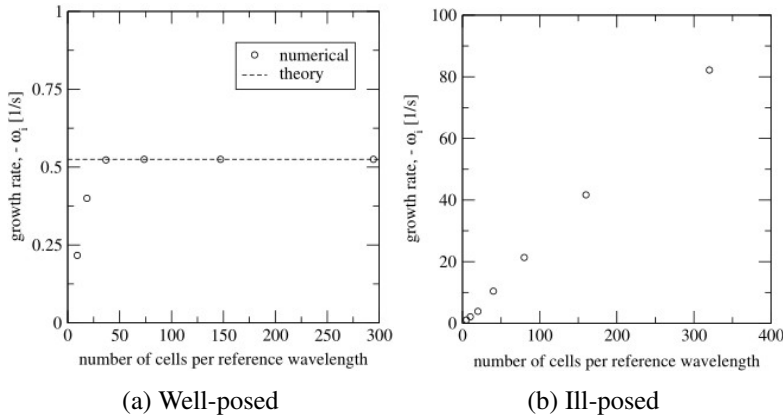
Figure 4.9: Illustrating of manifestation of ill-posedness. Source: [13]

which bear striking resemblance to the IKH criterion (E.3), mounting to a balance between the Bernoulli suction and the hydrostatic forces. Also, for $\rho_l \gg \rho_g$, well-posedness becomes equivalent to $\kappa > 0$, where κ emerged naturally in the wave formulation (4.28) of LASSI. Infinite liquid depth need not be assumed in this criterion, contra to the regime stability condition. Bonizzi *et al.* [7] also showed that their extended two-fluid model, which includes gas entrainment in slugs, share the same criterion.

A problem in using numerically dissipative procedures such as the upwind scheme (used in all models discussed here) is that numerical diffusion tent to dampen and mask the symptoms of ill-posedness. For many years this has damaged the credibility of methods utilising the two-fluid model [13]. Physically, ill-posedness in the two-fluid model can be explained by the the model's neglection of certain aspects, such as surface tension and more complex viscous effects [37].

Indeed, after Ramshow and Trapp raised the problem of ill-posedness in 1978, doubts about the applicability of the two-fluid model became wide spread. In later years, as ill-posedness of the two-fluid model was seen in light of the model (stratified flow) stability limit, confidence has been somewhat restored; though the limit of well-posedness is

marked by the IKH-criterion, viscous forces prove destabilizing to the flow [3], causing flow transition to a new flow regime in *viscous* fluids to take place at lover relative velocities, marked by the VKH-criterion [13]. A state in between these criteria should therefore lead to flow transition without becoming ill-posed. This has in recent years boosted the confidence in the two fluid model as a means by which automatic slug capturing, rather than applying initiation mechanisms, may be utilised. Practising some moderation in the choice of relative velocities will however be required.

Experiments have further confirmed that instability in the continuous two-fluid model corresponds well with physically observed instability and transition to a non-stratified flow regime. Some scepticism still remains over what happens when approaching the limits of these domains. Finally, as was demonstrated by Bonizzi [6], also *numerical* issues tend to arise as the two-fluid model approach the limit of well-posedness. Thus, the domains of physical instability, model instability, numerical instability and ill-posedness of the two-fluid model are similar and overlapping. These relationships are illustrated in Figure 4.10
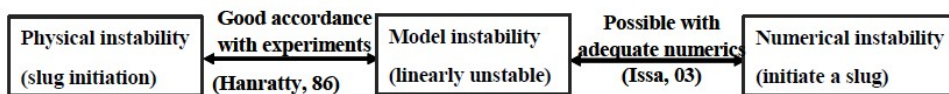
Figure 4.10: Slug initiation principle in the LASI scheme. Figure source: [37]

As LASSI scheme retains the same model stability domain of the original two-fluid model, the approach implemented in LASSI is then to assign a minimum value for $\kappa \geq \kappa_{min}$[14] to ensure well-posedness while the model instability will ensure slug initiation.

These considerations supplies the LASSI method with an advantage over methods which are to different from the two-fluid model to share its stability domain; hydrodynamic slug initiation happen automatically driven by the appropriate physical mechanisms which are retained in the method through the Reimann-solving wave procedure. This makes LASSI a slug capturing method, yet far less computationally expensive than the finely gridded, iterative Eulerian two-fluid representation model of Issa *et al.*

In this respect, none of the versions of SLUGGIT solve the Reimann problems of wave propagation. Since SLUGGIT v.2 applies a two-fluid model in stratified regions, it may be slug capturing, but only with very fine border spacing. The other methods (v.1, v.2s) are simplified to the extent that their model stability domain probably does not match the physical one, and so cannot be used as capturing methods. Instead, the hydrodynamic slugging phenomena have to be modelled through a criterion and clugs artificially initiated. Such models are often questionable in complex geometries [37] and the terms composing such criteria often come at large computational expense[15]. The same goes for the perhaps most commercially popular multiphase pipe flow code on the market: OLGA [5].

5 Benchmark tests

5.1 Liquid conservation

This section concerns the methods' ability to conserve mass. For reasons of simplicity, only liquid conservation is considered.

Introducing two ways of computing the liquid volume contained in the pipes:

$$V_{\int dz, l}(t) = A \int_{z_i}^{z_o} \alpha_l(z, t) \, dz = A \sum_{j=1}^{N} \alpha_{l,j} \delta z_j \tag{5.1a}$$

and

$$V_{io,l}(t) = V_{\int dz, l}(t_0) + A \int_{t_0}^{t} \left[\alpha_l(z_i, t^*) \, u_l(z_i, t^*) - \alpha_l(z_o, t^*) \, u_l(z_o, t^*) \right] dt^* \tag{5.1b}$$

where subscripts i and o indicate 'inlet' and 'outlet', respectively. The V-section geometry of Figure 5.1 is tested. It is composed of two $2\,m$ long pipes with opposite inclination $\phi \in \pm \{0°,\ 30°,\ 60°\}$. The pipe diameter is $1.2\,cm$.
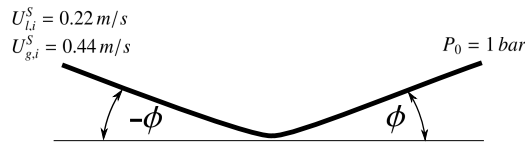
Figure 5.1: Configuration used to thest liquid consercation in Figures 5.2 and 5.3.

---

[14]After inspecting the source code [36] it is found that the value of κ_{min} currently implemented is a fraction of the hydrostatic force: $\kappa_{min} = 0.2 \frac{\rho_l - \rho_g}{\rho_l} g \cos \phi \left(\frac{d\alpha_l}{dh_l} \right)^{-1}$

[15]Experienced from the SLUGGIT v.2 code.

Figures 5.2 and 5.3 depict the pipe liquid volumes computed using (5.1b) and (5.1a). The times t_{mid} and t_{out} presented in the captions are respectively the times at which the liquid fronts first reach the mid section (the bend) and the outlet of the pipeline, which initially is free of liquid. It is clearly visible that, while SLUGGIT appears to conserve the liquid mass appropriately, LASSI produce a biased liquid error highly dependant on the pipe inclination. This is visible in the plots as rates of error accumulation change at $t = t_{mid}$, which is the time at which liquid reach the intersection change of the first and second pipe segment. For horizontal pipes and pipes where the inclination angle is small, this error is not large enough to be directly visible from the hold-up animations generated in PLOTIT [31]. Increased angles are associated with increased volumetric errors. Errors occurring with steep pipe inclinations, $|\phi| \geq 60°$, are clearly visible in the animations. Simulations performed wherein only a single inclined pipe section have produced the same error as if it had been preceded by a horizontal pipe section, indicating that the bend itself is not the main source of error.

The computed liquid flux at the outlet is slightly imprecise due to the slugging and momentary nature of the output data, which is why the time series are cut around when liquid first reaches the outlet. This occurs at $t = t_{out}$

It should be pointed out that the V-section geometry and all simulation parameters corresponds to the simulations presented in the second paper of [37]. In these simulation the inclination angles range from $\phi \in [-15°, 30°]$. As is evident from Figures 5.2b and 5.2c, the errors are small in this inclination regime. However, in the third paper of [37] a S-riser is simulated whose upstream rise is close to 55° and downstream rise near 75°.

In order to investigate the errors apparent in LASSI further, and illustrate some of the problems inconsistent masses will impose on simulations of a deep water riser case, the same mass conservation test is applied to a riser case of similar dimension to the Girassol field. Figure 5.4 presents a schematic. Figure 5.5 depict the volume calculations (5.1) vary-

ing the inlet liquid velocity and TargetLength parameter.[16] The gas velocity is the same as in the previous case, *i.e.* 0.44 m/s, and the inlet hold-up is kept at a constant $\alpha_l = 0.5$. The timestep used is $\delta t = 0.01$ s. Geometrically, the pipe configuration is a horizontal pipe section of 10 m followed by a 85° inclined riser long enough so that the liquid front never reach the outlet during a simulation period.
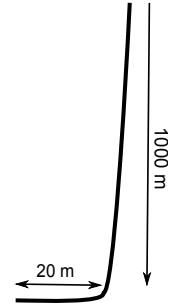
Figure 5.4: Riser geometry used to test LASSI liquid volume error in Figures 5.5.

Varying the time step appears to have some minor impact on the results, also in the horizontal pipe section, but this influence is small compared to that of the inlet velocities and the TargetLength parameter. Figures 5.5 show that increasing the liquid inlet velocity $U_{l,i}$ reduces $V_{\int dz,l}$ relative to $V_{io,l}$. Likewise, increasing TargetLength reduces $V_{\int dz,l}$ relative to $V_{io,l}$. The reasonable appearance of Figure 5.5c ($U_{l,i} = 0.50$ m/s, TargetLength = 0.1 m) should not be confused with a solution to the volume error problem; it is merely the intersection of over- and under-predictions of $V_{\int dz,l}$ – reducing either time step or TargetLength will not lead to an asymptotic reduction in error.

The consequences of this failure to conserve liquid mass in the available LASSI code [36] is fatal, as seen in Figure 5.5e. Here, the liquid in the pipe $V_{\int dz,l}$ reaches a constant value long before any liquid ever reaches the riser outlet. In other words, even as new liquid is pushed in through the inlet *ad infinitum*, no liquid will ever reach further than the first metres of the riser, all new inserted liquid mysteriously disappearing from the system.

The κ-values (Equation (4.28), $\kappa < 0 \Leftrightarrow$ well-posedness criterion (4.30) for $\rho_l \gg \rho_g$) are giver in
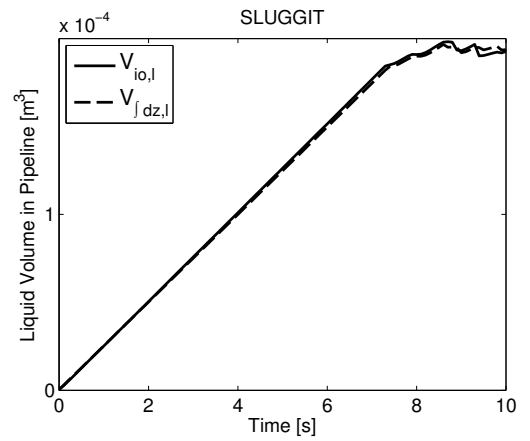
---

[16] TargetLength is not an universal section length, but is the length of sections at the inlet and half the length at which sections split in two. The timestep also influence the average section length through the CFL criterion [37, paper 1, p. 60]
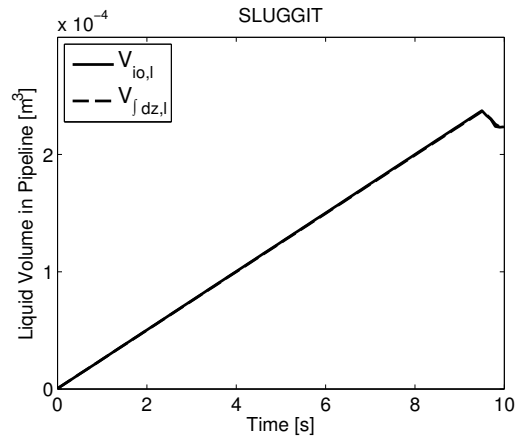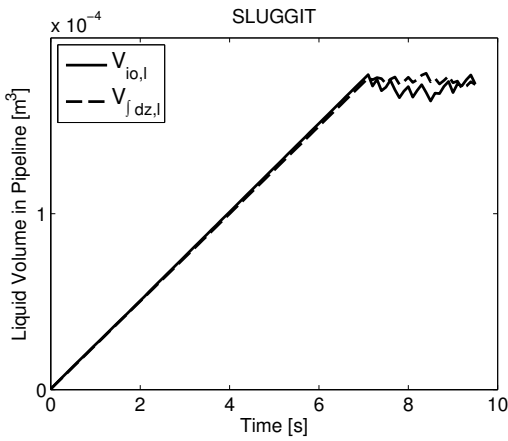
(a) $\phi = 0°$, $t_{mid} = 4.65$ s, $t_{out} = 9.55$ s
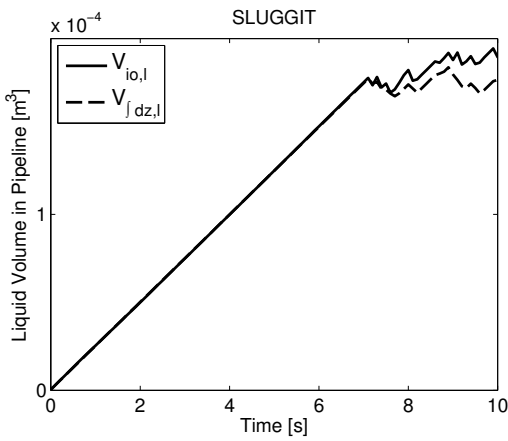
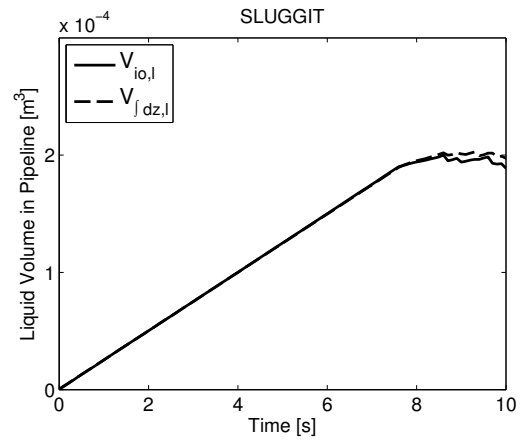(b) $\phi = \mp30°$, $t_{mid} = 1.85$ s, $t_{out} = 7.15$ s

(c) $\phi = \pm30°$, $t_{mid} = 5.40$ s, $t_{out} = 7.35$ s
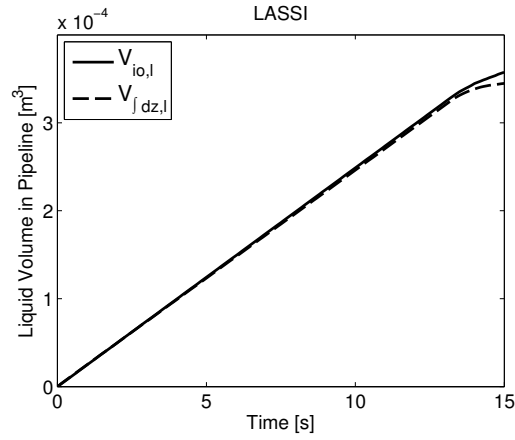
(d) $\phi = \mp60°$, $t_{mid} = 1.80$ s, $t_{out} = 7.15$ s
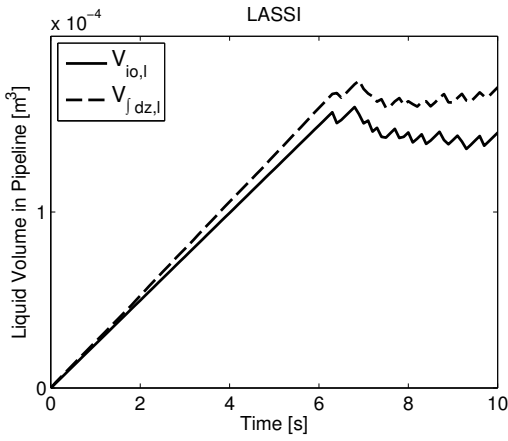
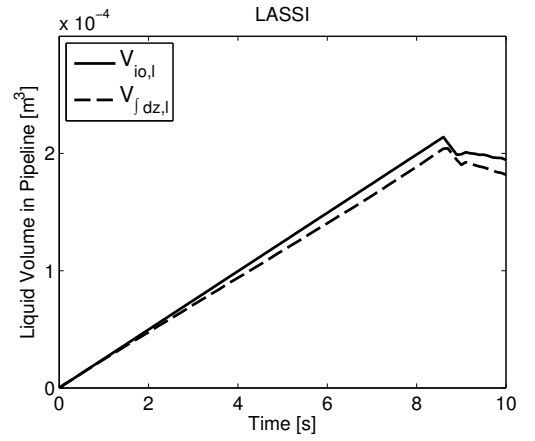(e) $\phi = \pm60°$, $t_{mid} = 5.25$ s, $t_{out} = 7.65$ s

Figure 5.2: Liquid volume conservation, SLUGGIT v2. V-section configuration, as in Figure 5.1. ($\delta t = 0.01$, $D = 0.012$, $\alpha_{l,i} = 0.275$)
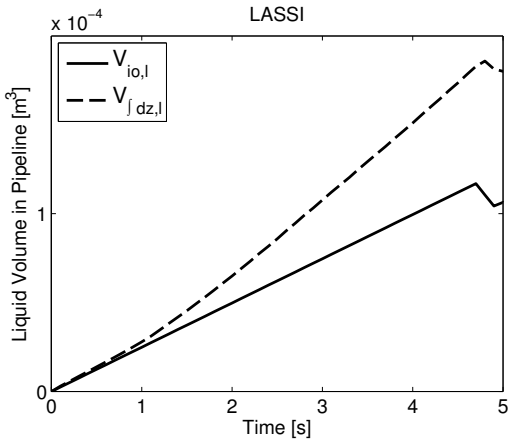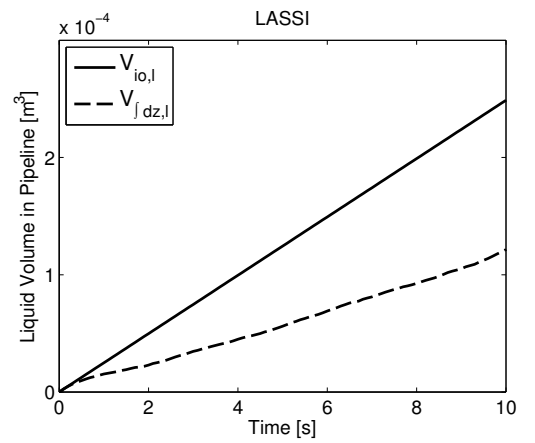
(a) $\phi = 0°$, $t_{mid} = 5.80$ s, $t_{out} = 13.30$ s

(b) $\phi = \mp30°$, $t_{mid} = 1.50$ s, $t_{out} = 6.35$ s

(c) $\phi = \pm30°$, $t_{mid} = 5.50$ s, $t_{out} = 8.70$ s

(d) $\phi = \mp60°$, $t_{mid} = 1.15$ s, $t_{out} = 4.80$ s

(e) $\phi = \pm60°$, $t_{mid} = 9.30$ s, $t_{out} = 10.50$ s

Figure 5.3: Liquid volume conservation, LASSI. V-section configuration, as in Figure 5.1. ($\delta t = 0.01$, $D = 0.012$, $\alpha_{l,i} = 0.275$)

Fiugres B.4 and B.5. It is seen that the V-section simulations, for which lack of mass conservation was documented, is well posed. Unsurprisingly, the same can not be said about the riser case due to the steep riser inclination. Since the flow is slugging here, the 'stratified' Taylor bubbles are in any event no longer than a few sections long.

It is evident that the available LASSI code [36] cannot be applied to the riser stability study undertaken within this work. In consideration of the reasonable results published in [37] for slightly inclined pipelines, and in reviewing the details of the scheme, it seems probable that the absence of liquid conservation is due to some error in the code implementation – possibly within the section management procedure.

5.2 Gas expansion in riser

The slug tracking schemes discussed in this work all have two basic flow elements – the Taylor bubble and the slug. It has been assumed that with these two elements most flow regimes can be approximated, and the appropriate basic flow system characteristics obtained. In this section, the methods ability to handle riser expansion will be tested. A short, closed inlet with mass sources will be used to make the physical regime bubbly and challenge the slug-flow approximation. Mass sources are chosen to correspond to those active in the larger field case study to come.

In Appendix A, a unit-cell type steady-state method developed for analysis of the total void fraction in the riser. A discrete procedure for finding the profile of the mean void fraction $\langle \alpha_g \rangle(z)$ is presented in Section A.1. These models have been developed during the present work.

Figure 5.6 shows the gas volume profiles from the steady state computation of Appendix A.1 against temporally averaged dynamic simulations with SLUGGIT v.2. The mean profile is here determined by computing

$$\langle \alpha_g \rangle(z) = \frac{1}{t_N - t_0} \int_{t_0}^{t_N} \alpha_g(t', z) \, \mathrm{d}t' = \frac{1}{t_N - t_0} \sum_{i=1}^{N} \alpha_g(t_i, z) \, \delta t_i$$

becoming a sample average in discrete space. Here,

N is the total number of temporal samples. The basic steady-state model code can be found in Listing 7, Appendix D, while Listing 5 presents the procedure for averaging the SLUGGIT simulation data by means of interpolating projection. Gas and liquid mass sources representative of the Girassol oil field [47, 43] are applied to a closed inlet. Four values of the parameter `MAX_BUB_COEF` were tested: `MAX_BUB_COEF` $\in \{1\,000, 200, 100, 50\}$. This parameter dictates how long a bubble section can be, in terms of pipe diameter multiples, before it is split into smaller sections. `MAX_BUB_COEF` = 100 is not included in Figure 5.6 as it overlaps `MAX_BUB_COEF` = 50 and 200 nearly perfectly.

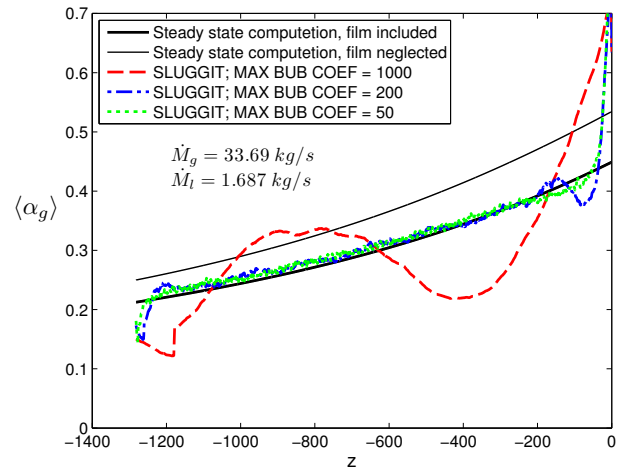
Figure 5.6: Gas volume fraction profile $\alpha_g(z)$. Dynamic simulations vs. steady state analyses. Closed inlet. $\dot{M}_g = 33.69$ kg/s, $\dot{M}_l = 1.687$ kg/s

The numerical steady-state model including the liquid bubble film from Appendix A.1 produce a near perfect match with the finely spaced section simulations, even though friction effects have been neglected in the steady-state models. These are in any case low in the simulations conducted here ($\mu \sim 10^{-3}$ Pa/s). The simplified version, SLUGGIT v.2s, give equally good results, except that the amplitude of the sinusoidal `MAX_BUB_COEF` = 1 000 curve is less, suggesting that the simplified scheme is less affected by slug entrance and exit effects. A possible explanation for this is a damping of the entrance and exit disturbance obtained since pressure equalisation in the pipeline bubble unit happens instantaneously, not dependent on internal gas flux.
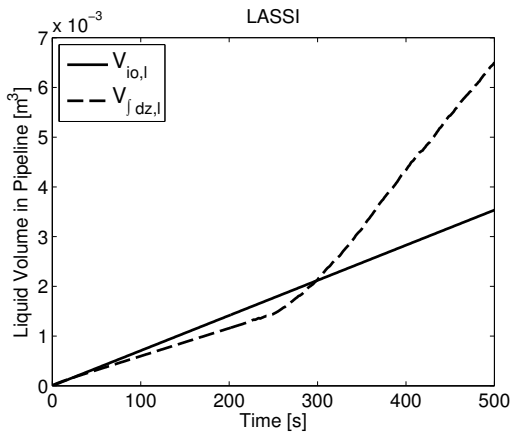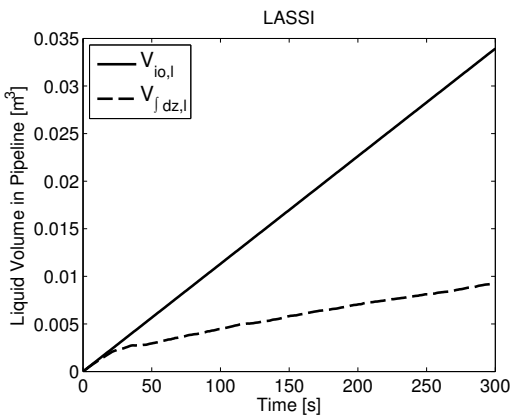
(a) $\begin{bmatrix} \text{TargetLength} & = & 0.1\,\text{m} \\ u_{l,i} & = & 0.125\,^{\text{m}}/_{\text{s}} \\ t_{mid} & = & 138\,\text{s} \end{bmatrix}$
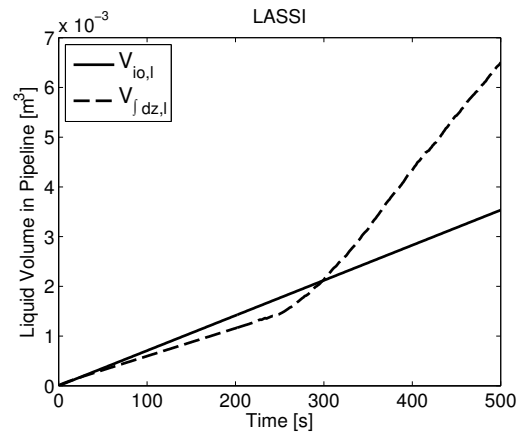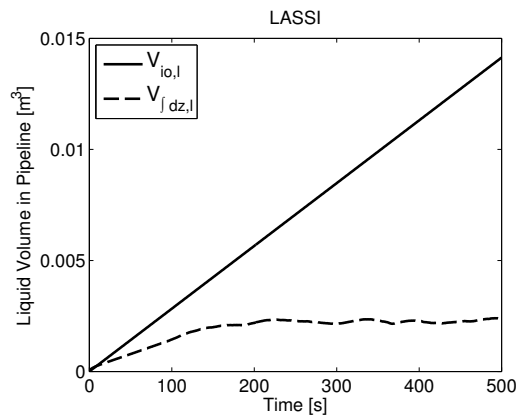
(b) $\begin{bmatrix} \text{TargetLength} & = & 0.01\,\text{m} \\ u_{l,i} & = & 0.5\,^{\text{m}}/_{\text{s}} \\ t_{mid} & = & 44\,\text{s} \end{bmatrix}$
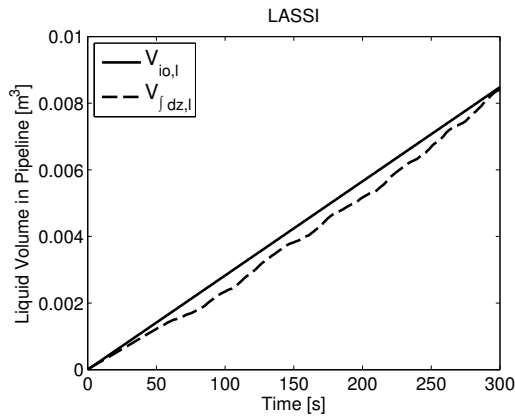
(c) $\begin{bmatrix} \text{TargetLength} & = & 0.1\,\text{m} \\ u_{l,i} & = & 0.5\,^{\text{m}}/_{\text{s}} \\ t_{mid} & = & 52\,\text{s} \end{bmatrix}$

(d) $\begin{bmatrix} \text{TargetLength} & = & 0.1\,\text{m} \\ u_{l,i} & = & 2.00\,^{\text{m}}/_{\text{s}} \\ t_{mid} & = & 17\,\text{s} \end{bmatrix}$

(e) $\begin{bmatrix} \text{TargetLength} & = & 1.0\,\text{m} \\ u_{l,i} & = & 0.5\,^{\text{m}}/_{\text{s}} \\ t_{mid} & = & 100\,\text{s} \end{bmatrix}$

Figure 5.5: Liquid volume conservation, geometry as in Figure 5.4, LASSI. ($\delta t = 0.01$, $U_{g,i} = 0.44$, $D = 0.012$, $\alpha_{l,i} = 0.5$)

49

Although the present result is quite satisfying, it should not be forgotten that both SLUGGIT and this steady-state model rely on the same bubble nose velocity expression for closure. The ancestor model on the other hand, in which the liquid film is neglected, grossly over-predicts the void fraction profile, indicating that this model was too simple.

Interestingly, section length dependant profile oscillations are uncovered. Large amplitude, low frequency oscillations dominate the large-bubble-section simulation profile (`MAX_BUB_COEF` = 1 000). A low amplitude, high frequency component is also visible here. In the small-bubble-section profile (`MAX_BUB_COEF` = 200 and 50,) it is the high frequency oscillations that dominate, while these are far less severe than in the aforementioned case. From Figure 5.6 one can see that the `MAX_BUB_COEF` = 200 simulation bears larger oscillations near the riser in- and outlet, indicating that this is a slug entrance and exit phenomenon increasing with slug length.[17]

A possible complimentary explanation for the profile oscillations' dependency on the parameter `MAX_BUB_COEF` may lie in how bubble volumes themselves have a tendency oscillate in the deep water cases, especially when the pressure conditions are altered as bubbles enter and exit the riser. This is rooted in the large hydrostatic heads pressing on the bubbles and the inertias of the liquid columns. Allowing for larger bubble lengths increases the average bubble volume in the riser (see Figures 5.7), increasing the bubble compressibility. These bigger bubbles causes longer periods of oscillation with larger total changes in volume during the bubble rise. Also, the times steps are significantly larger for simulations allowing longer bubbles as this places a less strict CFL criterion on the simulation. It is important to note that the SLUGGIT simulations were performed in a simple geometry with only four pipe segments, allowing for bubbles to take on the maximum length. Including short pipe sections ahead of the riser (such as small jumpers) would have a similar effect as reducing the parameter `MAX_BUB_COEF`.

Studying the animations generated form the simulation data provides an alternative explanation. As the maximum bubble section length decreases, the model is capable of capturing the rise in hold-up similar to a hydraulic jump at the inlet to the first horizontal pipe segment. This was seen for `MAX_BUB_COEF` = 100 and `MAX_BUB_COEF` = 50 (see Figures 5.7c), and allows for some hydrodynamic to take place, similar to the finely gridded capturing methods of, *e.g.*, Issa and Kempf [13]. This makes the average bubble length shorter. Therefore, when a bubble enters the riser, a smaller amount of gas mass is subtracted from the riser inlet pipe section. Conversely, with a large value on the `MAX_BUB_COEF` parameter, all slug initiation upstream of the riser is killed off by numerical damping. A similar influence hydrodynamic upstream slug initiation on the riser dynamic code has already been documented by Kjeldby [19] using the same SLUGGIT v.2 code.

Because the inlet is closed, a bubble being sucked into the riser inlet will cause a significant reduction of gas in the horizontal riser inlet pipe, causing a pressure reduction at the inlet. Upstream pressure reductions causes a deceleration of the bubble once in the riser, making it's occupation time in the lower section of the riser longer (first local maximum if Figure 5.6.) As the gas source once again fill the first horizontal pipe with gas, the pressure rises and the bubble accelerates through the middle part of the riser (middle local minimum in Figure 5.6,) before a new bubble enters the riser, again causing a pressure drop and a deceleration in the riser (final local maximum.) This effect is further reflected in the phase portraits of Figures 5.8a and 5.9b, and described in Cycle F.

In Figures 5.8 the $\Phi_l - p$ phase portraits (normalised scatter-plots of total riser liquid fraction vs. riser inlet pressure) are shown for the two cases `MAX_BUB_COEF` = 100 (b) and `MAX_BUB_COEF` = 1 000 (a) – two of the three simulations whose $\langle \alpha_g \rangle$-profile was shown in Figure 5.6.

For the case of `MAX_BUB_COEF` = 100, and all smaller values of this coefficient, the phase diagram appears fairly random, though askewed, indicating a

---

[17]This is more clearly seen in simulations of intermediate `MAX_BUB_COEF` values, not shown here.

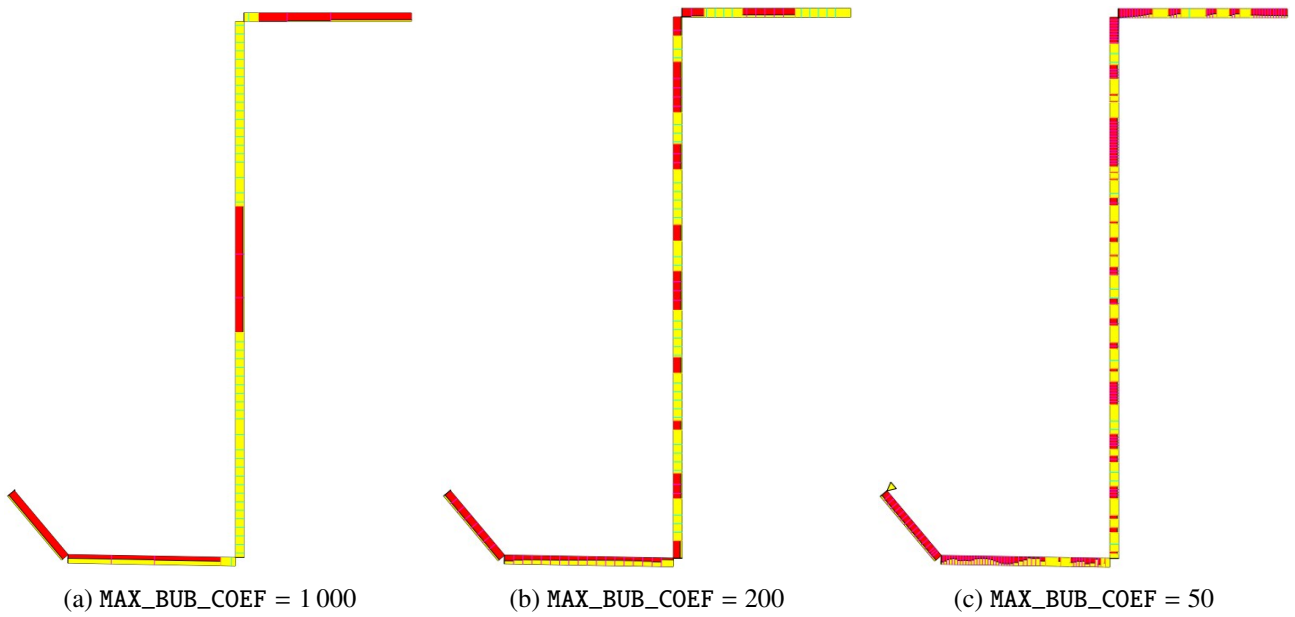(a) MAX_BUB_COEF = 1 000   (b) MAX_BUB_COEF = 200   (c) MAX_BUB_COEF = 50

Figure 5.7: Snapshot of bubbles in simple riser system. Image pipe diameter rescaled for visibility. (This is also done in all pipeline images throughout this text.)
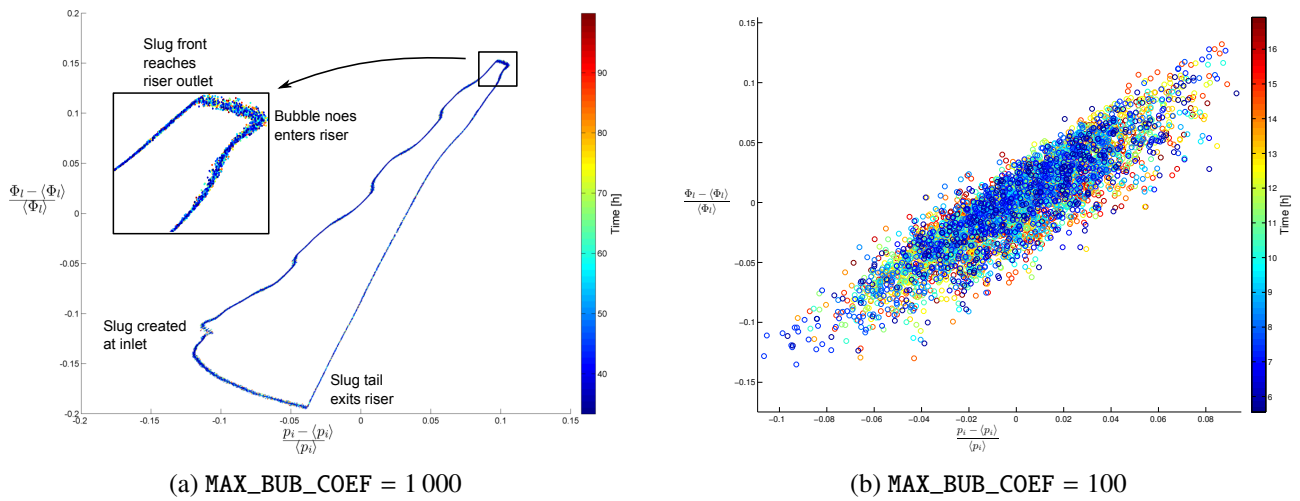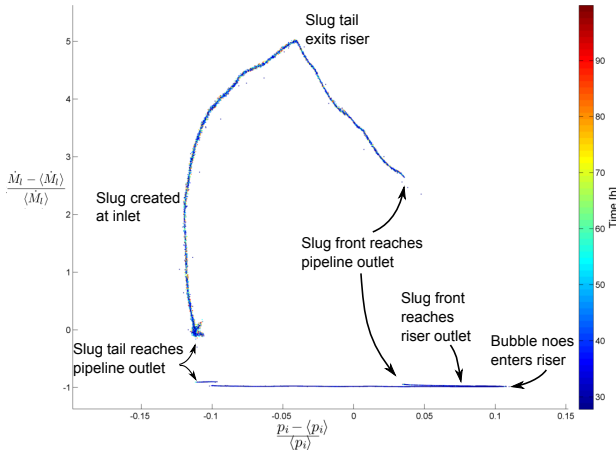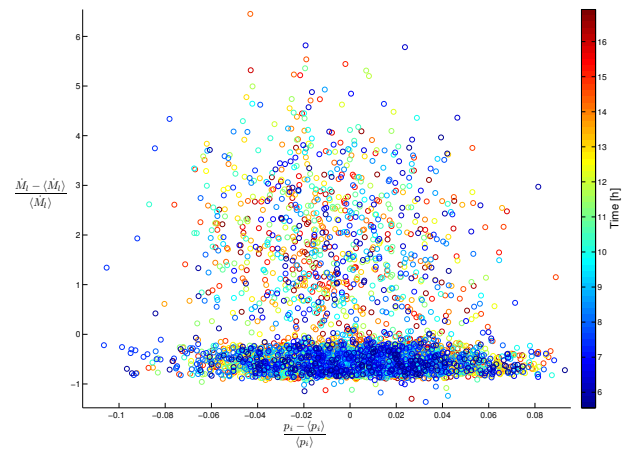

(a) MAX_BUB_COEF = 1 000   (b) MAX_BUB_COEF = 100

Figure 5.8: $\Phi_l - p$ phase portraits of simulations in Figures 5.6 and 5.7.

(a) `MAX_BUB_COEF = 1 000` – Snapshot Figure 5.7a

(b) `MAX_BUB_COEF = 100`

Figure 5.9: $\dot{M}_l - p$ phase portraits of simulations in Figures 5.6 and 5.7.

correlation between inlet pressure and riser void. Only analysing the riser system in a hydrostatic frame, one would rather expect a perfect correlation (points forming a positively inclined line,) but transient momentum effects and a near constant riser void fraction due to small bubbles causes scattering. It is likely that, if run long enough, the simulation with `MAX_BUB_COEF = 100` would also converge to a steady cycle pattern. However, time in computation this would require can simply not be afforded.

The $\Phi_l - p$ phase portrait for `MAX_BUB_COEF = 1 000` (Figure 5.8a) is significantly different. Here, the data points form a distinct bacon shape as a cy-

cle is repeated. Specific events form the four corners of phase portrait shape as the system state moves clockwise along a thin line in $\Phi_l - p$ space. The time spans $t \in [35, 100]$ hours, after the system has come to a steady-state cycle[18]. Smaller data point marker than those in Figure 5.8b have here been used to indicate how narrow the line of this pattern is. Even so, nearly only the point from the first hours are visible as these overlap those following. A single cycle takes about three minutes, making the number of cycles shown more than one-thousand. The events forming the cycles are manifested in the corners of the shape and are the following:

Cycle F. $\Phi_l - p$ *cycle; Figure 5.8a*

F.1 Lower left corner: A slug is formed in the horizontal upstream the riser and this slug front enters the riser inlet. The liquid fraction in the riser increases and the inlet pressure increases as the inlet is blocked and upstream volume is reduced. This corner is not 'sharp' because the cross section area of the gas phase $\alpha_g A$ at the riser inlet narrows before slug initiation ($\alpha_g > 0.95$ at inlet).

F.2 Upper left corner: The front of the slug highest positioned in the riser reaches the riser outlet and enters the downstream horizontal. Riser liquid fraction reduces as the topmost slug is blown out.

F.3 Upper right corner: The slug entering the riser in Step F.1 has completely entered the riser. The column of slugs and bubbles in the riser is pushed higher towards the riser outlet and the inlet volume is increased, reducing the pressure. The topmost slug is pushed out of the riser

F.4 Lower right corner: The slug exerting the riser outlet in Step F.2 has completely left the riser. Liquid is no longer drained from the riser and the liquid fraction increases form the riser inlet.

---

[18]Characteristics of entire cycle is time independent.

Snapshot 5.7a is taken in the narrow time slot between Step F.2 and F.3, marked and magnified in Figure 5.8a.

The `MAX_BUB_COEF` = 1 000 $\dot{M}_l - p$ phase portrait shown in Figure 5.9a becomes discontinuous and only vaguely similar to the phase portrait example Figure 3.5a presented in the introductory discussion (outer ring in this image). Still, the process has a circular, counter-clockwise moving portrait pattern with a flat bottom where production becomes zero. The discontinuity is a characteristic of the slug tracking method; the discontinuity of hold-up in slug fronts and tails produce jumps in production as unit borders pass through the outlet. Here, the 'production' $\dot{M}_l$ is taken form the pipeline outlet. Measuring $\dot{M}_l$ at the riser outlet will give a somewhat different portrait where the production delay due to transport in

the upper horizontal is less.

Code samples used in producing these portraits are given in Listings 3 and 4.

In Figure 5.10, the pressure times series corresponding to the `MAX_BUB_COEF` = 100 and `MAX_BUB_COEF` = 1 000 cases are shown. It is clear that the larger bubble units causes the amplitude of the pressure fluctuations to be 3 − 4 times that of the case with more finely spaced bubble sections. Also apparent is the fact that the simulation of `MAX_BUB_COEF` = 100 has not reach an equally steady cycle as at this time interval as for the coarser section case.
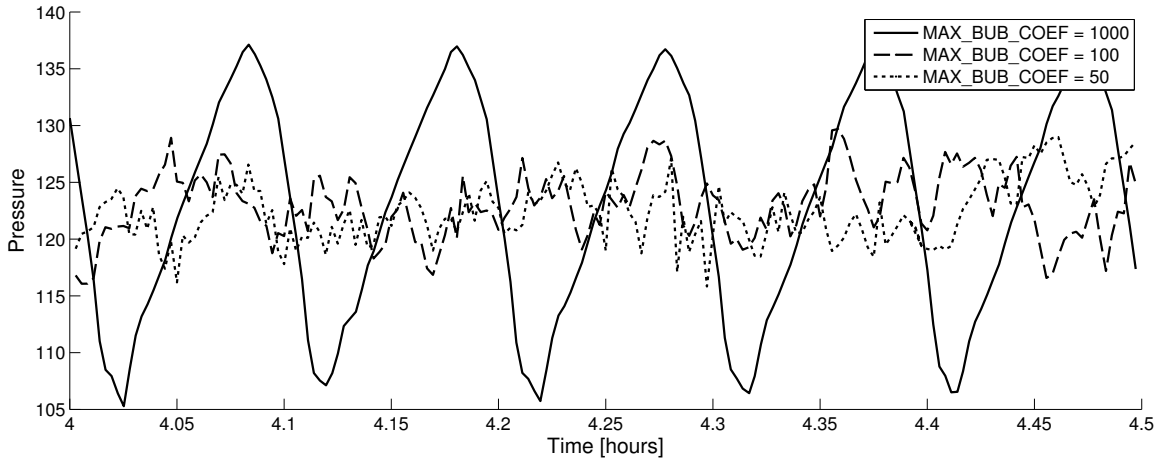

Figure 5.10: Pressure profiles of simulations in Figures 5.6 to 5.9.

Sharp pressure fluctuation profile like those from the `MAX_BUB_COEF` = 1 000 case is characteristic of terrain slugging, but is slugging flow the physically accurate solution? The severe slugging result can be seen in connection with the theory of Taitel from Section 3.3. Criterion (3.2), telling whether the riser is table and can easily be checked: Approximating the properties of (3.2) from the plots available through PLOTIT [31], it is found that $L = 600\,\text{m}$, $H \approx 1300\,\text{m}$, $\langle\Theta_g\rangle \approx 0.6$, $Po = 37\,\text{bar}$, $\langle\Phi_l\rangle \approx 0.69$ and α'_g was found to be of the order 0.9 in [41]. Due to the shortness of the horizontal inlet, the RHS of (3.2) becomes nega-

tive and marks the riser as securely stable according to Taitel's model.

Likewise, the Bøe criteria (3.1) can be checked. It may be rewritten:

$$\text{Type I slugging} \;\Rightarrow\; \dot{M}_l^s \geq \frac{RT}{g\alpha_g L}\dot{M}_g^s \qquad (5.2)$$

Feeding inn the numbers the RHS evaluates to $0.4970\,kg/s$ – the necessary criterion for terrain slugging type I is satisfied. Accordingly, the system is in the enclosed rectangular region of the flow map in Figure 3.3. Therefore, it is likely that the physi-

cally accurat solution should be either cyclic without fall-back, or steady flow.[19]

Judging from the pressure time series in Figure 5.10, it seems likely that the the physical system would be stable. All simulations have come to a reasonably steady state, in the sance that the average signal amplitudes and statistical moments have been established. Only the simulation with `MAX_BUB_COEF` = 1 000 is operationally unstable per present definition. Further, no consistent pressure fluctuation pattern or cycle is found, making the signal appear as a steady state pressure with white noise. Obviously, the small variations in pressure for `MAX_BUB_COEF` ≪ 1 000 are caused by the same slug entrance and exit effects as in Cycle F, though the riser bubbles are far smaller and far more numerous, causing a more complex dynamic and supplying the signal with a random element.

The pressure population standard deviation (second moment) s_p of the inlet pressure time series are

$$s_p\big|_{1\,000} = 9.1\,\text{bar} \qquad s_p\big|_{100} = 3.8\,\text{bar} \qquad s_p\big|_{50} = 2.7\,\text{bar}$$

where the numbers refer to the value of `MAX_BUB_COEF`. This amounts to a reduction in standard deviation proportional in order of magnitude to the reduction in bubble section length, which is not unexpected. The pressure fluctuations will be proportional to the slug lengths as these are formed. Bubbly flow will be dominant in the physical steady state case which the slug-stratified flow model converge towards as the bubble sections approach infinitesimal lengths.

The influence of section lengths on the system dynamics makes it clear that the section length parameters does not only affect accuracy and numerical stability. Even though coarse resolution (vast sections) may give reasonable results (as they do in the Girassol field case), these should be validated against more finely resolved simulations to ensure that the main dynamics are not significantly altered.

5.3 Influence of gas lift on riser void fraction

Using the models from Appendix A, the void fractions representative for the Girassol field case [47] have been computed ($H = 1278\,\text{m}$, $d = 0.2032\,\text{m}$, $p_o = 37\,\text{bar}$, $T = 59\,°\text{C}$ – isothermal approximation.) The spatially discretised model A.1 with the Girassol production state $\dot{M}_l = 33.7\,\text{kg/s}$, $\dot{M}_g = \dot{M}_g^{well} = 1.69\,\text{kg/s}$ ($152\,\text{kSm}^3/\text{d}$), finds a average void fraction $\langle\Phi_g\rangle = 0.345$, while the void fraction found for $\dot{M}_g = \dot{M}_g^{well} + \dot{M}_g^{gl} = 2.35\,\text{kg/s}$ is $\langle\Phi_g\rangle = 0.422$. The void fraction attributed to the gas lift is then $0.3645 - 0.290 = 0.0774$, or a head reduction from the pure liquid case of $\Delta H^{well} = 98.9\,\text{m}$.

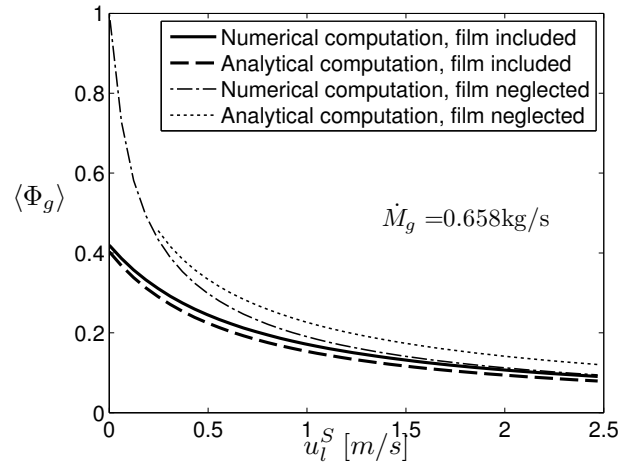Using the analytical model of Appendix A.2 yields $\Delta H^{gl} = H(0.4064 - 0.3254) = 103.5\,\text{m}$.

Figure 5.11: Void fraction as a function of superficial liquid velocity, $\dot{M}_g = 0.658\,\text{kg/s}$ ($70\,\text{kSm}^3/\text{d}$)

Figure 5.11 shows the total void fraction's dependency on the liquid flow rate for the gas. In comparing this with Figures A.4 in the appendix, it is clear that the simpler liquid film neglecting analysis in Annex F supplies an acceptable approximation only when liquid flow rates are high relative to gas flow rates.

If there is no liquid flow and the system has come to a stand-still, the void fraction produced by a gas lift will be fare more significant. In a stand still sit-

---
[19]note that Figure 3.3 is only an example – the the domain of steady flow inside the Bøe criterion may be larger than it appears here.

54

uation ($\dot{M}_l = \dot{M}_g^{well} = 0$) with a gas lift flow rate $\dot{M}_g^{lg} = 0.658\,\mathrm{kg/s} = 70\,\mathrm{kSm^3/d}$ the numeric liquid-film-including analysis of Appendix A.1 predicts a total void fraction $\langle\Phi_g\rangle(0.658, 0) = 0.4193$, and the analytic approximation (A.10) of Appendix A.2 predicts $\langle\Phi_g\rangle(0.658, 0) = 0.4031$. This constitutes a gas lift riser head reduction of $\Delta H^{gl} = 535.9\,\mathrm{m}$ and $\Delta H^{gl} = 515.1\,\mathrm{m}$, respectively. Reducing the static head by 40% will in most cases be enough to prevent the system from comming to a stand-still, even at relatively low well pressures. In the dayly operation of the Girassol field, the gas lift flow rate is about $150\,\mathrm{kSm^3/d} = 1.41\,\mathrm{kg/s} - \langle\Phi_g\rangle(1.41, 0) = 0.59$, or more than half the static head at stand-still.

In Section 7.3, SLUGGIT simulation results of full-geometry simulations with a productivity index boundary condition are presented. The entire system coming to a stand-still is amongst the results encountered. Obviously, were gas lift to be included in these simulations, the steady state outcome would be severely affected. Probably, a system stand-still would not be amongst the simulation outcomes.

Strictly speaking, Taylor bubble Assumption D.4 in the model derivation is not entirely valid in this case as gas usually enter the riser base as tiny bubbles which, driven by buoyancy, will propagate more slowly than Taylor bubble. The analysis still provide an order of magnitude estimate, approving in accuracy as coalescence ensures Taylor bubble formation.

5.4 SLUGGIT and the riser flow map

The testing so far has raised the question of whether the slug tracking methods are capable of predicting appropriate operational stability situation due to the 'lack' of a dispersed flow regime (Assumption A.1.) Here then, the ability of SLUGGIT v.2 to reproduce the four types of stable and unstable riser flow discussed in Section 3.3 will quickly be tested. This study will aim to find the simulation flow map, but only at a few points to give an overall impression. To evaluate the results, experimental data published by Taitel *et al.* will be used for comparison. The pipe diameter is $d = 2.54\,\mathrm{cm}$, the inclination is $\phi = 5°$, the length form pipeline inlet to riser inlet is $L = 19.1\,m$, whereat gas is injected at the pipeline inlet itself and liquid injected at $z = 10\,\mathrm{m}$ downstream this inlet. Figure 5.12 shows the stability map for this geometry, where the data points are tabularise in the original publication [41]. Those data points marked with diamond markers have been simulated using SLUGGIT v.2 without active slug initiation at the bend. Pressure time series from these simulations are shown in Figure 5.13.
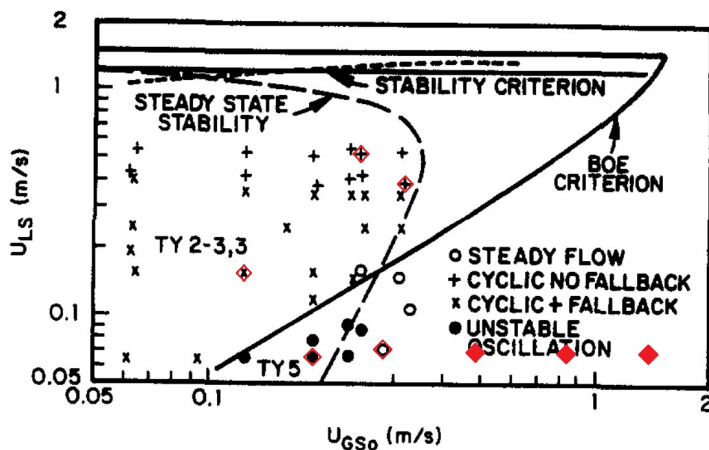

Figure 5.12: Flow map, $L = 19.1$, $\phi = 5°$, $d = 2.54\,\mathrm{cm}$. Liquid injection at $z = 10\,\mathrm{m}$. Source: [41]
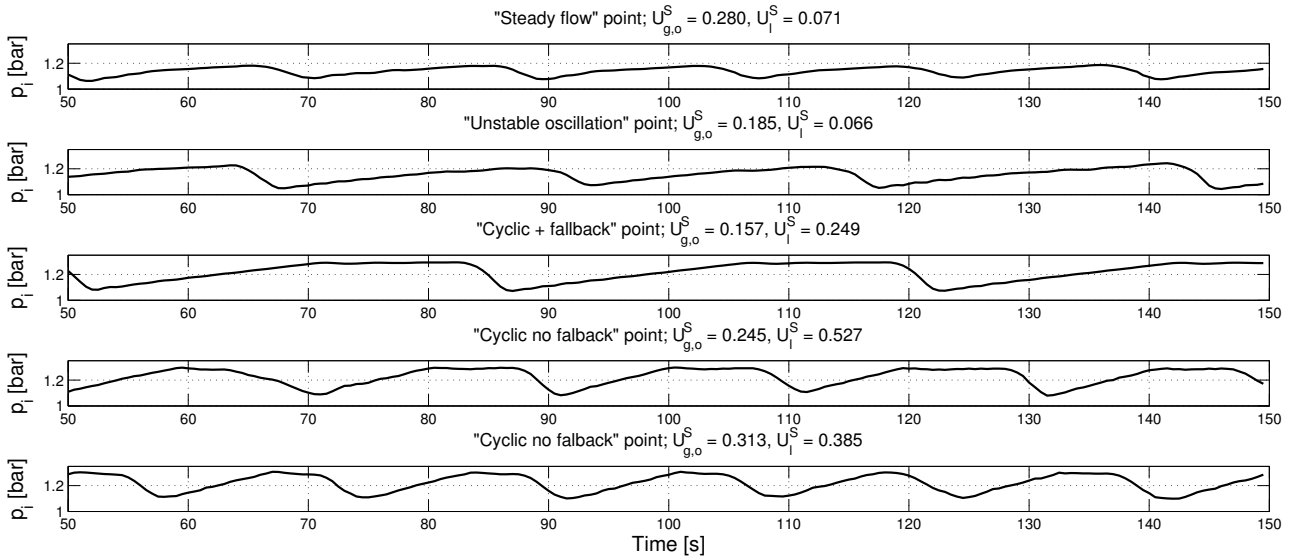Diamonds mark points simulated with SLUGGIT *cf.* Figure 5.13
$U_{g,o}^S = \{0.280, 0.185, 0.157, 0.245, 0.313\}$
$U_l^S = \{0.071, 0.066, 0.249, 0.527, 0.385\}$
Filled diamonds mark additional simulations *cf.* Figure 5.14

The following can be said about these simulations from viewing their inlet pressure time series and their PLOTIT [31] animations:

'Steady flow' point Cyclic flow pattern wherein the slug tail never penetrate far into the upstream pipeline (equivalent of continuous gas penetration). Cycle appears equivalent dt that described in Cycle E, Section 3.3, which is termed 'Unstable oscillations' in [40, 41, 14] and Figure 5.12. Snapshots of this cycle

55
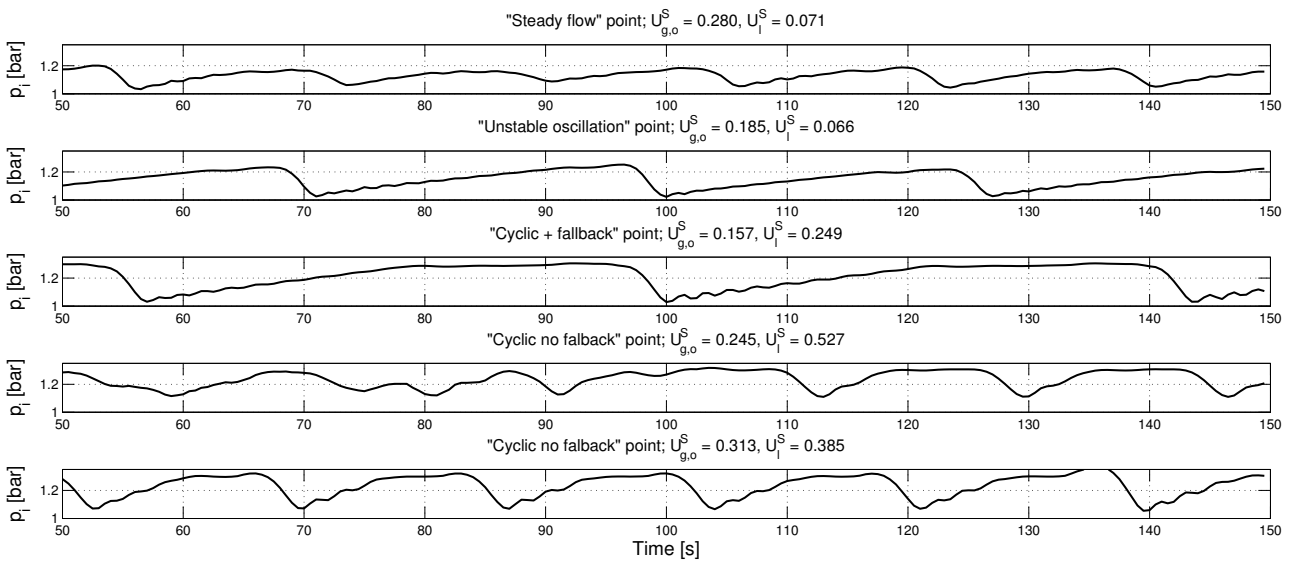
(a) SLUGGIT v.2

(b) SLUGGIT v.2s (simplified)

Figure 5.13: Pressure time series simulated with SLUGGIT v.2, `MAX_BUB_COEF` = 5, no active slug initiation in bend. Flow conditions *cf.* Figure 5.12 – diamond markers.

are presented in Figure B.2, Appendix B.

'Unstable oscillations' point Unstable oscillations as described in Cycle E. Compared to the 'Steady flow' point, the gas penetration rate is less and the gas-liquid interface re-establishes itself at a lower height after blow-out.

'Cyclic + fall-back' point Severe slugging (slug longer than riser at blow-out), as described in Cycle C. Interface re-established about midway up the riser after blow-out.

'Cyclic no fall-back' points Severe slugging with some fall-back. The fall-back is less than in the 'Cyclic + fall-back' point, and smallest in the point $U_{g,o}^S = 0.313 \, \text{m/s}$, $U_l^S = 0.385 \, \text{m/s}$, which is visible in the pressure time series by shorter oscillation periods and disappearance of the flat-topped profile.

Evidently, the lack of a non-intermittent dispersed flow regime tend to make bubbly flow patterns in the riser less stable. Consequently, the region called 'Unstable oscillations' if Figure 5.12 extends further to contain a wide range of gas flow rates. Also a consequence is the region in which liquid fall-back takes place after the blow-out, even though the experiments indicate no fall-back. This latter may be explained by too much liquid being cleared from the riser since gas can only travel in the form of Taylor bubbles which pushes more liquid ahead of them than would smaller bubble formations. Adopting the simplified scheme SLUGGIT v.2s, as seen in Figure b does not affect the time series significantly. Somewhat larger amplitudes, longer periods and fine-scale disturbances are here observed.

The most important observation to take from these brief tests is that is a word of warning. In the later sections of this work the SLUGGIT programme will be utilised in an attempt to understand operational instability in a real-life oilfield, yet it has just been shown that this method may fail in detecting some stable flow states at low liquid flow rates. Figure 5.14 give an impression of the further flow pattern development as the gas flow rate is increased form the 'Steady flow' point. The second pressure moment is not reduced below 5% of the unearated riser pressure (0.015 bar) until the gas velocity is about twice that of the original data point.

5.5 Comment

The type of benchmark testing preformed in this section of the SLUGGIT v2/v2s codes may seem extensive and somewhat diverging from the aims of the present work. On the contrary, it has proven to be immensely valuable (though time consuming) in revealing unexpected shortcomings in the newest SLUGGIT code versions. As the SLUGGIT v2/v2s code [21] is being continuously developed by more than once participant, its behaviour is altered with time, though precise track of what changes are is easily lost. The reasonable results presented so far stem from simulations generated by a SLUGGIT code version dated 19th of Match. When first carried out, later versions of the code were used which, surprisingly, gave significantly different results. A version dated to the beginning of June managed to correctly give steady flow in the point $U_{g,o}^S = 0.280 \, \text{m/s}$, $U_l^S = 0.071 \, \text{m/s}$, something the older version failed to do. Unfortunately, this version also predicted all other selected points to be stable. Even newer versions again exaggerated the instability domains. These versions also compared less favourably the the steady state model from Section 5.2.

Figure 5.15 show the $\Phi_l - p$ and $\dot{M}_l - p$ phase portraits for the same `MAX_BUB_COEF` = 1 000 case, as in Section 5.2, using the version from early June which gave steady flow at every flow map point. The animation of this run looks quite the same, except for two elongated bubbles occupying the riser rather than just the one. Also, it appears as if the slug is initiated at a slightly different location near the riser inlet. Similar, jet more diffused phase portraits are seen. Since two bubbles are active in the riser simultaneously, a cycle consists of two 'loops' in the $\Phi_l - p$ portrait. Importantly, the scales in these phase portraits are about an order of magnitude less than those in Figure 5.8 and 5.9, indicating the much lower fluctuations and higher resilience towards model instability.
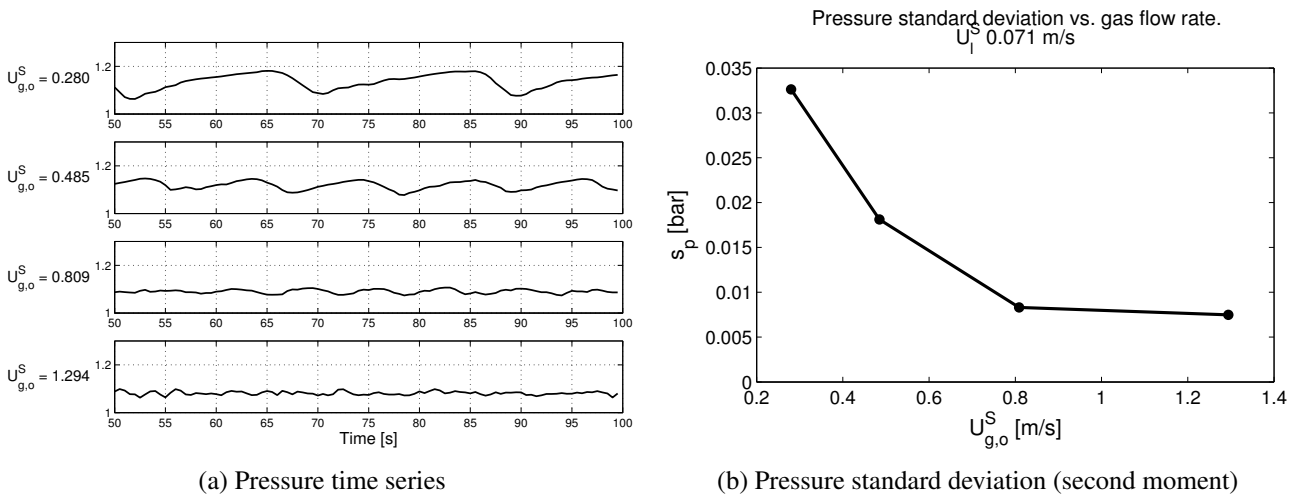
(a) Pressure time series

(b) Pressure standard deviation (second moment)

Figure 5.14: Attempt at obtaining steady flow by increasing gas flow rate (filled diamonds in Figure 5.12)

What causes these differences is version behaviour is, unfortunately, unknown. The alterations are numerous and included changes in evaluation of friction terms and management operations such as splitting and merging procedures. Despite time consuming investigation, a precise understanding of what causes these differences has yet not been established. Future investigation seems necessary. All investigation so far suggest that the model stability issue is strongly dependant on somewhat arbitrarily chosen management procedures.

To ensure compatibility, the code dated 19th of March, without any severe modifications, will be used in the reminder of the present work as this version gave reasonable stability behaviour for riser systems.
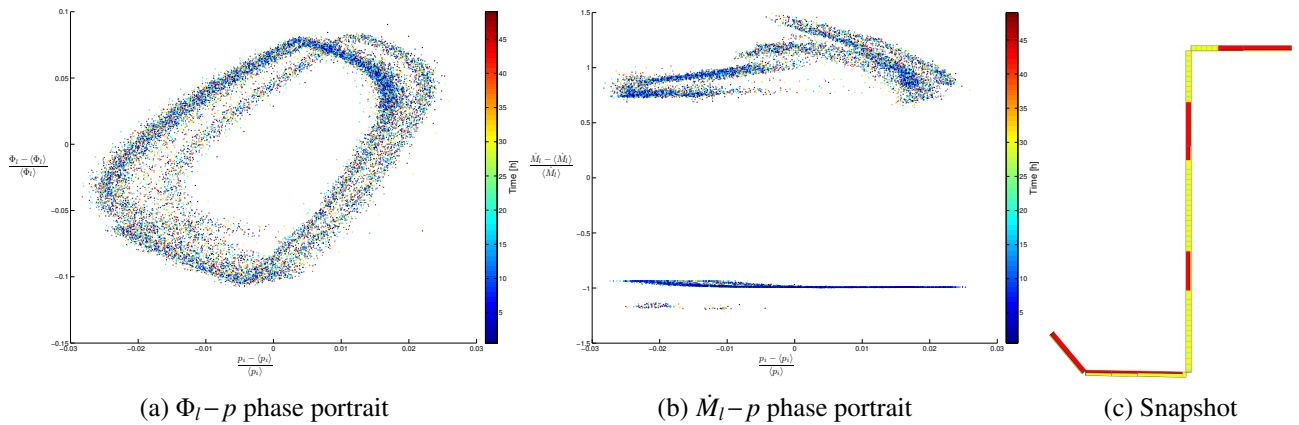

(a) $\Phi_l - p$ phase portrait

(b) $\dot{M}_l - p$ phase portrait

(c) Snapshot

Figure 5.15: Analogue to Figure 5.8a and 5.9a using newer version giving more steady solutions

6 Compromises

A great misfortune with respect to the slug tracking codes available at EPT is that there codes as implementations of similar schemes, yet implemented in totally separate and independent frameworks. This means that little time has been afforded to make each implementation robust, and the further development of one implementation will not benefit the others. Another resulting disadvantage is that in exploiting all methods, familiarisation with three vast codes rather than just one is required.

At the present state of each code, the time required to preform the adjustments and 'tinkering' needed to perform both simulation and analysis for all versions is simply not available. Some compromise is therefore required. Presently, the SLUGGIT v.1 code [23] does not compile and is significantly less developed than the SLUGGIT v.2/v.2s code [21]. Many of the special feature of the v.1 scheme is incorporated into the simplified v.2s alternative procedure, as discussed in Section 4.2. The main remaining differences are liquid velocities implicitly computed in sections rather than borders and gas entrainment in slugs. In future code development it is highly recommended by the author that the development takes place in a unified framework, preferably the v.2/v.2s code [21]. For these reasons, the v.2s implementation will be studied in favour of the v.1 code in the remainder of this work.

In Section 5.1 it was shown that the LASSI code [36] is presently not at a state which allows for analysis of riser systems. The amount of work required to remedy this problem (find the bug) is unknown. The scheme was originally developed for smaller lab-scale systems using fairly high grid resolution. Also the LASSI code lacks many of the inlet, management and automated timestep adjustment procedures available in SLUGGIT v.2/v.2s, making comparisons more challenging. For these reasons the study of the LASSI scheme will be confined to the theoretical description hitherto presented, keeping the scheme concepts and ideas in mind during the continued analysis.

7   Field simulation results

The goal of this section is to gain insight into what type(s) of instability(ies) causes to oscillations observed in the P50 Girassol pipeline as the gas injection rate is decreased below $100^{\,\mathrm{kSm^3}}/\mathrm{d}$ (see Figure 1.3.) Simulation capability of the SLUGGIT v.2/v.2s code [21] in deep-water cases is also tested. Figure 7.1 shows the gas and liquid $\dot{M}-p$ phase portraits generated with the field data [43]. [20]

---

[20]This point is fraught with some controversy; the value of $\langle \dot{M}_{l,i} \rangle = 33.7^{\,\mathrm{kg}}/\mathrm{s}$ corresponds to that reported by Zakarian and Larrey in [47]. On the other hand, this is inconsistent with the supplied field data [43] from which all the pressure information originates. Taking the average over the time period during which the gas lift rare was $70^{\,\mathrm{kSm^3}}/\mathrm{d}$, liquid mean volumetric flow rate is here found to be $1\,288^{\,\mathrm{Sm^3}}/\mathrm{d}$, which is about $14.9^{\,\mathrm{kg}}/\mathrm{s}$, or less than half half what has been taken as the 'proper' liquid flow rate.

(a) $Q_g^{ST} - p$ phase portrait

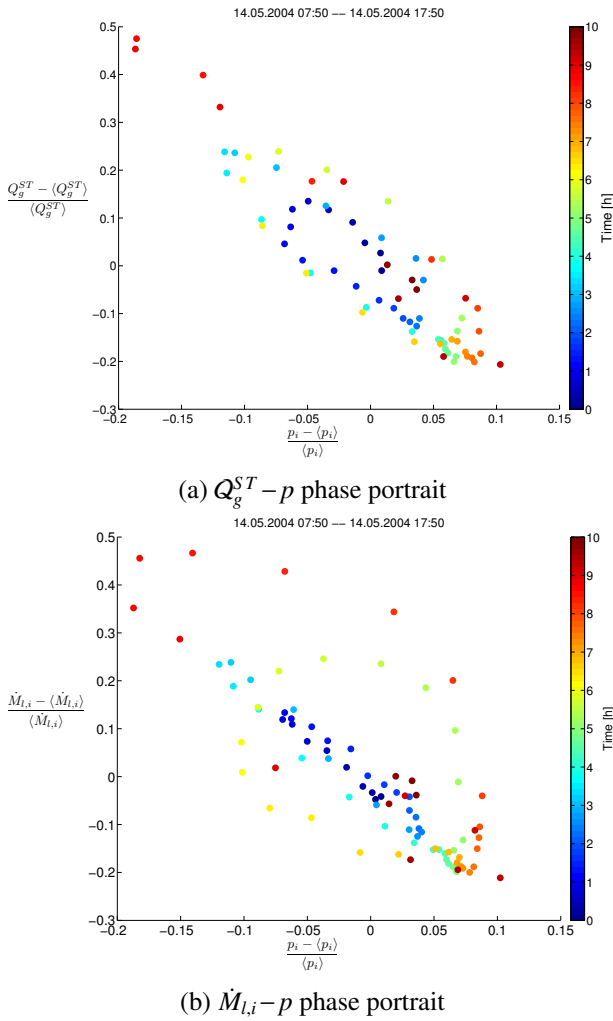(b) $\dot{M}_{l,i} - p$ phase portrait

Figure 7.1: Girassol data. Wells on manifold P5011

Note that, contrasty to the flow rate phase portraits of Sections 5.2 and 7.2, which are defined at the outlet, field data is only available near the inlet.

As in the the pure terrain slugging phase portraits exemplified in Figure 3.5, the field data portraits take on a circular form, spiralling anti-clockwise with time. They do however also take on a diagonal trend, flow rates decreasing with increasing pressure. Whereas the former suggests a terrain slugging dynamic, as seen in Section 3.3, the latter suggests an influence of the well characteristic; increasing pressure at the inlet will reduce well production. This latter possibly indicates a void, concentration or surge wave phenomenon.

7.1 Fixed inlet pressure – jumper influence

Khabibullin showed in [18] that the SINTEF multiphase dynamic pipe flow simulation code LedaFlow show oscillatory pressure profiles for vertical riser systems that are dependent upon whether jumpers are included upstream with riser. The riser is here similar to that of the Girassol P50 pipeline (see [47] and Section 1.2.1). A fixed pressure inlet boundary condition (a von Neumann type boundary condition) is applied with inlet pressure is $p_{inlet} = 145$ bar (a bit higher than found in the field data, though there is no gas lift in this simulation) and an outlet pressure $p_{outlet} = 37$ bar. The same dynamics as observed by Khabibullin have here been recreated using SLUG-GIT v.2.

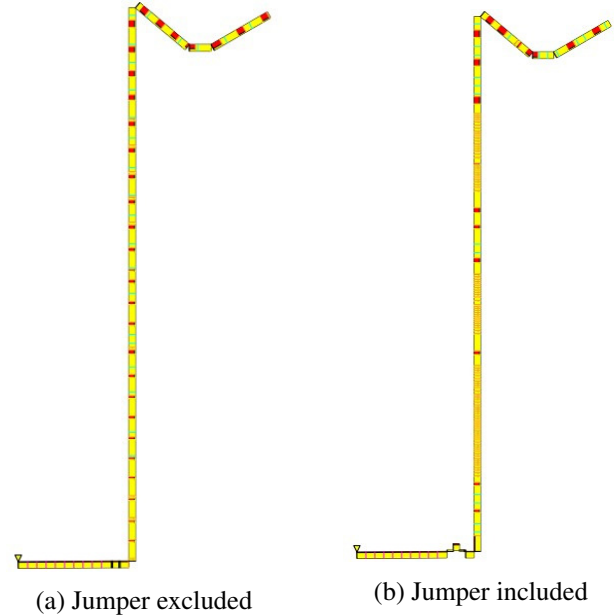(a) Jumper excluded   (b) Jumper included

Figure 7.2: Short open inlet with fixed out- and inlet pressures $p_{outlet} = 37$ bar, $p_{inlet} = 145$ bar. Slight positive inclination of horizontal pipe upstream riser.

Figures 7.2 present two snapshots – one with, and one without, a jumper afront the riser. A steady stream of bubbles and slugs are observed in the no-jumper case, and the pressure profile measured at the riser inlet is approximately constant. When a small jumper was included ahead of the riser, short bursts of gas occasionally released form the jumper, followed by streams of smaller bubbles, were observed. These bursts appear to take place at regular intervals.

60

7.1.1 Jumper-caused pressure oscillations

Comment The analysis of this section, carried out at an early stage of this work, is sensitive to changes in parameters and geometry, and also by the rather large maximum section length applied. For this reason the results themselves should be considered with some reservations. Still, they do indicate that the U-bend in the P50 pipeline geometry may play a part in an upstream dynamic – a notion which is not to be discredited.

Simulation To avoid the fixed inlet pressure influencing the upstream pressure measurements, the whole horizontal of the Girassol geometry was included in simulations using SLUGGIT v.2. To avoid the system coming to a stand still, it was found necessary to increase the inlet pressure to $p_{inlet} = 167$ bar so that both increased friction and the static head (no gas lift) could be overcome. The geometries used are shown in figure 7.3 and the pressure time series at the riser inlet in Figures 7.4. To demonstrate the influence of the jumpers and their placement, three cases are presented: One with the jumpers placed approximately as in the field geometry [43], one in which the jumper placement in altered slightly, and one where the jumpers have been removed altogether.

Figure 7.3: Simplified Girassol geometries. Pressure profiles at riser inlet shown in Figure 7.4. Pipe diameter rescaled by a factor 75

In the simulation where the jumpers are placed in accordance with field geometry (Figure 7.4a,) the pressure occasionally plunges sharply with about 16 bar during the initial stages of simulation as gas expulsions form the jumpers enter the inlet. These events occur on average at intervals of about half an hour. After two hours these events abruptly cease and a transient/annular steady state is reached. The dynamic changes as the positions of the jumpers are slightly altered, the jumper closest to the riser being moved further upstream (Figure 7.4b and middle geometry in Figure 7.3.) Here the regular pressure-plunges continue throughout the time series. To demonstrate that the jumpers are sources to pressure disturbances, the pressure time traces when all jumpers are removed are included in Figure 7.4c. As expected, this simulation show no sign of pronounced pressure fluctuation.

The manifold pressure time series form the field data [43] as also included for comparison, continuing the pursuit of Khabibullin in [18]. The simi-
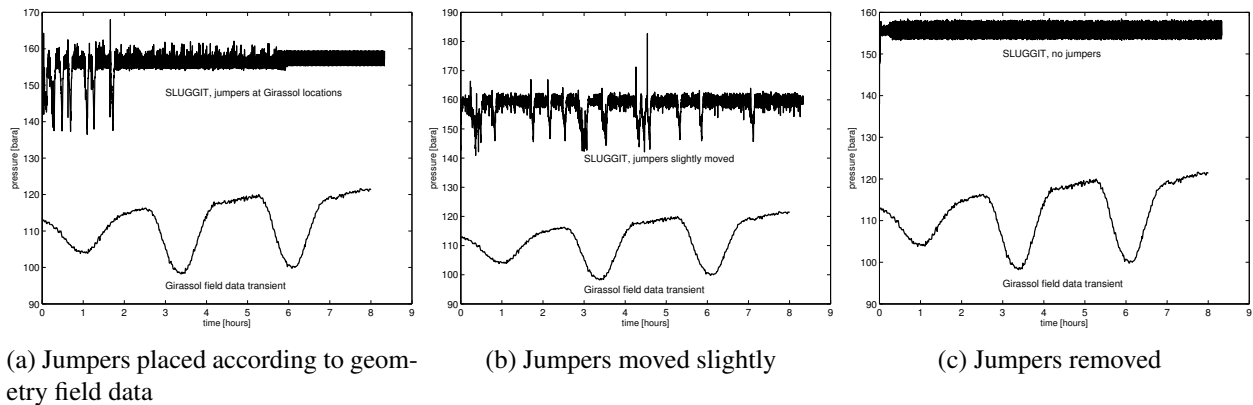
61

(a) Jumpers placed according to geometry field data

(b) Jumpers moved slightly

(c) Jumpers removed

Figure 7.4: Pressure time series at riser inlet. SLUGGIT simulations with simplified Girassol geometries (Figure 7.3, top ↔ a, middle ↔ b, top ↔ c) fixed out- and inlet pressures $p_{outlet} = 37$ bar, $p_{inlet} = 167$ bar. Also shown are field data [43] as gas lift is quickly reduced from 100 to 70 $^{kSm^3}/d$ at $t = 0$.

larities are not convincing. The pressure series in Figure 7.4b are amongst the few results managing to obtain oscillations where both period and amplitude are of the same order of magnitude, though pipeline geometry manipulation was needed to achieve this.

More precisely, the jumpers has to be moved further upstream, indicating that the field instability involve also some length of the horizontal pipeline.

Oscillation dynamics   The simulation data from this open inlet jumper case have been studied using visualization provided by the EPT PLOTIT visualization tool [31].   The jumpers, which are always filled with gas, are observed to periodically go through the following stages:

Description A.

A.1 Separated flow through the jumper and pipeline.

A.2 The gas volume in the jumper begin to oscillate. Volume fluctuation amplitude and frequency increase progressively in the jumper.

A.3 A small, additional amount of gas is released into the horizontal pipe from the jumper. This is immediately followed by a short slug and travels downstream the horizontal as a density wave.

A.4 As the additional gas reaches the riser and begins to expand, the oscillations in the jumper stabilize and the cycle repeat itself.

It is also found that the cycle in a single-jumper system is probably quite regular. The simulation which gave the pressure trace in Figure 7.4b has three jumpers. These influence each others' cycles and cause the observed disregularity.

In Section 1.2.2, a suspected causality between jumper gas release and riser expansions was mentioned. The idea was that a gas expulsion from the jumper would travel up the riser and reduce the hydrostatic head, causing upstream expansion and further gas expulsion. Instead, it appears form the ani-

mations that the activity in the jumpers become less vigilant as the void wave progresses up the riser (see accompanying animations.) The animations further unveils that a long slug forms ahead of the void wave in the riser. When this slug reaches U-bend near the outlet, U-bend terrain slugging will cease. As U-

bend slugging stops, also the high-frequency density oscillation seen in the jumper form which the void wave originated cease. This may suggest and inter- esting jumper-riser-U-bend negative feedback coupling – a possible cycle of causality is hypothesised:

Description B.

B.1 From steady state, terrain slugging initiate and progress in intensity and frequency in the upper U-bend.

B.2 This produces oscillations in the jumper void through pressure fluctuations propagating upstream. These oscillations allow for irregular gas entrainment in the jumper.

B.3 Pressure oscillations, and therefore jumper gas volume oscillations, progress in relation with the U-bend dynamics until a gas surplus is released into the pipeline form the jumper.

B.4 When this void wave reaches the riser, the disturbance is sufficient to initiate a slug formation quickly travelling up the riser.

B.5 Once the slug front (propagating much faster than the bubble noes) reaches the outlet, the U-bend is flooded and U-bend oscillations cease.

B.6 In turn, the pressure fluctuations will come to and end and the jumper volume will steady with little entrapped gas and at relatively higher static riser head.

B.7 As the slug is expelled, a separated regime is again resurrected and slugging flow may begin to developed in the U-bend. The cycle is repeated.

This presents an interesting prospect where oscillatory phenomena are coupled across approximately 1 500 meters of piping by means of pressure propagation upstream and void wave advection downstream. Figure 7.5 presents two illustrative snapshots.
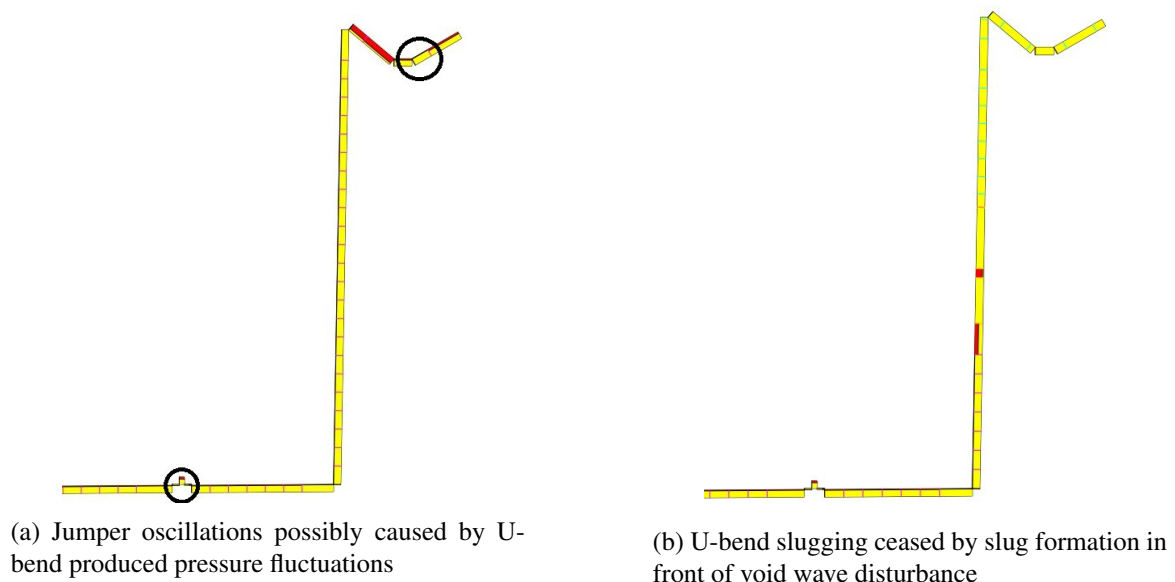

(a) Jumper oscillations possibly caused by U-bend produced pressure fluctuations

(b) U-bend slugging ceased by slug formation in front of void wave disturbance

Figure 7.5: Open inlet, jumper-riser-U-bend oscillations

Figure 7.6 presents three hold-up time series – one at the jumper closest the the riser inlet, one at the riser inlet itself, and one at the U-bend, at a point where the inclinations is positive and slugging occurs. Two hours of the eight hour simulation time is depicted, during which no void wave travels form any of the two jumpers further upstream. It is clear that as soon as the gas enters the riser base (negative spikes in the middle graph) periods of calmer jumper hold-up lasting about 10 minutes can be observed (top graph). As this happens, a quickly expelled slug floods the riser and U-bend (visible in the bottom graph). The expulsion of this riser slug manifest itself as a large drop in hold-up in the U-bend as the expanded gas emitted form the jumper reaches the outlet. These downward spikes in U-bend hold-up (bottom) infallibly marks the re-initiating of oscillations in the upstream jumper (top). This is consistent with the hypothesis, but does not prove any causality.

Naturally, simulations without any bend atop the riser have been performed to strengthen or kill the aforementioned hypothesis. Figure 7.7 shows the found steady state solution.

This simulation quickly reaches a steady state solution of stratified flow from the inlet to the second jumper, and bubble-slug flow from there to the outlet. Pressure fluctuations at the riser base (Figure 7.7b) are on order of two bars – the flow is considered stable. The horizontal in Figure 7.7a has zero inclination all over, so it is interesting that the change of

flow regime should occur at the middle jumper.

7.1.2 Expansion driven unstable production

From here, the simple representation of the U-bend from the previous Section is replaced by a more detailed U-bend representation of the Girassol P50 pipe using field geometry data [43]. The well piping is still not included, but will be studied in Section 7.3. Figure 7.8 display the geometry. The horizontal section is retained somewhat simplified (pipe segments of $\phi = 0°$ and $\phi = 0.4°$ inclination where field geometry has slightly negative inclination.)

Quite accidentally, expansion driven instability, as described in Cycle A, is here stumbled upon. The best way to understand the predicted dynamic is by viewing an animation of the simulation, and so the reader is encourage to view the accompanying PLOTIT output files. Also helpful are the snapshots in Figure B.1, Appendix B

Pressure time traces are shown in Figure 7.9. These pressure series are similar to those fount for the simplified U-bend (Figure 7.7b), but the mechanism responsible for the pressure fluctuations appear to be different when viewing the animations.

In the case of the geometry where the jumper positions are slightly altered (the last jumper is moved upstream), the cycle is more regular as jumper placement coincide better with bubble positions at the expansion event.
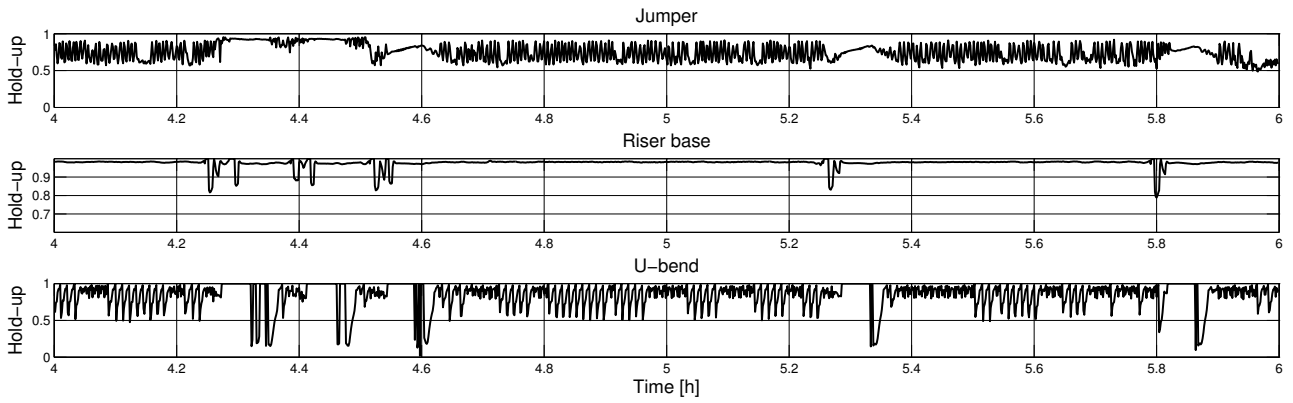
Description C. *Expansion driven unstable production*

C.1 No production occurs. Gas is entrapped in and around the jumpers. There are a couple of bubbles at the bottom of the riser. The liquid column surface in the riser is slightly too low to reach the outlet U-bend.

C.2 As the bubbles travel up the riser, their size increase, riser void increases, bottomhole hydrostatic pressure is reduced and the liquid hight in the riser increases. When the bubbles are about half-way up the riser, the riser liquid height is heigh enough for the liquid to reach the outlet.

C.3 The liquid production increases the liquid flow, transporting gas from the rightmost jumper into the riser, replacing the riser inlet bubble in Step C.1. This bubble enters the riser about the same time as the expanding, liquid producing bubble exits the riser and the riser again floods with a liquid column surface below the riser outlet.

C.4 Production is sustained as gas escaping a jumper is replaced by gas travailing from the upstream jumper neighbour.

Figure 7.6: Hold-up at last jumper (top), riser base (middle) and slugging portion of U-bend (bottom)

(a) Geometry

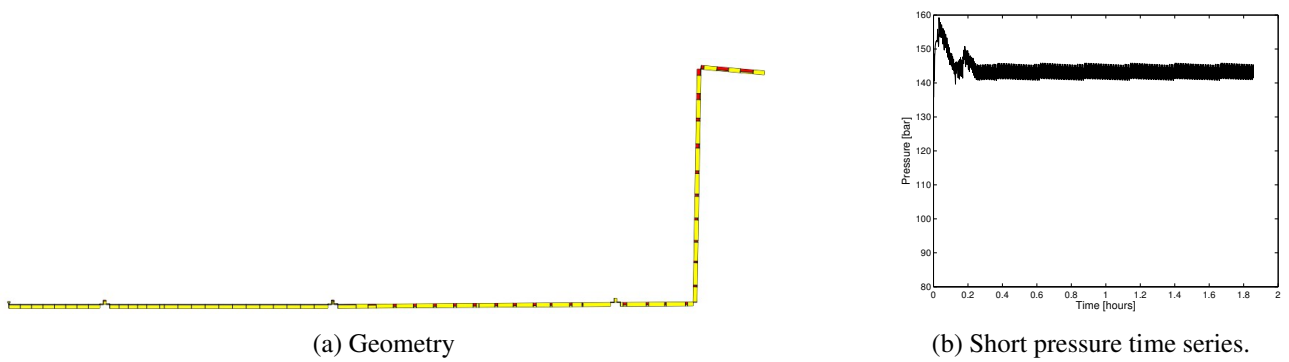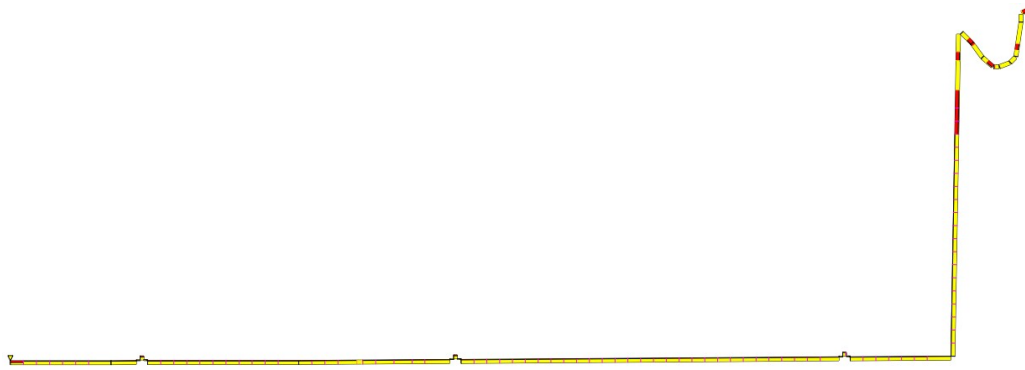(b) Short pressure time series.

Figure 7.7: Open inlet. Geometry equivalent to that in Figure 7.4b without U-bend atop the riser.

(a) Jumpers slightly displaced

(b) Jumpers placed according to field data

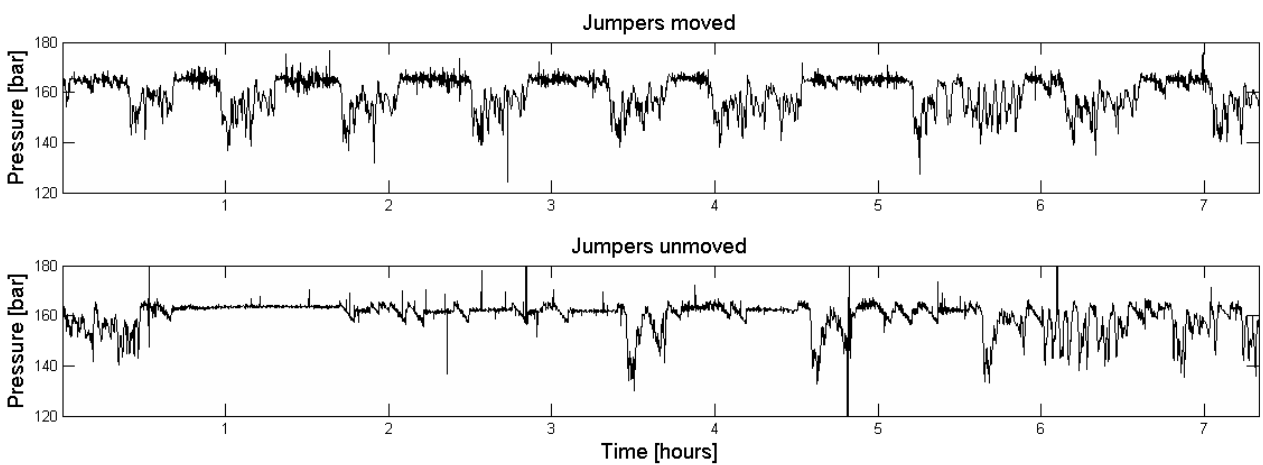Figure 7.8: Simplified Girassol geometry with complete U-bend

Figure 7.9: Pressure time series at riser base. Top graph ⇔ geometry Figure 7.8a, bottom graph ⇔ geometry Figure 7.8b

See Figure B.1b of animation snapshots to get a visual impression of the dynamic. The period of steady riser pressure seen in the top graph of Figure 7.9 happens as there is no liquid production (the liquid does not reach the top of the riser) and the amount of liquid in the riser remains unchanged. This lasts for about 30 minutes, which is not the time needed for the base bubbles to travel all the way up the riser, but the time needed for the bubbles to travel up the riser a distance far enough to expand sufficiently. This expansion volume equals the volume in between the riser outlet and an unaerated liquid column surface. As is evident from top plot graph in Figure 7.9, this time interval is fairly constant and periodic. Variations in duration of steady pressure are caused by uneven amounts of gas being left in the riser base after a cycle.

In the case where the jumper is placed close to the riser (Figure 7.8b) the dynamic can be described as follows:

Description D.

D.1 Liquid blocks the riser inlet. The jumper and piping upstream the riser contains gas that trickles forward.

D.2 The gas trickles into the riser. At some point, the trickle is large enough to suck the entire gas amount entrapped in the last jumper into the riser. The system may stay idle for hours before this happens.

D.3 As the gas expands, the liquid production increases and gas is pulled from the inlet. Gas present in the horizontal is pulled further downstream.

D.4 Depending on the amount of released gas and the momentum of the liquid, gas pulled from upstream regions reach the riser inlet before the gas in the riser may reach the outlet. If it does, the liquid production continues by means of the buoyancy and expansion provided by the newly arrived gas.

D.5 Eventually, new gas will not reach the riser inlet. Instead, the gas transported from upstream the riser will reach the final jumper and accumulate a gas storage here. The cycle is repeated.

– see Figure B.1a.

The duration of system idleness is here quite unsteady and unpredictable. From the bottom plot of Figure 7.9 it is seen that this period can last as long as three hours, all depending on the tiny movement necessary to transport a sufficient amount of gas the short distance from jumper to riser inlet. Basically, the main jumper-caused difference between the behaviour seen in Descriptions C and D is that the jumper placement does not correspond equally well with bubble movement for replacement of the riser inlet bubble to be guaranteed – Step C.3 and D.4.

Some important features of these simulations should be underlined:

Inlet pressure In a case study such as this, with fixed inlet pressure, there is only a narrow interval of inlet pressures within which this type of instability is possible. In the present case, the inlet pressure was $p_i = 167$ bar. Should however the inlet pressure be higher than this then the pressure inlet-outlet difference is high enough to allow for production even with no void in the riser. The dynamic then will be a fast flow of slugs and bubbles, as previously seen in the beginning of this section. Though this may itself be subject to density wave instability and other forms of instability, the dynamic presented in Description D and C cannot be replicated.

In reducing the inlet pressure too far below the static head of a pure-liquid riser column, the void produced by gas expanding while travelling up the riser will not increase the riser liquid surface height sufficiently to reach the outlet. In this case, no liquid production will take place at all, the gas will leave the riser, and the system will settle to a stand-still.

The upper snapshots of Figures B.1a and b shows

how little additional head is needed on the inlet to drive the system into continuous production.

Inclination of horizontal pipeline Attempts have been made to reproduce the type on instability described above using the exact Girassol P50 pipeline geometry. This has proved impossible. The reason is that the longest segments of piping on the P50 pipeline have an inclination of $\phi \approx -0.8°$. Negative inclination makes the pipeline prone to terrain slugging, but buoyancy constantly works to prevent new gas from entering the riser. From simulations it was found that some promising expansion slugging could be seen at the initial stages of the simulations, as gas was pulled into the riser by the momentum of the liquid. At some point however, the liquid will come to rest and the gas may begin to evacuate up towards the inlet. Again then, if the inlet head is less than the riser height the system will come to a stand still. Alternatively, were will be continuous production in which buoyancy forces are does not drive the production (buoyancy may on the other hand still affect operational stability.) In other words, since periods of no liquid production is a part of the expansion driven unstable production seen in this section, the system must be able to endure periods of near stand-still while allowing gas to enter the riser.

7.2 Closed inlet, fixed flow rates – Terrain slugging

Figure 7.10: Closed inlet geometry

The fixed flow rates inlet boundary condition is available in all EPT slug tracking codes. Here, all mass fluxes through the inlet are fixed, either by fixing the inlet superficial velocities $U_{k,i}^S$ and pressure (density), or by denying any flow through the inlet and fixing mass sources somewhere in the pipeline. This is a Dirichlet type boundary condition that forces changes in gas density, accommodating elasticity

into the dynamic. Compared with the open inlet, fixed pressure boundary condition, the closed inlet promotes a quite different system response.

Again, the Girassol field P50 pipeline will be in focus as a test case. The P50 pipeline is perhaps a more natural test case choice for the closed inlet boundary as the combination of compressibility and downward-sloping terrain produce a setting prone to terrain slugging. Terrain slugging has already been discussed introductorily in Section 3.3 and has been past of benchmark testing in Section 5.4. As before, the well is excluded from geometry. This time, the exact horizontal and riser geometry is used [43], which is shown in Figure 7.10 – notice the downward inclination of the horizontal, which is $\phi = -0.74$ upstream the two jumpers, and $\phi = -0.83$ downstream.

Mass sources are added close to the inlet; at $z = 1.0$ m a gas source pumping $\dot{M}_g^s = 1.69$ kg/s is placed, while a liquid source $\dot{M}_l^s = 33.7$ kg/s is placed at $z = 250$ m. These sources ensure mass fluxes corresponding the average well production measurements published by Zakarian and Larrey in [47]. The pressure response time series at the riser base is presented in Figure 7.11
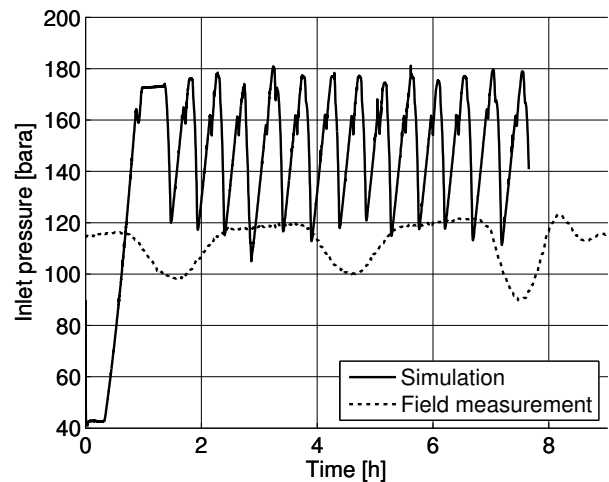

Figure 7.11: Pressure time series upstream riser from P50 pipeline geometry. Closed inlet, constant mass sources $\dot{M}_g^s = 1.69$ kg/s, $\dot{M}_l^s = 33.7$ kg/s. SLUGGIT v2 simulation vs. Girassol manifold measurements [43, 18, 47].

Again, in order to draw a parallel to Khabibullin's project thesis work [18], the pressure time trace is plotted against the Girassol P50 manifold pressure measurements just after the gas lift has been reduced form 100 to 70 $^{kSm^3}/_d$. A description of the dynamic is here not necessary; a textbook case of *severe* slugging plays out, and is already described in Cycle C in Section 3.3. Snapshots of animation can be found in Figure B.3 in Appendix B.

The severe slugging result can be seen in connection with the theory of Taitel from Section 3.3. Criterion (3.2), telling whether riser is table, can easily be checked. Approximating the properties of (3.2) from the plots available through PLOTIT [31], it is found that $L \approx 4600\,m$, $H \approx 1300\,m$, $\langle \Theta \rangle \approx 0.5$, $P_o = 37\,bar$, $\langle \Phi_g \rangle = 0$ and α'_g was found to be of the order 0.9 in [41]. This makes the RHS of (3.2) equal $125\,bar$, which is significantly more than P_o, confirming riser instability.

Likewise, the Bøe criteria (3.1) may be checked, using the re-written formulation (5.2). This produce a RHS of $7.93\,^{kg}/_s$ – the necessary criterion for terrain slugging type I is satisfied. Using the alternative to the Bøe criterion from [32] give than same result.

Figure 7.12 show the riser phase portraits of the severe slugging simulation. The portraits show distinct resemblance to the portraits in Figures 5.8a and 5.9a in Section 5.2 where oscillations are caused by coarse resolution.

Adjusted gas injection rate

During the final weeks of work the present master thesis it was found, through communication with Eldar Khabibullin, that there has been a misunderstanding concerning the input data used in the above considerations. It would appear that the flow rates supplied ($\dot{M}_{oil} = 14.36\,^{kg}/_s$, $\dot{M}_{H_2O} = 19.33\,^{kg}/_s$, $\dot{M}_g = 1.69\,^{kg}/_s$) are in fact the phase flow rates the fluid mixture would obtain under standard condition pressure and temperature, not under the inlet conditions. In other words, these flow rates are not adjusted for phase transition associated with the state change from standard to inlet conditions. The appropriate inlet mass flow rates as recently supplied by Eldar Khabibullin are $\dot{M}_{oil} = 15.96\,^{kg}/_s$, $\dot{M}_{H_2O} = 19.59\,^{kg}/_s$,

$\dot{M}_g = 0.295\,^{kg}/_s$, which correspond to a pressure $p_i = 122\,bar$ and temperature $T_i = 63.5\,°C$. This amounts to a gas mas flow rate less than a fifth of the original inlet condition.

Unsurprisingly, the character of the flow now changes significantly. The horizontal is now mostly filled with liquid, the gas forming Taylor bubbles in a liquid filled horizontal rather than a stratified region stretching from inlet to the bend-blocking slug. The temporally and spatially averaged liquid hold-up in the horizontal is found to be $\langle \Theta_l \rangle = 0.84$. In comparison, the same average in the previous case, with $\dot{M}^s_g = 1.69\,^{kg}/_s$ and severe slugging, was found to be $\langle \Theta_l \rangle = 0.60$. This means that, with the new gas flow rate, the horizontal compressible volume is about halved. Upstream compressibility is a key ingredient in the terrain slugging cycle C and reducing this will reduce the severity of the slugging.

With the new reduced gas injection, liquid production is uninterrupted. The riser is mostly filled with un-aerated liquid, occasionally disturbed by a Taylor bubble penetrating from the horizontal. Total average liquid riser hold-up is $\langle \Phi_l \rangle = 0.95$
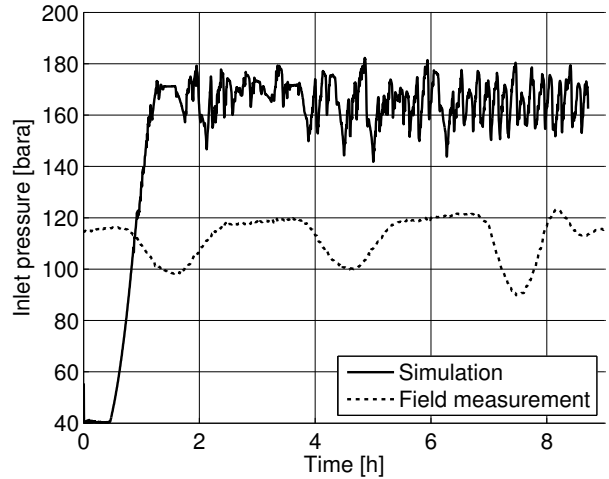

Figure 7.13: Pressure upstream the riser from P50 pipeline geometry (Figure 7.10). Closed inlet, constant mass sources $\dot{M}^s_g = 0.295\,^{kg}/_s$, $\dot{M}^s_l = 35.55\,^{kg}/_s$. SLUGGIT v.2 simulation vs. Girassol manifold measurements.

A pressure time series of a simulation performed using these new inlet boundary conditions is presented in Figure 7.13. The pressure fluctuations have
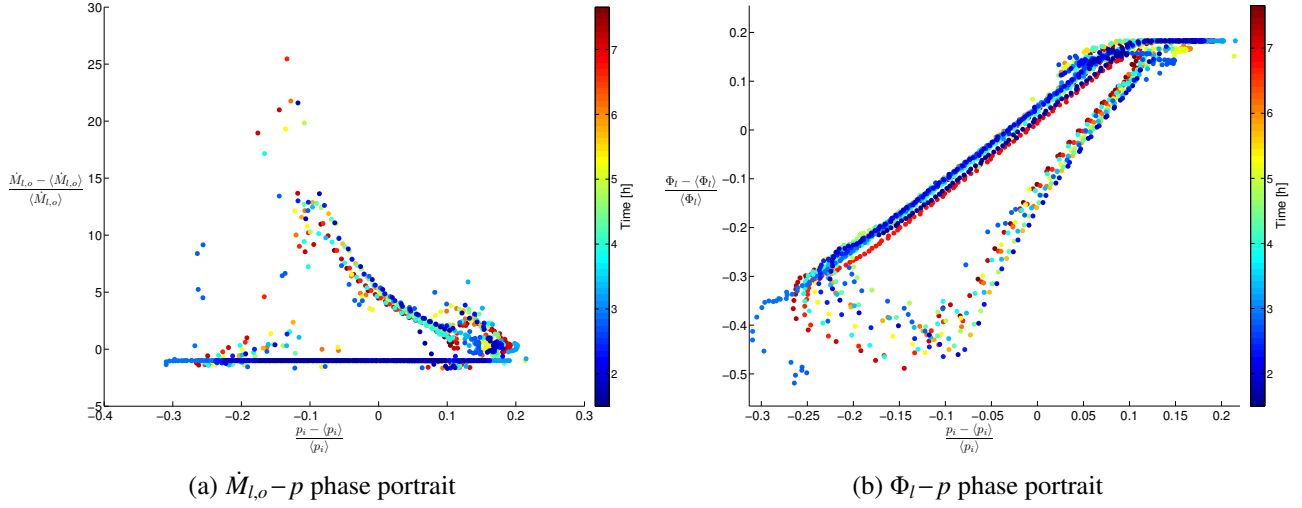
(a) $\dot{M}_{l,o} - p$ phase portrait

(b) $\Phi_l - p$ phase portrait

Figure 7.12: Closed inlet with fixed mass sources $\dot{M}_g^s = 1.69\,\mathrm{kg/s}$, $\dot{M}_l^s = 33.7\,\mathrm{kg/s}$. Geometry as in Figure 7.10
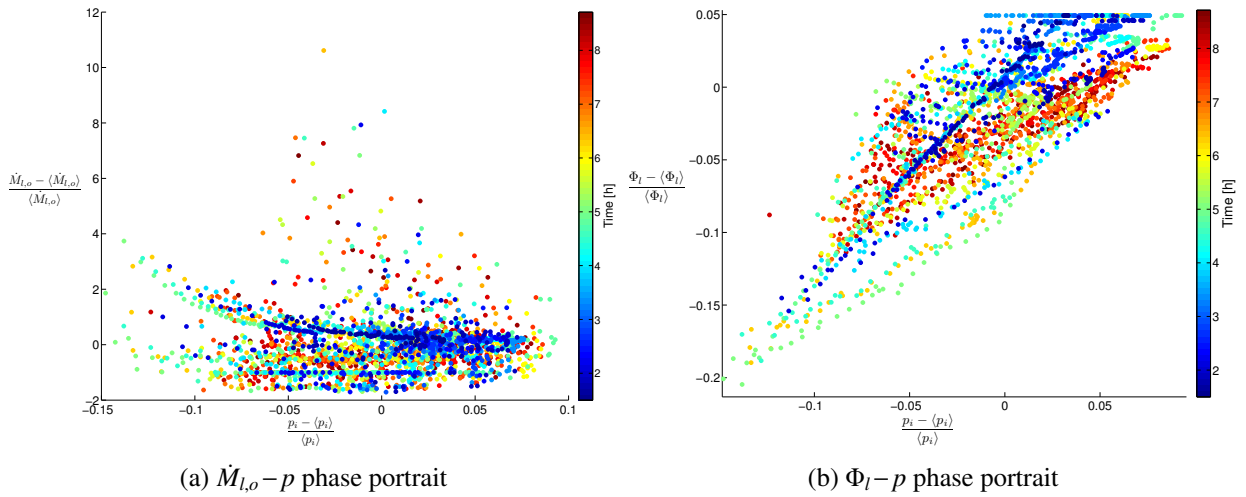

(a) $\dot{M}_{l,o} - p$ phase portrait

(b) $\Phi_l - p$ phase portrait

Figure 7.14: Closed inlet with fixed mass sources $\dot{M}_g^s = 0.295\,\mathrm{kg/s}$, $\dot{M}_l^s = 35.55\,\mathrm{kg/s}$. Geometry as in Figure 7.10

a period of about 10 min and peak-to-peak amplitude around 20 bar. These fluctuations are again ladened with more noise of higher frequency and smaller smaller amplitude.

Figure 7.14 present the phase portraits of the adjusted SLUGGIT simulation. Though some trends may be discearnable, it is clear that these portraits does not show patterns in the way seen in the severe slugging simulation, Figure 7.12. It is quite interesting to note that even under these flow conditions, fluctuations with amplitude in the order of those measured at the Girassol field are seen. The oscillations in pressure are formed by gas occasionally penetrating into the riser and expanding therein. PLOTIT animation [31] further reveals that the Tailor bubbles in the horizontal tends to 'shake' back and forth as they slowly propagate downstream. This happens as bubble tails are temporarily turned into bubble noses so that the bubbles move a short distance upstream. Interestingly, the temporary changes in bubble propagation direction appears to be caused by the disturbances generated as gas slugs in the U-bend atop the riser. It is difficult to tell whether this dynamic has influence on the pressure fluctuations, as well as whether it is physically appropriate or caused by the bubble nose criteria not being entirely appropriate when bubbles are nearly stationary in horizontal pipes. From the basic description of the SLIGGUT v.2/v.2s bubble nose logic, Section 4.9, it should be evident that capturing correct bubble propagation behaviour in near horizontal pipes can be somewhat tricky.

To investigate to what degree the pressure disturbances are caused by the bubble-riser penetration effect or terrain slugging in the U-bend, a new simulation is carried out. This time, the U-bend atop the riser replaced with a 400 m long perfectly horizontal pipe segment. All other parameters remains as in the previous simulation. The result is shown in Figure 7.15. A part of the fluctuation has disappeared and only the less frequent bubble-riser entrance events remain. The amplitude of fluctuation is here found to be slightly increased, possibly explained by the Taylor bubbles being larger since there is no flow disturbance from the U-bend. The corresponding $\Phi_l - p$ phase portrait shown in Figure 7.16b form nearly a straight line, which is consistent with a purely hydrostatic system consideration. This is

contrary to what was seen with the U-bend in Figure 7.14b, and confirms that the divergence from a straight line riser void/upstream pressure relationship in the former simulation was caused by slugging in the U-bend. This, of course, makes sense since pressure differences across an downstream slug is not accounted for in the riser liquid column.
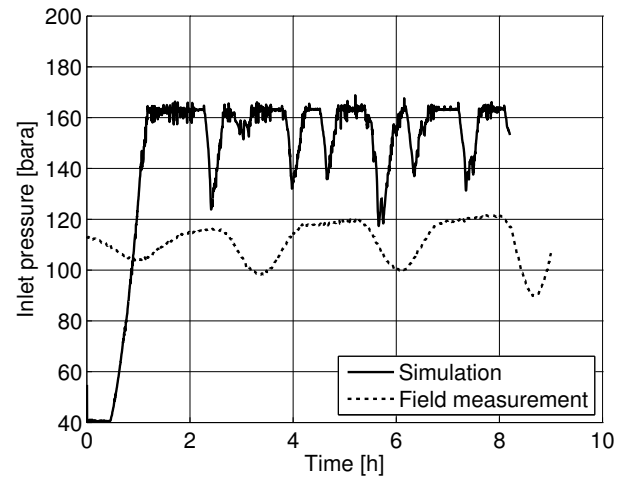

Figure 7.15: Pressure upstream riser from P50 pipeline geometry – as in Figure 7.10, only U-bend of pipeline geometry replaced with a horizontal pipe segment. Closed inlet, constant mass sources $\dot{M}_g^s = 0.295$ kg/s, $\dot{M}_l^s = 35.55$ kg/s. SLUGGIT v.2 simulation vs. Girassol manifold measurements.

Simulations performed by Eldar Khabibullin using SINTEF's LedaFlow model and the commercially popular OLGA code predicts the same high-frequency fluctuations as seen Figure 7.13, only these fluctuations were slightly more regular [18]. These simulations included a gas lift injection rate of 70 kSm³/d. Predicted fluctuation period of the LedaFlow simulation was 5 min with a peak-to-peak amplitude of about 11 bar. OLGA predicted similar fluctuations of 10 bar peak-to-peak amplitude and 24 min periods. The oscillations from OLGA were composed of steady double-pulse signal with a smaller pulsation followed by a larger one, similar to a heart beat. Compared with the 3 hour period and 35 bar amplitude of the field data [43], Figure 1.3, these simulations does not appear to capture the appropriate instability phenomena. 35 bar is the fluctuation amplitude reached before the gas lift injection rate was restored – it is unknown to what
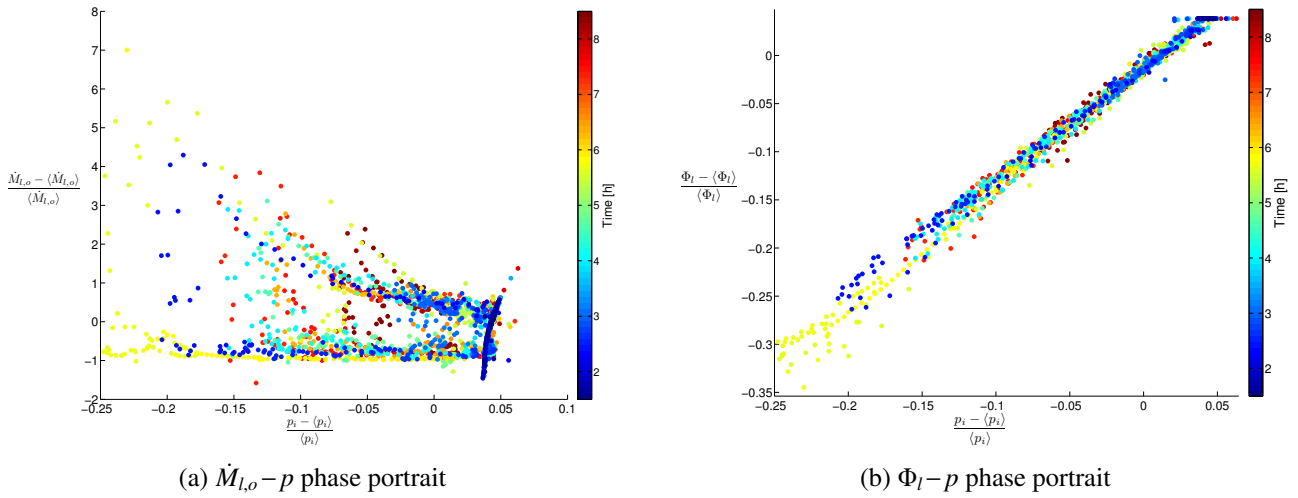
(a) $\dot{M}_{l,o}-p$ phase portrait

(b) Φ_l-p phase portrait

Figure 7.16: Closed inlet with fixed mass sources $\dot{M}_g^s = 0.295\,\mathrm{kg/s}$, $\dot{M}_l^s = 35.55\,\mathrm{kg/s}$. Geometry as in Figure 7.10, only U-bend is replaced with a horizontal pipe segment

amounts these fluctuations would grow if given time, nor what would happen if gas lift was eliminated altogether. In fact, the slugging high-frequency fluctuations found whit LedaFlow were found to be a consequence of predicted terrain slugging in the U-bend at the pipeline outlet, and not a riser slugging phenomenon [18]. With SLUGGIT v.2, the same U-bend terrain slugging is found, but also Tailor bubbles penetrating into the riser appears to generate pressure disturbances. Most likely it is these latter pressure disturbances who case the SLUGGIT fluctuations to be less regular that that of LedaFlow and OLGA.

LedaFlow further predicted bubbly flow in the horizontal and slugging flow in the riser.[21] Bubbly flow, though intermittent on the small scale within the flow itself, physically adopts a continuous character in cross-sectionally averaged properties. A steady and continuous transport of gas into the riser is therefore possible with simulation tools including dispersed flow regimes. No dispersed flow patterns are (presently) available in SLUGGIT, these instead manifesting themselves as bubble-slug flow. Coalescence thereby tend to form all gas in the horizontal into elongated bubbles, distributing the gas discontinuously and irregularly along the horizontal. These will disturb the pressure when entering the riser.

7.3 Full Girassol geometry with well

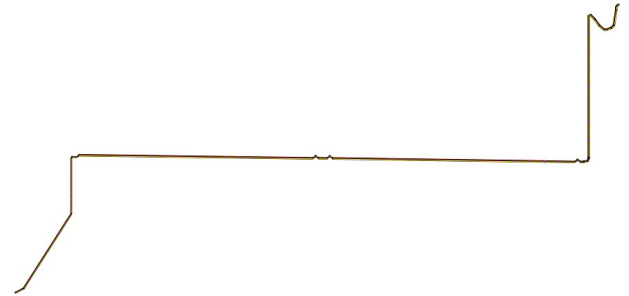Figure 7.17 depicts the full Girassol geometry including the sub-seabed well pipe sections.

Figure 7.17: Full Girassol pipe geometry with well

During the present work a linear pressure-flow rate inlet coupling has been implemented similar to that used in the commercial multiphase code OLGA [12]. Details of this performance index implementation can be found in Appendix C. The productivity index was implemented in order to increase the system similarity to the real Girassol field and comparability to the simulation results of collaborators who work with other models (see Section 1.2.3 and 1.2.1.)

---

[21]LedaFlow animations supplied by Khabibullin.

7.3.1 SLUGGIT v.2

Three simulations will here be described. All have the an inlet productivity index $K = 210\,^{Sm^3}/_{d \cdot bar}$, a well pressure $P_{well} = 252\,bar$, Gas-Oil Ratio $GOR^* = 48.316\,^{Sm^3}/_{m^3}$ and Water Cut $wc^* = 0\,^{m^3}/_{m^3}$ [47, 18]. The GOR and water cut are here adjusted from the field values of $GOR = 103$ and $wc = 0.531$ to approximate both oil and water as a single liquid phase.[22] Because it was found in Section 5.2 that allowing bubble sections larger than 200 times the pipe diameter may cause significant 'numerical numerical terrain slugging', 200 will be the above limit for the `MAX_BUB_COEF` parameter in this section.

The relative velocities under the present flow conditions are thought to be sufficiently high to make hydrodynamic slug creation a possibly significant influence. Two hydrodynamic slug initiation criteria will therefore be tested: The Slug Stability (Bendiksen) (SSB) criterion and the Invicid Kelvin-Helmholtz (IKH) criterion. The former is a criterion seen from the slugging regime, allowing slug initiation when the conditions are such that slugging flow can be sustained. This is simply achieved by initiating slugs when the gas velocity exceeds what would be the bubble nose velocity $v_{b,n}$ from Equation (4.19). The latter of these criteria is seen form the stratified region, and concerns when stratified flow can no longer fluid-dynamically be sustained. It is presented in Annex E. The inviscid version is chosen in order to reduce the computational expense of checking the criteria at each section, every time step. For further details on hydrodynamic slugging criteria, see *e.g.* [25, p. 66-74].

Two simulation cases are here given attention:

Case I: `MAX_BUB/SLUG_COEF` = 200. No modelled hydrodynamic slug initiation.

Description:

t < 0.3 h: Initial transient phase where the pipeline is filled by a stratified liquid hold-up front propagates through the pipeline.

0.3 < t < 0.5: Slugging initiated from the first jumper. Liquid is transported through slugs up the riser.

0.5 < t < 0.8: Slugging from jumpers cease (for some reason.) Separated flow throughout system without liquid production. Liquid builds up in riser as riser hold-up increases.

0.8 < t: Instantaneous formation of a slug in riser and well, blocking both with a full, un-aerated liquid column. The static head rises abruptly at the inlet and becomes larger than the well pressure ($p_i > P_{well}$.) As a result, the inflow through the inlet shuts down and the system comes to a stand still (no backflow through the inlet is allowed, as in OLGA [12].)

Case II: `MAX_BUB/SLUG_COEF` = 200. SSB modelled hydrodynamic slug initiation is active.

Description:

t < 0.25 h: Initial phase. Hydrodynamic slug initiation at beginning of the horizontal pipeline. The system is filled with liquid by a propagating slug-bubble front.

0.25 < t: Steady state production with slugging flow in the horizontal, riser and U-bend, and annular flow in the well. The slug-to-bubble length ratio in the horizontal is on average in the order of 0.1. Consequently, the point at which an increase in well production is balanced by the pressure drop due to friction is relatively high (high production).

---

[22]Even thought three phase simulations are supported in SLUGGIT, this is outside the scope of the present work.
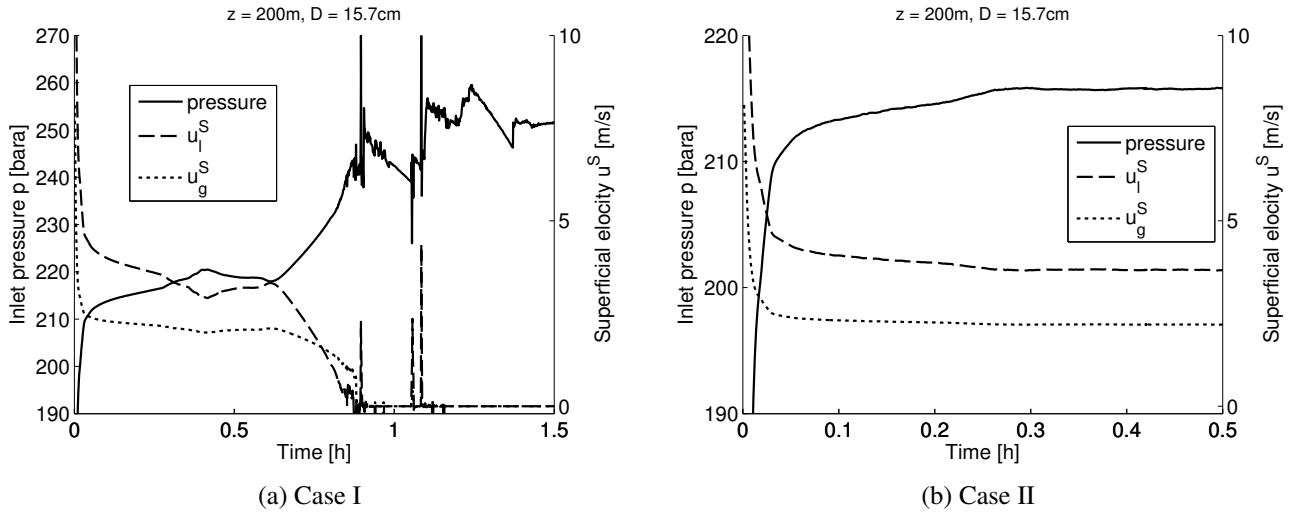
Figure 7.18: SLUGGIT simulated pressure and phase velocities using the performance index inlet boundary conditions. Time trace taken close to well inlet.

The velocity and pressure time traces close to the well inlet are shown for cases I and II in Figure 7.18. A simulation similar to case II has also been carried out using the IKH-criterion (E.3) to actively initiate hydrodynamic slugs. The same dynamic behaviour as seen in case II was then predicted, only slugs were more frequently initiated for then to be destroyed shortly after due to decreasing slug lengths. Consequently, the net difference in choosing the IKH criterion was larger computational expense.

For comparison with the mass source boundary conditions supplied by Eldar Khabibullin and applied in Section 7.2, the steady-state average mass flow rates are computed from the case II simulation. The average liquid production was found to be $\langle \dot{M}_{l,o} \rangle = 56.9$ kg/s, compared with $\dot{M}_{l,i} = 33.7$ kg/s as supplied by Khabibullin.[20] For the gas phase mass flow rate is found to be $\langle \dot{M}_{g,o} \rangle = 1.97$ kg/s, contrary to the supplied boundary condition $\langle \dot{M}_{g,i} \rangle = 1.69$ kg/s. Since phase transition is not presently included in the SLUGGIT code, this steady-state flow rate is constant throughout the pipeline (more on this later.) Naturally, the stand-still in case I results in no production.

It would appear that, depending on minor alterations on the simulation parameters, the predicted steady state solutions take on one of two opposite extremes. Either a complete stand-still solution is found if, at any point, a large enough slug blocks the riser. This is because the well pressure is less than the maximum static head in the Girassol geometry, and the SLUGGIT code lacs gas lift support. The event causing such a blockage usually takes the form of a 'collapse' in the riser; if the liquid fraction in an annular or lightly slugging vertical flow regime is allowed to built up, the upstream pressure will increase and there may come a point where liquid hold-up locally reaches unity. As this happens, the blockage causes a sudden flow retardation and fall-back throughout the riser, turning all riser liquid into a long, un-aerated slug nearly instantaneously. The large hydrostatic pressure increase cased by this event occurring in the riser immediately causes the same event in the well, and to the hydrostatic pressure suddenly increases beyond the well pressure.

Alternatively, the system always manages to clear enough liquid to avoid liquid build-up and blockage. In this situation, a positive feedback takes place during the initial stages; a reduction in riser and well liquid reduces the hydrostatic head, which in turn increases the well production. In the case studied here, increasing well production reduces the overall system liquid fraction, reducing the inlet head even further. At some point, the inlet pressure will be dominated by frictional rather than gravitational forces, forming a high-velocity equilibrium point. Compensating for gas lift by *e.g.*, reducing riser and

74

well length has the effect of eliminating the former flow solution, all predictions becoming the high-velocity ones.

These solutions are contrary to solutions found when computing the same case with LedaFlow or OLGA [18]. The solutions found using these codes are steady, but with less void in the system than the high velocity solutions found with SLUGGIT.[23] These simulations predict bubbly flow regimes in the long horizontal and the annular regime in the riser. Bubbly and droplet flow regimes are not yet implemented in SLUGGIT v.2, and the void in all slugs is assumed to be zero. This may in part explain the difference in prediction.

It is also interesting to investigate whether finer resolution affects the results. A simulation with `MAX_BUB/SLUG_COEF` = 100 is carried out without hydrodynamic slug initiation, along with the exaggerated case of `MAX_BUB/SLUG_COEF` = 1 000. It is hoped that the high relative phase velocities possible in this case study may be sufficient to produce some natural hydrodynamic slug capturing, though obviously not sufficient to be undamped.

Case III: `MAX_BUB/SLUG_COEF` = 50. No modelled hydrodynamic slug initiation.

Description:

t < 0.27 h: Again, initial transient phase where the pipeline is filled by a stratified liquid hold-up front propagates through the pipeline. Slug initiates form first jumper.

0.27 < t < 0.4: Formation of small slugs in the riser. These are blown out. All slug generation ceases.

0.4 < t < 0.5: All-over separated flow. A surge wave of high hold-up propagates up the riser.

0.5 < t < 0.6: Annular flow in the riser collapses and the riser is flooded with un-aerated liquid. The wave front has by then reached about 500 m up the riser.

0.6 < t Annular flow regime in the well collapse. $p_i > P_{well}$ and the system comes to a stand-still.

Case IV: `MAX_BUB/SLUG_COEF` = 1 000. No modelled hydrodynamic slug initiation.

Description:

t < 0.3 h: Initial phase. Separated flow throughout entire system. Vaguely increasing liquid hold-up in riser and well.

0.3 < t: Equilibrium obtained. Steady state production without any slug formation.

Pressure and superficial phase velocity time traces are shown in Figures 7.19. Obviously, `MAX_BUB/SLUG_COEF` = 50 is not a sufficiently fine resolution to obtain any form of hydrodynamic slug capturing. This should perhaps not be surprising as Issa, Kempf and Bonizzi [7, 13] found that a ratio $\ell/D \geq 0.4$ would be necessary for capturing to be reasonably unaffected by further refinement. What is interesting, however, is that a separated flow steady-state solution was found for the coarsely resolved case VI.

The gas and liquid production rates in case VI are found to be $\langle \dot{M}_{g,o} \rangle$ = 0.994 kg/s and $\langle \dot{M}_{l,o} \rangle$ = 28.7 kg/s, respectively. Compared with case II, the flow rates are a little less.

In cases I and III the flow remained stratified some time before a collapse occurred in the riser, while in case VI the flow obtained a steady-state solution with stratified flow throughout the horizontal.

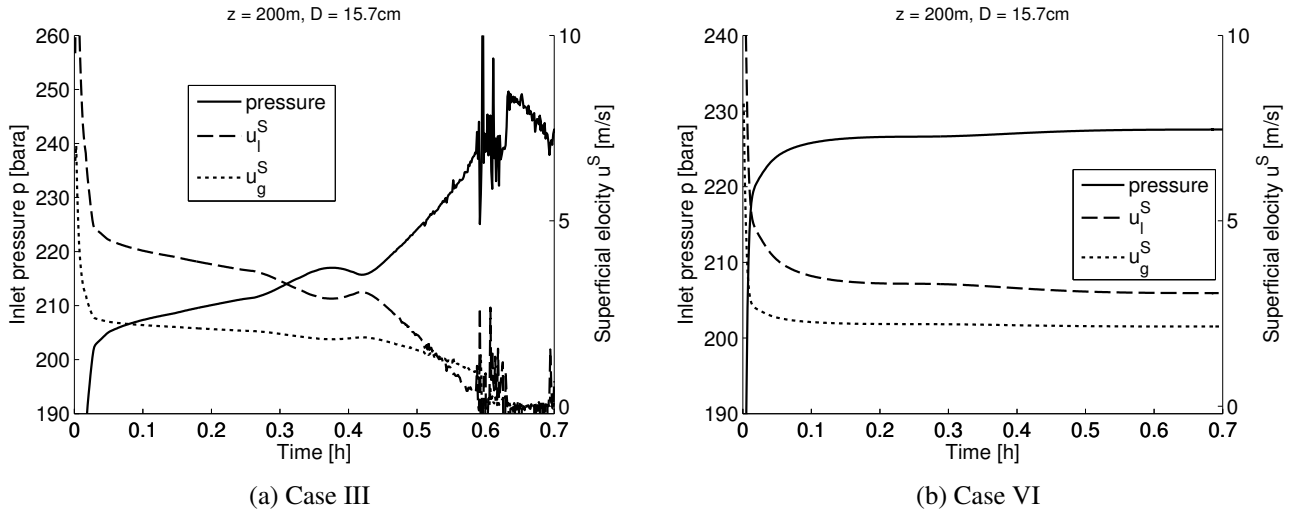[23]Private communication with Eldar Khabibullin.

Figure 7.19: SLUGGIT v.2 simulated pressure and phase velocities using performance index inlet boundary conditions. Time series taken close to well inlet.

Due to the high relative velocities in these cases, one would expect a non-stratified regime in the physical flow. Figures 7.20 and 7.21 display the left and right hand side of the inviscid Kelvin-Helmholtz criterion (E.3) from Annex E at $t = 0.25\,$h and $t = 1.0\,$h from cases III and VI, respectively. The tricky term $\left(\frac{d\alpha_l}{dh_l}\right)$ is handled by a geometric consideration of the sketch in Figure 4.3, where the interface angle γ is found by solving $\frac{1}{2\pi}(\gamma - \sin\gamma) - \alpha_l = 0$ in MATLAB® using the built-in iterative function fzero. $\left(\frac{d\alpha_l}{dh_l}\right) = \frac{4}{\pi D}\sin\frac{\gamma}{2}$ is then obtained. Alternatively, a linearisation provided in [25, p. 49] may be applied within an accuracy of $\pm 2\,\%o$.

Evidently, the IKH-criterion is violated throughout the pipeline. Because the domain of VKH stability is smaller than that of the IKH-criterion, a stratified flow regime should not be able to persist physically as a steady state flow pattern. Some form of hydrodynamic slug initiation mechanism, as in case II, is therefore justified. Further, as was proven by Bonizzi *et al.* [6, 13, 7], the IKH-criterion also marks a necessary criterion for the stratified two-fluid model to have real characteristics (be well-posed) and produce physically reliable solutions. Similar figures of the well-posendess criterion (4.30) are not shown here as they are nearly identical to Figures 7.20 and 7.21. Ill-posedness can manifest itself in un-physical, resolution-dependant disturbance

(see Section 4.11.2). However, due to numerical diffusion, they seldom manifest themselves in discretised sachems unless grid resolution is exceptionally high[24] [13]. Consequently, the ill-posedenss (of the underlying continuous two-fluid model) remain undetected and its influence, if any, unknown. Case VI, where the 'grid' is very coarse indeed, may be a prime example of this, wherein no symptoms are visible, yet the continuous two-fluid model would be ill-posed and the physical solution should, according to the IKH-criterion, be non-stratified.

Also shown in Figures 7.20 and 7.21 are the pipe inclination angles, of which the RHS of the IKH-criterion is dependant. In vertical pipe segments, the RHS of (E.3) reduce to zero and the criterion is unconditionally violated. Physically, this means that a stratified flow cannot be sustained vertically. Instead, if separated, the regime will be annular. In the SLUGGIT model however, only the wetted and interfacial perimeters S_κ, S_{int} are adjusted. These are weighted as a function of pipe inclination to give a smooth transition to an annular flow pattern topology. At the same time, the stratified two-fluid model is solved as if the flow is stratified, including the $\partial_z h$ term in the momentum equation (4.16). Though this term vanishes as the inclination approaches $\pm 90°$, the mid-region of high inclinations is poorly de-

---

[24]It is the *continuous* formulation of the two-fluid model which becomes ill-posed.

fined, assuming partially annular surface perimeters while retaining a phase hight hydrostatic pressure term based on stratified flow. This aside, a separated flow regime, as modelled in the SLUGGIT v.2 scheme in vertical risers, will have complex eigen-

values as the scheme basically incorporates a coarse two-fluid model [16], all be it with adjusted friction terms. Though appearing unproblematic from experience running the code, the effect of ill-posedness in this scenario is not altogether understood.
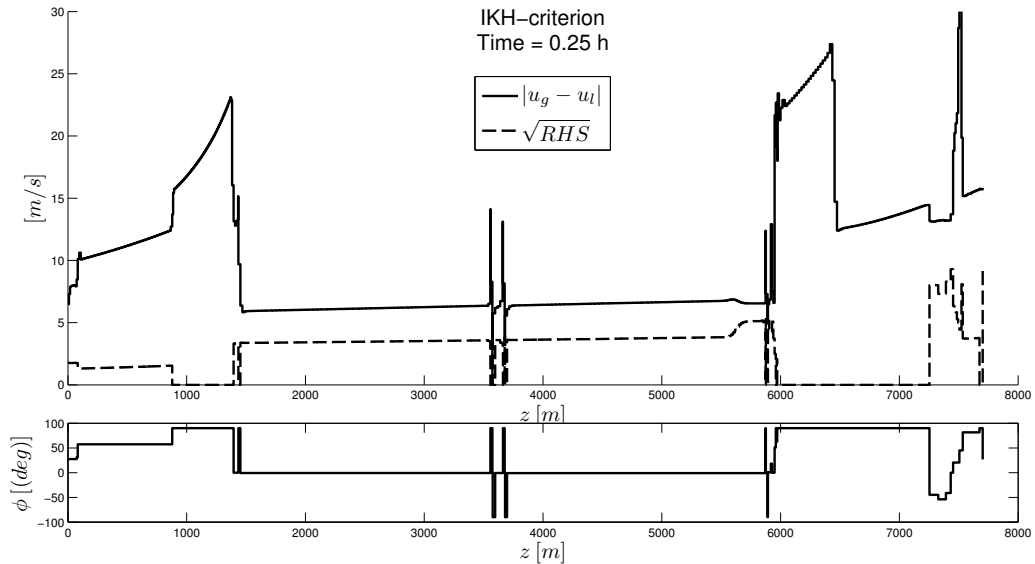

Figure 7.20: Case III simulation. (Square roots of) left and right hand side of inviscid Kelvin-Helmholtz inequality criterion (E.3)
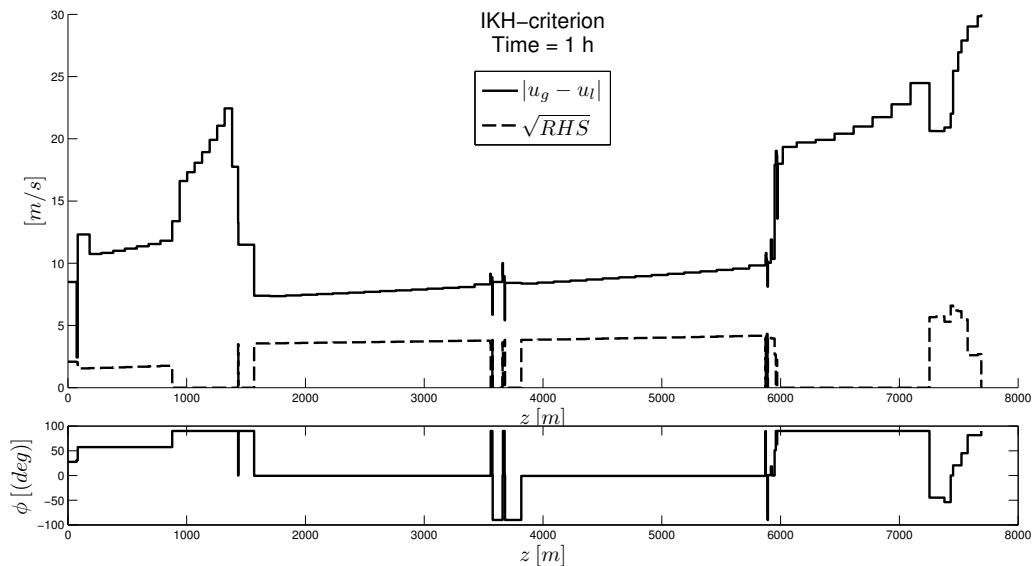
Figure 7.21: Case VI simulation. (Square roots of) left and right hand side of inviscid Kelvin-Helmholtz inequality criterion (E.3)

7.3.2 SLUGGIT v.2s

For comparison, case I is re-simulated using the simplified scheme SLUGGIT v.2s:

Case I-s: `MAX_BUB/SLUG_COEF` = 200. No modelled hydrodynamic slug initiation. Simplified scheme.

Description:

t < 0.25 h: Slug formation takes place only some 50 meters away from the inlet. Slugging flow (slugs and bubbles of about equal length) propagates through the pipeline and up the riser.

0.25 < t < 0.4: Slugs in the horizontal die away as the total liquid fraction in riser increases. The flow slows down, increasing the liquid fraction in the well also.

0.4 < t: In a gradual manner, the inlet pressure approaches the well pressure and the system comes to a stand-still. No liquid production has taken place.

Figure 7.22 shows the pressure and superficial velocities close to the inlet. The simulation shows much higher fluctuations than in the non-simplified case of the previous section. The reason for this is onset of slugging close to the inlet. Notice also that data is taken form the location $z = 20\,\mathrm{m}$, where the diameter is $D = 14\,\mathrm{cm}$, rather than $z = 200\,\mathrm{m}$, where $D = 15.7\,\mathrm{cm}$, as was done previously. The reason for choosing $z = 200\,\mathrm{m}$ was the large section lengths of Case VI, while the location $z = 20\,\mathrm{m}$ in Case I-s was chosen because further away from the inlet the flow was slugging, which gave very intermitted and untidy curves.
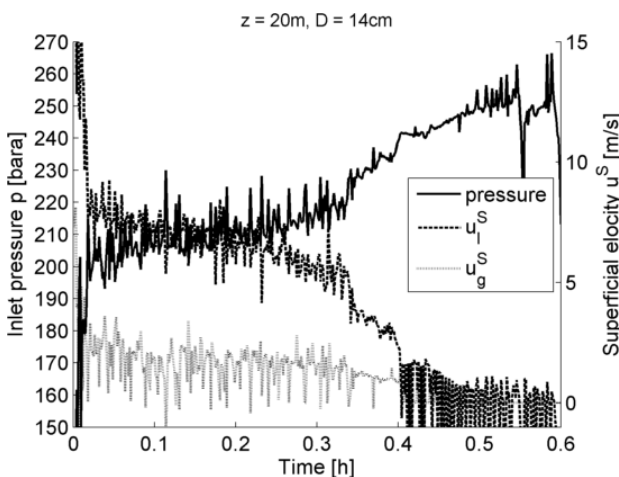

Figure 7.22: Case I-s simplified simulation. pressure and phase velocities using performance index inlet boundary conditions. Time series taken close to well inlet.

So why the difference in prediction? The explanation lies of course in the main method simplifications as they are described in Section 4.2 and Tables 2.

Most importantly, assuming uniform pressure in stratified units denies gas acceleration thought pressure transients, which are likely to be important in the initial formation of the separated regime seen in the unsimplified model. Transient pressure forces counteract liquid build-up. This is demonstrated in Figure 7.23, which shows the spatial pressure profile during the initial stages ($t = 20\,\mathrm{s}$) of the Case I and Case I-s simulations. Here, both simulations show liquid propagation by means of a negative pressure gradients. The non-simplified scheme manages to create this gradient in the stratified/annular regime as gas accelerates and column weight decreases. Due to uniform stratified unit pressure, this is not a possible solution in the simplified scheme. Rather, the formation of slugs are required in order to manifest a pressure gradient. Also seen in Figure 7.23 is how the pressure at the most upstream slug front in the simplified scheme always will equal the outlet pressure. Consequently, this warrants huge mass flow rates initially

Uniform stratified pressure also dismisses the Bernoulli suction phenomenon and the possibility of slug capturing – the area of model stability now differs from that of the two-fluid model. An interesting note to add here is Renault's discovery that first order upwind schemes with velocity-staggered grids (Figure 4.7b), will tend to 'misplace' this Bernoulli suc-

tion one section downstream [37]. Velocity staggered grids are quite common in transient codes, and is found in *e.g.*, SLUGGIT v.2, TRIOMPF and OLGA. A consequence of this is that suction physically causing increasing hold-up locally will numerically induce a pressure gradient in the counter-flow direction, which produce a suction ahead of single-section slugs, possibly promoting liquid propagation and a separated regime in the non-simplified scheme. This gives an incentive for considering pressure-staggered schemes as a substitution.

Further, in excluding the convection terms in the liquid momentum equation, injected liquid is given no initial momentum with which it is transported away from the inlet.

Contrary to the intention and intuition, the simplified scheme ends up requiring a significantly longer computation time than the non-simplified scheme because of the increased complexity accompanied with the slugging flow (particularly through the jumpers.)

The simplified scheme afforded a significantly longer computation time than the non-simplified scheme due to increased the complexity of the slugging flow

Adjusted GOR

Near the end of Section 7.2, an adjustment was made to the inlet flow rate conditions to correct for a misunderstanding that had arisen where mass rates had been defined at standard conditions and so not corrected for phase transfer. This mishap also affects the present section as the *GOR* allegedly also is defined in terms of gas-liquid separation at standard conditions, and not, as was initially though, as the separation at the inlet. Due to the present intrinsic lack of any PVT support in the models codes, the interpretation of the *GOR* as a boundary condition computes the mass flow rates under standard conditions and assumes these phase mass rates to be the mass rates at the inlet. Without PVT support, the conversion form standard cubic meters was done by finding the ratio of density at inlet and standard conditions – see Appendix C.

Conversely, the 'appropriate' way of applying

the supplied *GOR* value is to find the gas-oil-water separation at standard conditions and compute the separation of this mixture back to the inlet conditions using PVT software. The main difference here is that the gas mass at the inlet in considerably less as phase transition causes gas condensation at the increasing pressure.

Khabibullin provided a new approximation of the *GOR* at the inlet under the conditions $p = 122\,\mathrm{bar}$, $T = 63.5\,^\circ\mathrm{C}$, namely $GOR = V_g/V_{oil} = 259\,\mathrm{m^3/d}/1839\,\mathrm{m^3/d} = 0.14\,\mathrm{m^3/m^3}$. Since all PVT support is yet to be implemented in the SLUGGIT code[25], the same procedure as earlier must be employed, only the standard conditions are redefined to closer match the inlet. The 'adjusted standard conditions' are $p^{ST^*} = 122\,\mathrm{bar}$, $T^{ST^*} = 65.3\,\mathrm{K}$. Water cut is assumed unchanged at 53% (though it in reality slightly increased). As before, the *GOR* is further adjusted to an all-oil single phase liquids $GOR^* = (1 - 0.53) \cdot 0.14 = 0.0658$, $wc^* = 0$

Figure 7.24 show pressure and superficial velocity plots for the new *GOR* and 'adjusted standard conditions.' The profiles are seen to be similar to Case I and Case III in Figures 7.18a and 7.19a, respectively. The main difference lies in the reduced volumetric gas flow rate due to the correction for phase transition. Overall liquid fraction increases therefore, also when slugs are hydrodynamically initiated (bubbles between slugs become shorter). Consequently, the liquid fraction in the riser and well become too high, and the flow collapse once the front of the slug-bubble regression has reached some distance up the riser.

It should be emphatically pointed out that adjusting the GOR-value as done here is no a solution to the present lack of PVT-management in the SLUGGIT codes. Earlier it was seen that the difference in gas mass flow rates due to phase transition at the well and outlet conditions are large. Changing the gas mass flow at the inlet does not account for the phase transition which occurs in the riser as local pressure decreases. Consequently, adjusting for a correct gas mass flow rate at the well will generate an
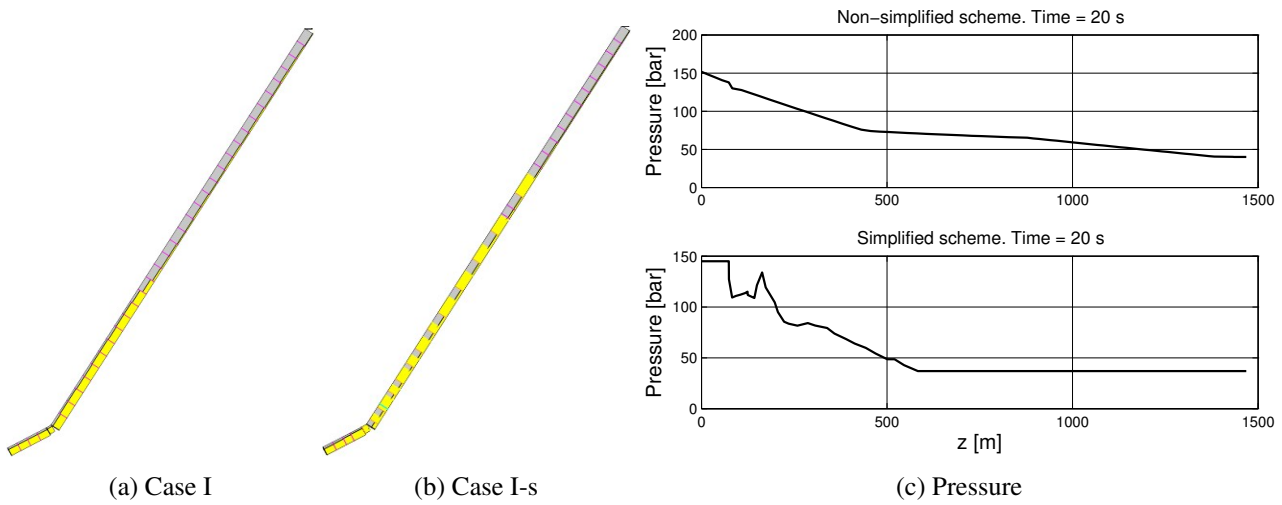
---

[25]This is being done presently by Tor Kjelby.

(a) Case I   (b) Case I-s   (c) Pressure

Figure 7.23: Initial development, simplified vs. non-simplified SLUGGIT scheme $t = 20\,\text{s}$

under-prediction of gas mass flow rate near the outlet. PVT-support is therefore a necessary component in deep-water simulation tools.
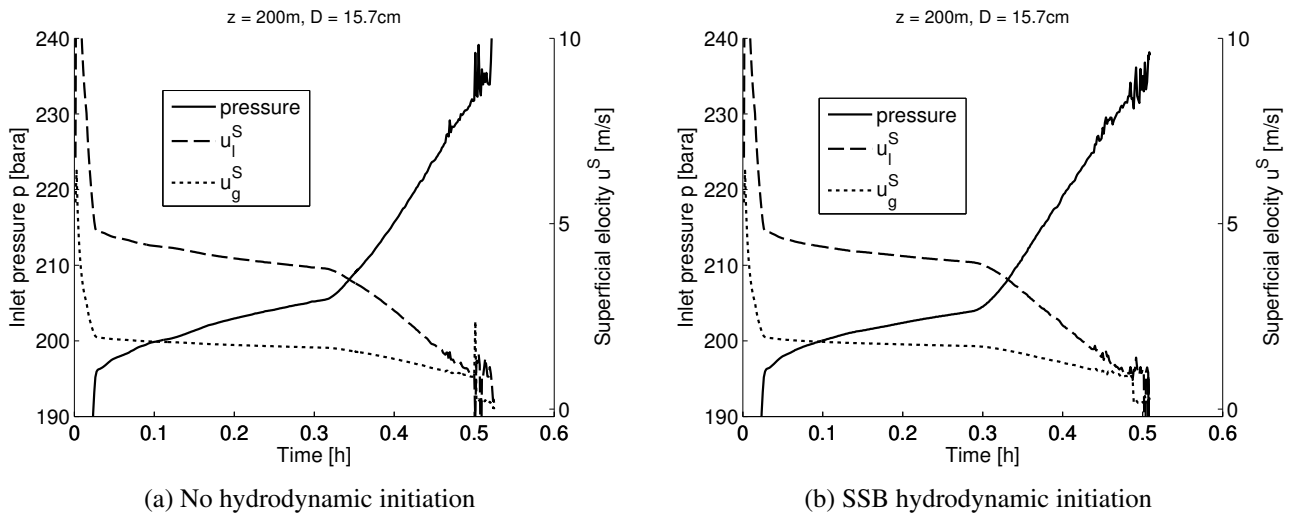

(a) No hydrodynamic initiation   (b) SSB hydrodynamic initiation

Figure 7.24: Adjusted GOR computation. `MAX_BUB/SLUG_COEF` = 200

8   Discussion and recommendations

8.1   Girassol instability

Finding the origin of the P50 Girassol pipeline instability has proven to be challenging task. Though multiple forms of operational instability were generated, none had a period of oscillation in the range of the field data.

Over-predicting slugging frequency seems to be a common problem in most multiphase codes [35]. For the SLUGGIT code, the following obstacles have shown to be particularly troublesome:

Gas lift No field data is available in which the gas injection is switched off altogether. Neither does the data from which it is at its lowest ($70 \, ^{kSm^3}/_d$) ever reaches a steady amplitude of fluctuation. In fact, it is not altogether know whether the P50 pipeline has any production at all without active gas lift. Neither any of the SLUGGIT codes nor the LASSI code has in them any well-functioning support for generating a gas lift in the riser (*i.e.*, placing a gas source at the riser base.) The reason for this is that technical challenges arise when a slug object passes the point at which the gas source is placed. Kjeldby implemented a method for tackling these challenges in his master thesis work [20], though this method caused some pressure disturbances and did not function ideally. Modified gas lift procedures are possible and are likely to be implemented in the near future. An alternative and perhaps preferable way of overcoming the gas source challenge is to implement gas entrainment into slugs. Void in slugs is also recommended to improve the methods' capability of predicting dispersed flows.

PVT treatment It has already been demonstrated, though quite unintentionally, that retrieving the appropriate thermodynamic PVT fluid mixture properties is important in fields where pressure changes are significant. Mainly the issues are those of phase transition, which in this field is found to be of the same order as the produced gas. The influence of this may very well affect the system dynamic as a whole.

Field data controversy The for publication reported by Zakarian and Larrey [47] does not altoghther match the field data [43] from which all the pressure information originates. Where the former supplies a liquid flow rate $\langle \dot{M}_{l,i} \rangle = 33.7 \, ^{kg}/_s$, the mean volumetric flow rate is found to be $1\,288 \, ^{Sm^3}/_d$ in the latter, or $14.9 \, ^{kg}/_s$. Though there probably exist a natural explanation for this, it does serve to reduce confidence in the data.

Limited flow regimes All of the EPT slug tracking methods presently rely on the base assumption that all simulated flow regimes can be represented by slug and stratified flow objects. In Section 5 and 7, it was found that the limited number of flow regimes – particularly the absence of a dispersed flow – may reduce the domains of model stability.

In Section 5.4 it was found that the SLUGGIT v.2/v.2s codes had difficulty in obtaining steady flow at low liquid, high gas flow rates. This is particularly disconcerting since flow stability is here the main focus.[26] Similarly, it was found is Section 7.3 that the SLUGGIT v.2/v.2s codes predicted high pressure fluctuations in comparison to LedaFlow and OLGA simulations carried out by Khabibullin [18]. Occasional release of coalesced tailor bubbles into the riser was found to cause a part of the fluctuations in the SLUGGIT simulations, while LedaFlow and OLGA had predicted bubbly flow regimes in the horizontal. On the other hand, due to lack of gas lift and confusion surrounding inlet boundary conditions, the basis for comparison is questionable.

Implementation of gas entrainment in slugs is likely to improve this condition. The SLUGGIT v.1 code by Pascal Klebert already have this feature installed, but could not be tested during this work due to technical problems with the code. Bonizzi *et al.* [7] investigate the influence of entrainment into their slug capturing code TRIOMPF. In the limited and simple cases investigated in this publication it was found that the effect was not severe, but corrected an otherwise erroneous trend where increasing mixture velocity would also increases mean hold-up in the V-section case.

Limited focus on vertical flow All investigated slug tracking methods have been developed based on the principle of the stratified two-fluid model. During the present work, these methods have unquestioningly been

---

[26]Some reserves should here be made. It is not entirely clear whether this is due to the model fundamentals or short-comings in the current management procedure. The SLUGGIT v.2/v.2s are being continuously developed and differences in stability predictions within resent versions may suggest the latter.

applied to vertical risers. In the case where the flow regime is predicted to be slugging with short units (often method-equivalent of bubbly flow,) the SLUGGIT methods reduce to an empirical slug specification model in which the bubble propagation correlations and mass balances govern the flow.

Some assurance is provided by the fact that test simulations provided excellent correspondence to the steady-state model in Appendix A, provided a reasonable maximal section length. With high gas rates however, the riser flow will on the other hand be annular. Even with some correction for the friction perimeters, the liquid height gradient term $\partial_z h \cos \phi$ will disappear form the (stratified) two-fluid model. Consequently, the pressure treatment will be equivalent to applying the constant cross-sectional pressure assumption in a simplified two-fluid. As was shown in [16, p. 69-70], or in expression (4.30) for that matter, this simplified two-fluid model is then unconditionally ill-posed. Though this topic is somewhat controversial, it seems to this author at least that some effort must be made, either in ensuring well-posedness, or in proving an evidential basis, for it to be fully accepted in a scientific community.

Another point which presently seems weak in the LASSI and SLUGGIT codes is the 90°bend at the riser inlet. Appropriate slug formation here has been found to be vital for obtaining the correct flow pattern in the riser, which in turn has a strong effect on the system dynamic as a whole. Bend initiation criteria have not proven to be all together successful in this respect, partially because this criterion requires inflow towards a low-point from both directions. The presently developed pipe class for bent pipes may improve these matters, but would still require high section length refinement in bend regions.

Although the type of pressure fluctuations observed in the field data [43] (Figure 1.3) has not been recreated, much has been learned about the instability characteristics and how they apply to the Girassol field case. In Section 7.1, various forms of oscillatory behaviour related to the fixed-pressure 'open inlet' boundary conditions were discovered. Here, geometric features of the pipeline, centrally the jumpers and U-bend, were given special attention. Reproducing oscillations particularly caused by gas expansion in the riser was attempted successfully, including the dynamic described as 'expansion driven instability' in the assignment description of this thesis. Also a surprising feature of this investigation was that oscillations in the U-bend may play a role in operation instability dynamics involving pipeline upstream of the riser. Despite these findings, it was in general observed that the oscillating pressure profiles corresponded poorly with the field data measurements. Periods of gas accumulation in jumpers, and oscillation periods generated from the void waves created therefrom, were both found to be short (usually less than an hour.) These would yield pressure fluctuations that were occasional and spiky, rather than possessing a slow, sinusoidal character of the field data. Although riser expansion is likely to be a key component in the field instability, the suggested mechanism of expansion driven fluid accelerations 'pulling

with it' additional gas from jumpers (Cycle A) seems very unlikely for two reasons. Firstly, the proximity of the gas congestion would be too close to the riser to produce periods of three hours. Secondly, the entrapment volume of the risers and pipeline does not seem sufficient.

Gas release caused by upstream expansion is also a possibility. Again though, the only upstream entrapment volume big enough is likely to be the well itself. If so, the mechanism is actually equivalent to the favoured void wave Cycle B.

All the instabilities observed in the open inlet configuration appeared to be very sensitive to changes in geometry, and inlet hold-up and pressure. Small changes have been found to cause or reverse operational instability mechanise, and even uncovering unexpected new ones.

In Section 7.2, the fixed fluid flow rates boundary condition was tested. Severe slugging obtained using $\dot{M}_{g,i} = 1.69 \, \text{kg/s}$ and $\dot{M}_{l,i} = 33.7 \, \text{kg/s}$ was found to give slugging periods of about 30 min and tip-to-tip amplitudes of approximately 60 bar. Compared to the 3 h periods and 35 bar tip-to-tip amplitudes of the field data, the match is poor. The flat-top form sinusoidal of the field data also compares poorly with the sharp zig-zag pressure pattern of terrain slugging. In

terms of amplitude, it must again be underlined that it is unknown how the field pressure would develop if allowed to grow.

Recently made corrections of the mass source conditions gave a different response altogether. Here, the rate of gas injection was so low as to make gas production only occasional, as Tailor bubbles from time to time penetrated into the riser. The restricted gas amounts reduced the volume of upstream compressibility, while the riser was mostly un-aerated. Pressure fluctuations were found to originate both form the U-bend and the events wherein a Taylor bubble enter the riser. Again, fluctuation periods and amplitudes were too short.

The full geometry simulations with the productivity index inlet boundary condition of Section 7.3 was though to offer the greatest hope of reproducing the field instability. The main reason for believing so is the long oscillation periods in the field data. Should these oscillation be caused by a transport phenomena, as opposed to some sort of build-up as in terrain slugging type I or gas pocked build-up, the distance of transport need to be vast. It is likely that the entire pipeline – from inlet outlet – is involved.

Wave phenomena similar to that described in Cycle B seems the most plausible explanation in this respect, particularly due to the way such a cycle would generate a sinusoidal pressure profile, as well as be strongly dependant upon the operational state of gas lift injection – both in terms of how gas injection affects the flow in a stabilising manner, and in term of how a change in gas lift state would cause a disturbance kick-starting this type of operational instability. This was discussed in more detail in Section 3.2. Since well response is crucial for such density-wave instability dynamics to take place, further investigation into well-replicating boundary conditions on the inlet may be beneficial in investigating this field case.

Disappointingly, unless liquid accumulation in the riser was continuously counteracted by upstream hydrodynamic slugs, the system would come to a stand-still. Most simulation indicated the stand-still outcome, which is an easily verifiable solution as the un-aerated inlet static head of filled riser and well will exceed the well head. If not at a stand still, the system would show no signs of operational instability.

Again, these results appear to have been affected by the misunderstanding concerning the inlet conditions (*GOR* definition in terms of phase transfer). Only stand-still solutions were found when applying an approximate *GOR* based on 'adjusted standard conditions'. Adjusting the *GOR* and standard conditions is not a solution to the PVT problems, and the differences in prediction demonstrate that the productivity index implementation is not complete until such support is available. Naturally, the mix-up in inlet conditions also serves as a reminder of the importance of supplying detailed, accurate and verified case information.

8.2 Method considerations

LASSI: The investigatory part of this thesis began by testing the codes' ability to handle the vertical riser geometry. The LASSI code [36] failed these tests brutally, the cause rooted in a inclination-dependant failure to conserve mass. Since the formulation of the LASSI model is presented in an entirely mass-conservative manner in [37], it is assumed that the lack of mass conservation is due to an implementation error, possibly in the section management procedure. Whether finding and solving this bug would be a small or large task is unknown, but it is imperative if the scheme is to be applied for any future purpose.

Based on the results published in [37], one may postulate how this scheme may fare in comparison to the SLUGGIT schemes for this case study. In the horizontal of the Girassol case the LASSI scheme would probably hold certain advantages, such as waves and slug capturing. The method is however not developed for the purposes of vertical flow, and so would have little advantage in the riser and well. Further, simulating with the resolution required for grid-independent wave functionality would entail significant computational cost in a pipeline of the field dimension. In [37], section lengths at the or-

---

[27]Even though the LASSI code [36] is more simply implemented and so therefore runs significantly quicker than SLUGGIT for the same number of sections and time steps.

der of the pipe diameter is normally applied, which would be impossible in a field study.[27] On the other hand, also SLUGGIT simulations are clearly affected by section length when pushed beyond a limit. In field tests this was found to begin affecting the simulations as `MAX_BUB_COEF` passed 200. More specific statistical properties, such as slug frequency and length, are likely to be affected by resolution in SLUGGIT for far smaller section lengths.

SLUGGIT v.2s: In the full-geometry simulations, the simplified scheme gave slugging flow starting at the inlet due to intrinsically uniform pressure in stratified units. Though it should be mentioned that it is not really known what flow regime is physically appropriate at the inlet of the Girassol field case, it is an important drawback of the simplified scheme is that achieving an separated flow solutions in highly inclined pipe segments becomes nearly impossible. Only with massive interfacial friction forces can liquid be driven upwards without the assistance of a stratified/annular pressure gradient. Otherwise, the simplified scheme only really support slugging flow. Therefore, the simplified scheme is most appropriate when the physical flow regime consists of relatively short bubbles. If bubble units are single section sized, than, apart from neglecting the convective terms in the momentum equation, the simplified and non-simplified schemes are equivalent, removing the benefit of simplification altogether.

Perhaps it is possible to create a hybrid environment within which the simplified treatment changes if bubble units grow too long. This would however cause management challenges in the transition from 'short' to 'long' bubbles which probably would sabotage the intended simplicity.

8.3   Recommendations and suggestions

In order to perform reliable deep-water simulations the challenges listed in the beginning of Section 8.1 must be addressed.

In particular gas lift and PVT support seems vital. Alternative border restriction procedures for allowing gas sources to be placed independently of slug presence have been suggested. Though this would be interesting to test, enabling gas lift by means of implementing gas entrainment into slugs is the preferred approach since gas entrainment in itself also a suggested improvement. Further, the slug initiation routine during terrain slugging needs to be investigated with focus on operational stability regime.

Because density wave instabilities, as described in Section 3.2, seems a plausible cause of the field instability, further investigation into density waves may prove fruitful. Further development of the well relation applied to the inlet boundary may also be necessary in this endeavour.

Incorporating gas entrainment in slugs may reduce the fluctuations form Taylor bubbles entering the riser in low-gas systems, such as those seen in Figure 7.24. It may possibly also improve conformity to the terrain slugging flow map tested in Section 5.4.

All slug tracking method discussed here have been developed for near-horizontal flow. It may be necessary with further development of the method intrinsics with particular focus on vertical flow. In essence, this concerns expanding the extent of supported flow patterns so that they are appropriately defined in vertical pipes. On the other hand, expanding the methods excessively may go against the ideal of simplicity and 'reducing to essentials' on which the methods are founded.

During the flow map testing in Section 5.4, it was found that both criteria and the procedure by which slugs were initiated at the riser inlet dip were determining factors in the method's ability to reproduce experimentally determined operational regimes. Criteria and initiation procedures are however developed and changes continuously, affecting stability behaviour both for better and worse. In the opinion of the author, finding a general-purpose model which will be capable of generating appropriate terrain slugging for all possible pipeline configurations, similar to the bend initiation procedure, would be difficult and require much special case treatment. Rather, these areas of the geometry, which are subject to much activity and influence the system as a whole, need the appropriate resolution. Presently, the only way of reducing allowable section length is to do so across the entire pipeline.

It should, however, be a simple task to allow for location dependant length parameters. This could reduce computational time significantly while retain-

ing an appropriate resolution where it is needed. An important feature in this respect however, is that the dynamic time step regulation sets the time step according to the smallest Courant number found across the entire pipeline. Broadly stated, this implies that a local section refinement would still be accompanied by a proportional increase in computation time (which is better than the quadratic increase found otherwise – see Section 4.5). An idea in this concern is an intermediate computation; in a region of pipe where resolution is sought to be increased, say a distance reaching form one slug-bubble border to another, the local section lengths could be halved locally. Rather than making extra computations across the entire pipeline, an intermediate computation $n+\frac{1}{2}$ is computed in this region only. For the mass equation, this would be unproblematic since mass fluxes across bubble-slug borders are already computed explicitly. The implicitness of the pressure-momentum equation system would however be disturbed. This latter obstacle holds equally for the trouble of parallelising the code, which would also involve a 'seam' across which implicitness is broken.

When considering the simplified v.2s versus the non-simplified v.2 SLUGGIT schemes, it is the authors opinion that the simplified scheme will be suited for some special slugging cases only, and that in these cases the simplification benefit in terms of computational savings is limited. Instead, there is at the moment thought to exist a significant potential in optimising and improving the efficiency of the SLUGGIT v.2/v.2s code [21] as a measure for reducing computational costs. Also, though it may be that the simplified scheme has an advantage in terms of robustness, the non-simplified scheme has benefited from more development, debugging and testing.

Lastly, the author is absolutely adamant that the continued development should take place within one single unified framework. It is a great misfortune that the three codes, SLUGGIT v.1 [23], SLUGGIT v.2/v.2s [21] and LASSI [36], have all developed independently. Even the time afforded within a master thesis work did not prove sufficient to become ad-

equately familiarised with each code. Nor, for that matter, to find and remove enough bugs for the case simulation to run. It would appear unlikely, or at leas not recommendable, that the hours required in developing each of these codes to a robust level ever be afforded. Rather, the methodologies of each can be implemented in a unified framework, utilising as much as possible of the same management code and regulation features. This is also a vital point for the validity of comparison; are core method differences to be appreciated with clarity, all other features of management should remain the same (grid, time step, inlet, outlet, exception handling, closure relations, turning and hydrodynamic slug initiation criteria, etc..)

8.4   Final comments

It should not be forgotten that the field data to which a comparison has been attempted is the field response to a particular event, namely the momentary withdrawal of gas lift support from a stable to an unstable state. Possibly the oscillations seen is the beginning of a highly transient process which eventually would bring the system, from initial steady, gas-lift supported conditions, down to a stand-still. In this case, obtaining similar transients while initiating *from* a stand-still condition *without* gas lift would indeed be impossible. It may also be that the oscillations from the field data would continue to grow. In any event, since the data presents merely an uncompleted transition from one state to another, only comparison of the same transition process can be said to be appropriate. This is not possible at present.

The goals put forth in this thesis work was to investigate the EPT slug tracking schemes' ability to recreate real-life oilfield slugging dynamics using the P50 Girassol field pressure data as a benchmark for comparison. At the same time, finding the hitherto undocumented caus(es) of the oilfield's unstable operation was put forth as a supplementary goal. Accordingly, it has here been attempted to verify model behaviour using field data, *and* investigate operational instability mechanisms using those same models. This constitutes a type of 'mutual benchmarking' – always a questionable business indeed.

9 Conclusion

The slug tracking models, in combination with the PLOTIT visualisation tool, have shown to be particularly well suited in helping to understand pipeline flow dynamics. Not only in the clarity of visualisation does this become apparent, but also in the way in which the code is open and easily modifiable. This offers an unique ability to investigate the influence of phenomena and flow mechanisms by making them accessible for direct phenomenological manipulation.

At present, the SLUGGIT and LASSI codes does not seem mature enough handle deep water riser systems reliably. In particular, these codes still lack

- Support for gas sources capable of handling passing slugs (gas lift).

- PVT-support accounting for high-pressure compressibility and phase transition.

- Models developed for vertical and dispersed flow regimes.

Prediction sensitivity to mostly intuition-based management procedures is also an issue.

Although not directly reproducible, the present study indicates that the field instability is produced, at least in part, by some wave phenomena involving long stretches of pipeline, and probably also the well. The sinusoidal character of pressure measurements suggests density or surge waves, similar to Cycle description B.

References

[1] Andreas H. Akselsen and H.I. Andersson. The Effect of Near Wall Resolution on Turbulence Statistics using the Lattice Boltzmann method, 2011. Project thesis, NTNU.

[2] N. Apazidis. Influence of bubble expansion and relative velocity on the performance and stability of an airlift pump. *Int. J. Multiphase Flow*, 11(4):459–479, 1985.

[3] D. Barnea and Y. Taitel. Kelvin-Helmhotz stability criteria for stratified flow: viscous versus non-viscous (invicid) approaches. *Int. J. Multiphase Flow*, 19(4):639–649, 1993.

[4] K.H. Bendiksen. An experimental investigation of the motion of long bubbles in inclined tubes. *Int. J. Multiphase Flow*, 10(4):467–483, 1984.

[5] K.H. Bendiksen, D. Malens, R. Moe, and S. Nuland. The Dynamic Two-Fluid Model OLGA: Theory and Application. *SPE Production Engineering*, pages 171–180, 1991. Inst. for Energy Technology, Norway.

[6] M. Bonizzi. *Transient one-dimensional modelling of multi-phase slug flows.* 2002.

[7] M. Bonizzi and R.I. Issa. A model for simulating gas bubble entrainment in two-phase horizontal slug flow. *Int. J Multiphase Flow*, 29:1685–1717, 2003.

[8] S. Chandrasekhar. *Hydrodynamic and Hydromagnetic Stability*. Oxford University Press, 1961.

[9] Y.-H. Chenga, J.-R. Wangb, H.-T. Linb, and C. Shih. Benchmark calculations of pressurizer model for Maanshan nuclear power plant using TRACE code. *Nucl. Eng. Des.*, 2009.

[10] A. De Leebeeck and O.J. Nydal. Simulation of large amplitude waves in a slug tracking scheme compared to roll wave experiments at high pressure. *Int. J. Multiphase Flow*, 36:40–50, 2010.

[11] H. Dhulesia and D. Lopez. Critical evaluation of mechanistic two-phase flow pipeline and well simulation models. In *SPE Annual Technical Confrence and Exhibition*, pages 393–402, oct. 1996.

[12] Houston: SPT Group. *OLGA user manual - transient multiphase flow simulator*, 2006.

[13] R.I. Issa and M.H.W. Kempf. Simulation of slug flow in horizontal and nearly horizontal pipes with the two-fluid model. *Int. J. of Multiphase Flow*, 29:69–95, 2003.

[14] F.E. Jansen, O. Shoham, and Y. Taitel. The elimination of severe slugging – Experiments and modeling. *Int. J. Multiphase Flow*, 22(6):1055–1072, 1996.

[15] Monika Johansen and O.J Nydal. *An experimental study of the bubble propagation velocity in 3-phase slug flow*. PhD thesis, Norwegian University of Science and Technology. Department of Energy and Process Engineering, Trondheim, 2006.

[16] S.T. Johansen, T. Ytrehus, and K.E. Einarsrud. Modeling of Multiphase Flows. Compendium of PhD course EP8404, Multiphase Flow Modeling, Norwegian University of Science and Technology.

[17] E. Kaun and O.J. Nydal. Expansion driven Unstable Two Phase Flows in Long Risers and Wells. Master's thesis, Norwegian University of Science and Technology. Department of Energy and Process Engineering, Trondheim, 2011.

[18] Eldar Khabibullin. Multiphase pipe transport of oil and gass: Dynamic simulation of Girassol field case, 2011. Project thesis, NTNU.

[19] T.K. Kjeldby, R. Henkes, and O.J. Nydal. Slug tracking simulations of severe slugging experiments. In *World Academy of Science, Engineering and Technology 78*, pages 928–933, 2011.

[20] Tor K. Kjeldby and O.J. Nydal. Simulation of expansion driven flow instabilities in long risers. Master's thesis, Norwegian University of Science and Technology. Department of Energy and Process Engineering, Trondheim, 2010.

[21] J. Kjølaas, T.K. Kjelby, and A.H. Akselsen. Sluggit source code, 2012. Referred to as "SLUGGIT v.2" and "v2s" in the present work, documentation: [22].

[22] Jørn Kjølaas. *Plug propagation in multiphase pipelines: Modeling and small scale experiments*. PhD thesis, Norwegian University of Science and Technology. Department of Energy and Process Engineering, Trondheim, May 2007.

[23] P. Klebert and O.J. Nydal. Sluggit source code, 2004. Referred to as "SLUGGIT v.1" in the present work, documentation: [24].

[24] Pascal Klebert and O.J. Nydal. SLUGGIT, Models and numerical implementation, October 2004. Post-Doc work.

[25] Olav Kristiansen and O.J Nydal. *Experiments on the transition from stratified to slug flow in multiphase pipe flow*. PhD thesis, Norwegian University of Science and Technology. Department of Energy and Process Engineering, Trondheim, 2004.

[26] R.T. Lahey Jr. Void Wave Propagation Phenomena in Two-Phase Flow (Kern Award Lecture). *AIChE*, 37(1):123–135, 1991.

[27] E.W. Llewellin, E. Del Bello, J. Taddeucci, P. Scarlato, and S.J. Lane. The thickness of the falling film of liquid around a taylor bubble. *Proceedings of the Royal Society*, 468(A):1041–1064, 2012.

[28] T.S. Mayor, A.M.F.R. Pinto, and Campos J.B.L.M. Hydrodynamics of gas-liquid slug flow along vertical pipes in turbulent regime – A simulation study. *IChemE*, 2007.

[29] T.S. Mayor, A.M.F.R. Pinto, and Campos J.B.L.M. On the gas expansion and gas hold-up in vertical slugging columns – A simulation study. *Chemical Engineering and Processing*, 2007.

[30] B. Müller. Introduction to Computational Fluid Dynamics. Lecture Notes in Computational Heat and Fluid Flow, August 2011.

[31] O. Novak. PLOTIT (SLUGGIT, LASSI and OLGA data visualization programme), March 2012. Plotit is using and/or is based in part on the work of the Qt library, Qwt project and QwtPlot3D project. EPT, NTNU.

[32] O.J. Nydal. Excerzise 2 – severe slugging. Course TEP4250 - Multiphase Transport and the Norwegian University of Science and Technology.

[33] O.J. Nydal, M. Audibert, and M. Johansen. Experiments and modelling og gas-liquid flow in an s-shaped riser. 1998.

[34] O.J. Nydal and S. Banerjee. Dynamic slug tracking simulations for gas-liquid flow in pipelines. *Chem. Eng. Comm.*, 141-142:13–39, 1996.

[35] P.F. Pickering, G.F Hewitt, M.J. Watson, and C.P. Hale. The prediction of flows in production risers – truth & myth? Published online, `http://www.feesa.net`, 2001.

[36] Fabien Renault. Lassi source code, 2007. documentation: [37].

[37] Fabien Renault and O.J. Nydal. *A Lagrangian slug capturing scheme for gas-liquid flows in pipes*. PhD thesis, Norwegian University of Science and Technology. Department of Energy and Process Engineering, Trondheim, 2007.

[38] L. Sinègre and N. Petit. Distributed delay model for density wave dynamics in gas lifted wells. In *44th IEEE Conference on Decision and Control, and the European Control Conference*, pages 7390–7397, des. 2005.

[39] R. Skartlien, E. Sollum, P. Meakin, K. Furtado, and I.E. Smith. The Lattice Boltzmann Method with applications to multi-phase flow containing interfacially active components. Des. 2008. Institute for Energy Technology (IFE), Norway.

[40] Y. Taitel. Stability of severe slugging. *Int. J. Multiphase Flow*, 12(2):203–217, 1986.

[41] Y. Taitel, S. Vierkandt, O. Shoham, and J.P. Brill. Severe slugging in a riser system: Experiments and modeling. *Int J Multiphase Flow*, 16(1):57–68, 1990.

[42] H. Tennekes and J. L. Lumley. *A First Course in Turbulence*. The Massachusetts Institute of Technology, 1972.

[43] TOTAL, 2005. Field data from the Girassol oil field. Received with permission from TOTAL.

[44] M. van Dyke. *An Album of Fluid Motion*. The Parabolic Press, Stanford, California, 1982.

[45] H.K. Versteeg and W. Malalasekera. *An Introduction to Computational Fluid Dynamics: The Finite Volume Method*. Pearson / Prentice Hall, Harlow, 2 edition, 2007.

[46] F.M. White. *Fluid Mechanics*. McGraw-Hill, sixth edition, 2008.

[47] E. Zakarian and D. Larrey. A Systematic Investigation of Girassol Deepwater-Field Operational Data To Increase Confidence in Multiphase Simulation. Feb. 2009.

[48] M. Zastawny, G. Mallouppas, F. Zhao, and B. van Wachem. Derivation of drag and lift force and torque coefficients for non-spherical particles in flow. *Int. J. of Multiphase Flow*, 39:227–239, 2012.

Appendices

A A model of void in risers

In this section, a steady state model designed to compute the void fraction in vertical risers is developed from base principles. Although somewhat of a digression from the main topic of the EPT dynamic multiphase models, it is ventured upon as it will provide some basis of model comparison and evaluation. Though experimental measurements are perhaps preferred for the purpose of validation, the basis for comparison with the large Girassol field case [47] is not ideal. Also, this theoretical analysis may be used to gain some insight into how gas lift, or the lack such, affects the result when comparing with field data (Section 5.3.) A theoretical model with which to compare is, therefore and in of itself, valuable. Additionally, it opens for the inclusion of theoretical analysis into the present thesis work.
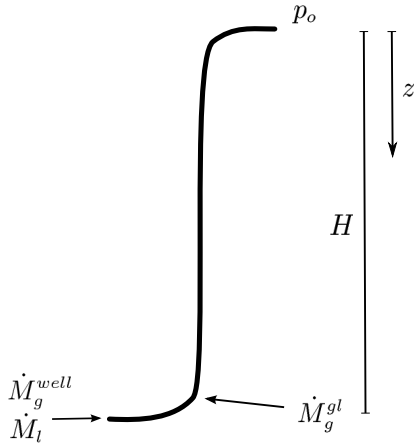
Figure A.1: Riser with gas lift
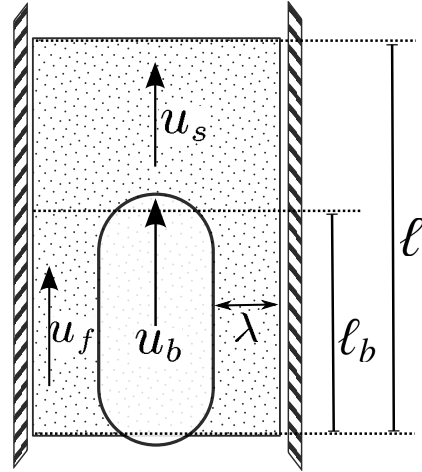
Figure A.2: Bubble-slug unit

Figure A.1 presents a sketch of the layout for this analysis. The gas inflow stem from both the well and the gas lift, so

$$\dot{M}_g = \dot{M}_g^{gl} + \dot{M}_g^{well}$$

while liquid is only supplied from the well.
The following assumptions are used:

Assumptions D. *Riser steady state void model*

D.1 The liquid phases can be approximated as a single phase (two fluids)

D.2 The production is at steady state, *i.e.* the mass fluxes of both fluids, are constant in time and space.

D.3 The riser is fully vertical.

D.4 The gas propagates as large Taylor bubbles so that the empirical bubble nose velocity from Section 4.8 can be used to approximate the gas velocity – *i.e.*, $u_b = v_{b,n}$

D.5 The local bubble area fraction $\alpha_b(z)$ never reach unity.

90

D.6 Bubble film thickness acquire a practically constant value some short distance downstream from the bubble nose.[28]

This analysis will be based on the schematic of Figure A.2. The ratio of bubble and slug lengths will be important in this respect, and so the following local, mean bubble length fraction Γ is defined, together with the local average bubble cross-section area fraction α_b

$$\Gamma \triangleq \frac{\ell_b}{\ell} \qquad \alpha_b \triangleq \frac{A_b}{A} = \frac{(r - \lambda_f)^2}{r^2}$$

Applying the steady state assumption D.2, mass balances may be applied using to mass rates to provide two equations. Also, doing a liquid mass balance across slug and bubble film, one can retrieve expression (4.21) in Section 4.8. As declared in Assumption D.4, the empirical bubble nose velocity expression of Section 4.8 is used to express average bubble velocity:

$$\dot{M}_g = \rho_g u_b A \Gamma \alpha_b \qquad\qquad \text{(A.1a)}$$

$$\dot{M}_l = \rho_l u_s A (1 - \Gamma) \cdot 1 + \rho_l u_f A \Gamma \cdot (1 - \alpha_b) \qquad \text{(A.1b)}$$

$$u_b = \frac{u_s - (1 - \alpha_b) u_f}{\alpha_b} \qquad\qquad \text{(A.1c)}$$

$$u_b = 1.2 u_s - U_v \qquad\qquad \text{(A.1d)}$$

As before, b, s and f denote 'bubble', 'slug', and (liquid) 'film', respectively.

Equations (A.1) produce a system of four equations and five variables $\{u_s, \ u_b, \ u_f, \ \alpha_b, \ \Gamma\}$. As it turns out, the variables Γ and α_b collapse into the variable of interest – the average gas volume fraction $\langle \alpha_g \rangle = \alpha_b \Gamma$. Solving system (A.1) is a tedious task, the details of which the reader will be spared. The procedure is to contract (A.1d) and (A.1c) into (A.1a), and then attack (A.1b), solving for Γ and multiplying by α_b. Gas density is handled by substitution using the ideal gas law. Using caution, this produces:

$$\langle \alpha_g \rangle = \frac{U_{c1}}{U_{c2} \, p + 1.2 U_{c1}} \qquad\qquad \text{(A.2)}$$

where the mean gas volume (void) fraction $\langle \alpha_g \rangle = 1 - \langle \alpha_l \rangle$ is defined by

$$\langle \alpha_g \rangle(z) \triangleq \lim_{t \to \infty} \frac{1}{t - t_0} \int_{t_0}^{t} \alpha(t', z) \, dt' = \alpha_b \Gamma(z)$$

and $U_{c1} = \dot{M}_g R T / A$ and $U_{c2} = U_v + 1.2 \dot{M}_l / (A \rho_l)$. A total riser void fraction Φ_g (neglecting the gas weight) may then be defines:

$$\Phi_\kappa \triangleq \frac{1}{H} \int_0^H \alpha_\kappa \, dz \qquad\qquad \text{(A.3)}$$

and, by Fubini's theorem:

$$
\begin{aligned}
\langle \Phi_g \rangle &= \lim_{t \to \infty} \frac{1}{t - t_0} \int_{t_0}^{t} \frac{1}{H} \int_0^H \alpha_g \, dz \, dt' \\
&= \frac{1}{H} \int_0^H \lim_{t \to \infty} \frac{1}{t - t_0} \int_{t_0}^{t} \alpha_g \, dt' \, dz \qquad \text{(A.4)} \\
&= \frac{1}{H} \int_0^H \langle \alpha_g \rangle \, dz
\end{aligned}
$$

A slight digression: Before it was known that the variables α_b and Γ would disappear from (A.2), it was originally thought that a final relation on the bubble film thickness λ_f would be necessary in order to achieve closure. Before this was known, some effort was put into finding an appropriate expression for the film thickness λ_f. Searching through the literature provided some such information. In particular, Llewellin *et al.* [27] give a nice summary of this topic and showed that the dimensionless film thickness λ_f / r is a function of the dimensionless inverse viscosity $\rho_l \sqrt{g d^3} / \mu$ only. For example, should bubble film thickness be a interesting characteristic of the dynamic simulation models, Brown's (1965) laminar analyses, attacking Navier-Stokes equations, could be applied:

$$\lambda_f = \frac{\sqrt{1 + ND} - 1}{N}, \qquad \text{where} \qquad N = \left[\frac{16}{9 Fr_b} \frac{\rho_l^2 g}{\mu^2} \right]$$

where $Fr_b = u_b / \sqrt{2 g r_b}$ is the bubble Froude number with bubble radius $r_b = r - \lambda_f$. Brown assumed a constant bubble Froude number $Fr_b = 0.351$ making the film thickness constant throughout the riser.

Expression (A.2) provide and express for the average phase volume fraction $\langle \alpha_\kappa \rangle$ and total void fraction $\langle \Phi_g \rangle$ as a function of the local pressure. However, the local hydrostatic pressure is itself an integral

[28]Empirically found to be valid [4]

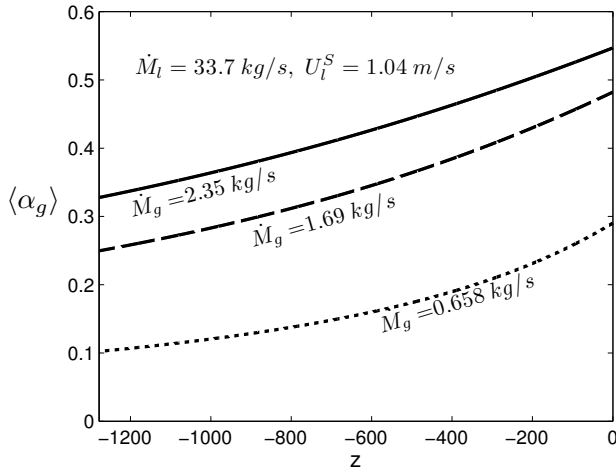function of the mean liquid volume fraction $\langle \alpha_l \rangle$:

$$p(z) = p_o + g\rho_l \int_0^z \rho_m \, dz'$$

$$= p_o + g \int_0^z \left[\langle \alpha_g \rangle \rho_g + \left(1 - \langle \alpha_g \rangle \right)\rho_l \right] dz' \qquad (A.5)$$

Two approaches, one discrete and one analytical approximation, are presented to tackle this challenge.

A.1 Discrete calculation

In this approach, the riser is divided into small, finite sections. Equation (A.2) is solved for each section using the information in the above sections; the pressure integral (A.5) for section j is evaluated as

$$p_j = p_o + g \sum_{\zeta=1}^{j-1} \rho_{m,\zeta} \, \delta z_\zeta$$

$$= p_o + g \sum_{\zeta=1}^{j-1} \left[\left(1 - \langle \alpha_g \rangle_\zeta \right)\rho_l + \langle \alpha_g \rangle_\zeta \, \rho_{g,\zeta} \right] \delta z_\zeta \qquad (A.6)$$

Note that only the fluid in the cells above the present cell j is included. It would be more precise to also include half the liquid weight of the liquid in the present section. This would however make the expression implicit and warrant the deed for iteration. Instead of iteration, a sequential approach may be take, regaining the accuracy by a finer grid. The procedure is then simply to loop through $j = 1$ to N (from riser outlet, down towards the inlet). At each step j, p_j is computed from (A.6), using the values $\langle \alpha_g \rangle_\zeta$, $\rho_{g,\zeta} = p_\zeta / RT$; $\zeta < j$ stored from the previous computations. Then, $\langle \alpha_g \rangle_j (p_{j-1}, p_{j-2}, \ldots)$ may be computed from (A.2) and stored as a profile. The total riser void fraction can the be found by:

$$\langle \Phi_g \rangle = \frac{1}{H} \sum_{j=1}^N \langle \alpha_g \rangle_j \, \delta z_j$$

(a) Mean local gas volume fraction profile $\langle \alpha_g \rangle$
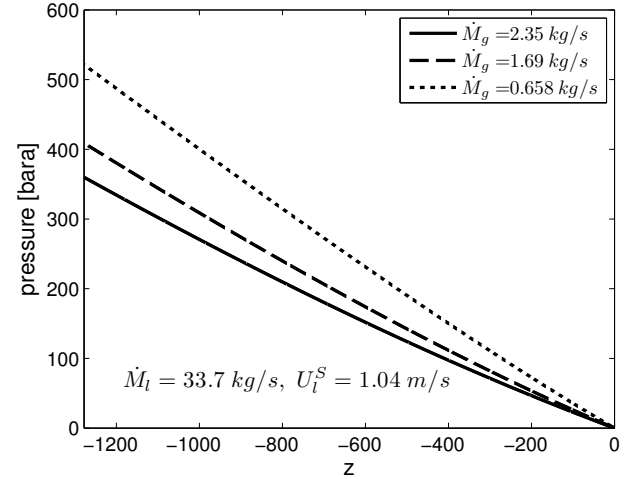
(b) Pressure profile $p(z)$

Figure A.3: Numerically computed profiles, $\dot{M}_l = 33.69 \, \text{kg/s}$, or $U_l^S = 1.04 \, \text{m/s}$. $H = 1278 \, \text{m}$, $d = 0.2032 \, \text{m}$, $T = 59 \, ^\circ\text{C}$, $p_o = 37 \, \text{bar}$

A.2 Analytical approximation

Even though the numerical procedure of Section A.1 is straight forward, a single analytical expression for the total riser void fraction may be useful. Here, this is acheived by attacking Equation (A.2) with the pressure from (A.5). Contrary to the numerical procedure, the gas weight will be neglected. Combining these equations, rearranging slightly and integrating from $z = 0$ to $z = H$ (outlet to inlet) yields:

$$U_{c2}g\rho_l \int_0^H \langle \alpha_g \rangle \int_0^z \langle \alpha_g \rangle \, dz' \, dz U_{c2} g\rho_l \int_0^H z \langle \alpha_g \rangle \, dz - (U_{c2}p_o + 1.2U_{c1}) \int_0^H \langle \alpha_g \rangle \, dz + U_{c1}H = 0 \qquad (A.7)$$

From here, the technique employed is to express (A.7) in terms of integrals of Γ from 0 to H, which is already defined in (A.3) as the sought-after average total riser void fraction $\langle \Phi_g \rangle$. The first term is handles easily as either integration by parts or substitution of $\mathrm{d}z$ by $\langle \alpha_g \rangle^{-1} \mathrm{d} \left(\int_0^z \langle \alpha_g \rangle \, \mathrm{d}z' \right)$ yields

$$\int_0^H \langle \alpha_g \rangle(z) \int_0^z \langle \alpha_g \rangle(z') \, \mathrm{d}z' \, \mathrm{d}z = \frac{1}{2} \left(\int_0^H \langle \alpha_g \rangle(z) \, \mathrm{d}z \right)^2 = \frac{1}{2} \left(\langle \Phi_g \rangle H \right)^2$$

The second term, $\int_0^H z \langle \alpha_g \rangle \, \mathrm{d}z \; \left(= \langle \Phi_g \rangle H^2 - \int_0^H \int_0^z \langle \alpha_g \rangle \mathrm{d}z' \mathrm{d}z \right)$, is far more troublesome – the author has not found any way of solving for it analytically as the running variable z requires information in the void profile itself. From the results of the numerical approach of Section A.1 (see Figure 5.6) it is observed that the slope of $\langle \alpha_g \rangle$ is smooth and does not change greatly across the riser. The approximation

$$\int_0^H z \langle \alpha_g \rangle \, \mathrm{d}z \approx \frac{1}{H} \int_0^H z \, \mathrm{d}z \cdot \int_0^H \langle \alpha_g \rangle \, \mathrm{d}z = \frac{1}{2} \langle \Phi_g \rangle H^2 \tag{A.8}$$

is applied, which is an approximation analogue to the key approximation of the handling of the flux terms in the finite volume method – *e.g.* Equation (4.2). Because the slope of $\langle \alpha_g \rangle$ slightly decreases as the outlet is approach, approximation (A.8) underpredicts the true term value by a small amount.

All terms may now be expressed in $\langle \Phi_g \rangle$ and known variables, producing a quadratic equation. Further rearranging gives the simplest form

$$\langle \Phi_g \rangle^2 - 2b \langle \Phi_g \rangle + c = 0 \tag{A.9}$$

where

$$b = \frac{1}{g \rho_l H} \left[p_o + 1.2 U_{c1} U_{c2} \right] + \frac{1}{2}$$

$$c = \frac{2}{g \rho_l H} \frac{U_{c1}}{U_{c2}}$$

The quadratic expression (A.9) has the well-know solution

$$\langle \Phi_g \rangle = b \pm \sqrt{b^2 - c} \tag{A.10}$$

$(\pm \;\to\; -)$ providing the physical solution.

Figures A.4 shows the numerical and analytical void model's response to changing liquid velocity into the riser at a constant gas mass flow rate of $\dot{M}_g = 1.69 \,\mathrm{kg/s}$ ($152 \,\mathrm{kSm^3/d}$). This is a gas lift flow rate taken from the Girassol P50 pipeline field data [43], along with the properties $H = 1278 \,\mathrm{m}$, $d = 0.2032 \,\mathrm{m}$, $T = 59 \,°\mathrm{C}$, $p_o = 37 \,\mathrm{bar}$. The liquid well flow rate associated with this field is $\dot{M}_l = 33.69 \,\mathrm{kg/s}$ or $u_l^S = 1.04 \,\mathrm{m/s}$ [18, 43, 47][29].

Figures A.4 also include computations from the further simplified models presented in Annex F. These models were developed leading up to the present one, and were simpler in that the the liquid film was neglected – *i.e.* the slug liquid velocity was computed directly from the liquid flux and mean hold-up. As can be seen from the figures, these models gave fairly similar predictions when the liquid mass rate is high relative to the gas mass rate. However, when a larger mean fraction of the riser cross section is occupied by gas, the accuracy decreases, notably – see Figure 5.6. The wish to improve this spatial void fraction profile near the riser outlet was the motivation for the present model.

A.3 Comment

---

[29]Temperature downstream riser choke applied.
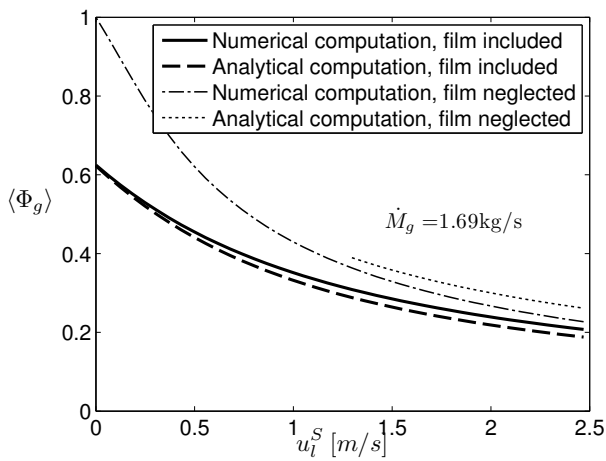
(a) Void fraction as a function of superficial liquid velocity, $\dot{M}_g = 1.69\,\mathrm{kg/s}$ (152 $\mathrm{kSm^3/d}$)
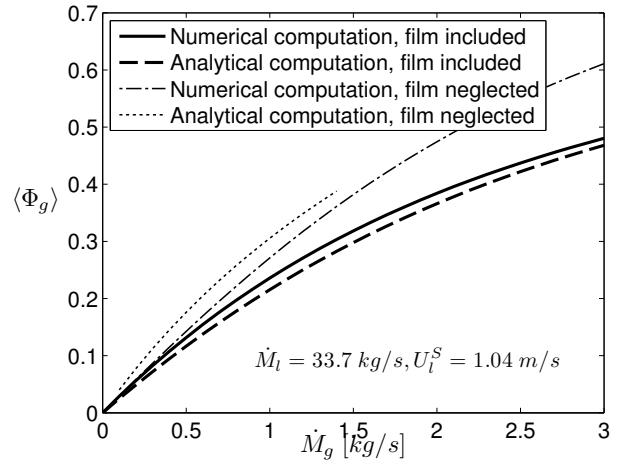
(b) Void fraction as a function of gas mass flow, $\dot{M}_l = 33.69\,\mathrm{kg/s}$ or $u_l^S = 1.04\,m/s$

Figure A.4: Approximated void fraction in riser

After the completion of this section, a dynamic expansion model by Mayor *et al.* [29, 28] was found in the literature. Encouragingly, this model applies much of the same methodology as employed here. The model of Mayor *et al.* differs in that they numerically organize the computation around bubbles which are tracked up the riser, quite similar to the slug tracking models which compose the main theme of the present work. Mayor *et al.* applies a Box Muller algorithm to set the bubble lengths at the riser inlet from a normal distribution, and the slug length from a dependant normal distribution. Additionally, iteration is needed in this method, making it altogether more complicated than the method of this section.
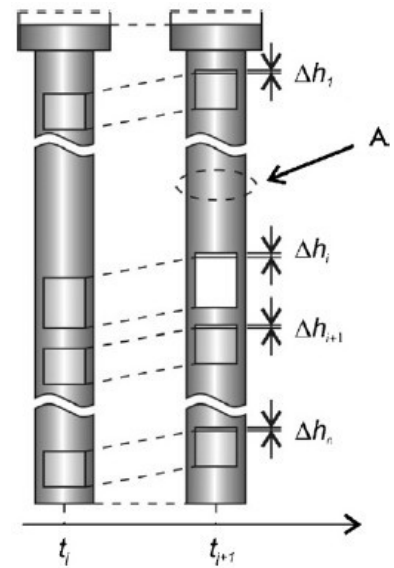
Figure A.5: Bubble expansion schematic of Mayor *et al.* Source: [29]

B Snapshots
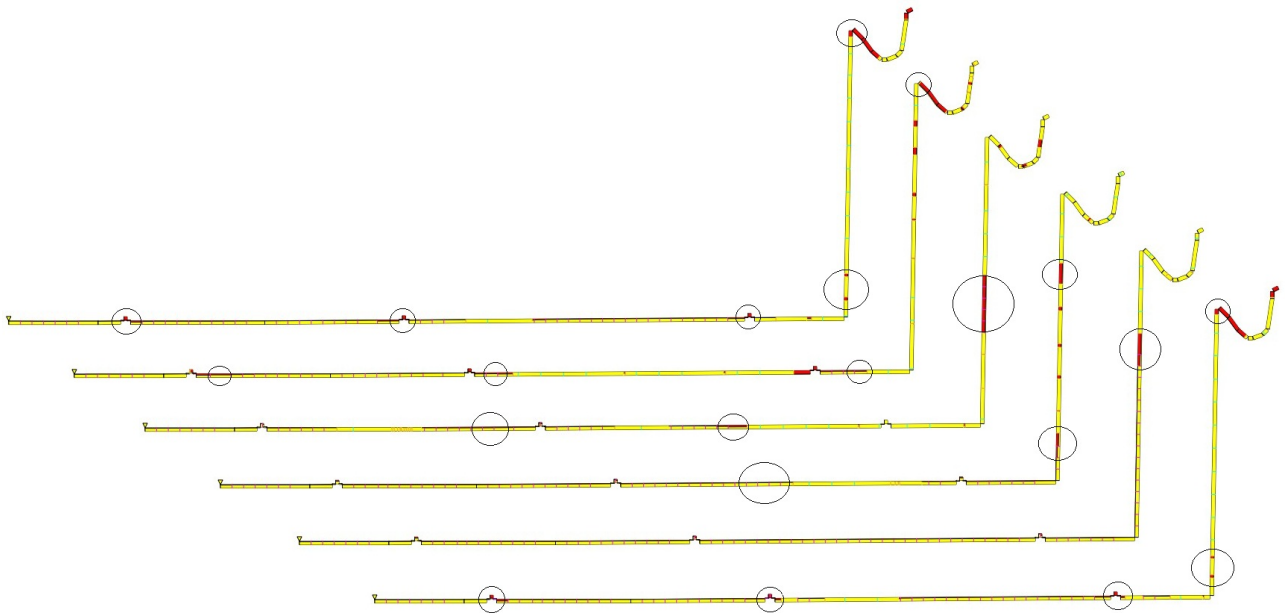
(a) Jumpers moved, see Description C.   The snapshots are taken at times (top to bottom) $t \in \{3\,220\,\text{s},\ 4\,840\,\text{s}\ 5\,040\,\text{s},\ 5\,460\,\text{s},\ 5\,960\,\text{s},\ 6\,570\,\text{s}\}$

(b) Jumpers unmoved, see Description D.   The snapshots are taken at times (top to bottom) $t \in \{12\,290\,\text{s},\ 12\,460\,\text{s}\ 12\,870\,\text{s},\ 13\,100\,\text{s},\ 135\,700\,\text{s},\ 13\,450\,\text{s}\}$

Figure B.1: Snapshots of expansion driven instability (see Section 7.1.2 and pressure times series in Figure 7.9). Circles included to underline void propagation and period of production
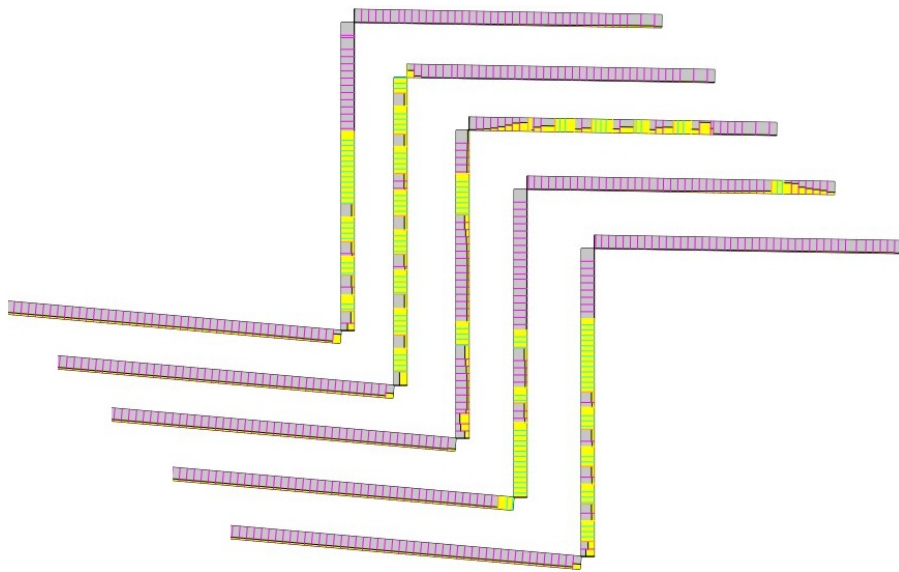
Figure B.2: Riser stability flow map bench-mark test – see Section 5.4. $U_{g,o}^S$ = 0.280 m/s, U_l^S = 0.071 m/s. The snapshots are taken at times (top to bottom) $t \in \{37.5\,\text{s},\ 46.5\,\text{s},\ 50.0\,\text{s},\ 55.0\,\text{s},\ 61.0\,\text{s}\}$. Experimental data from Taitel *et al* show this point to be stable.
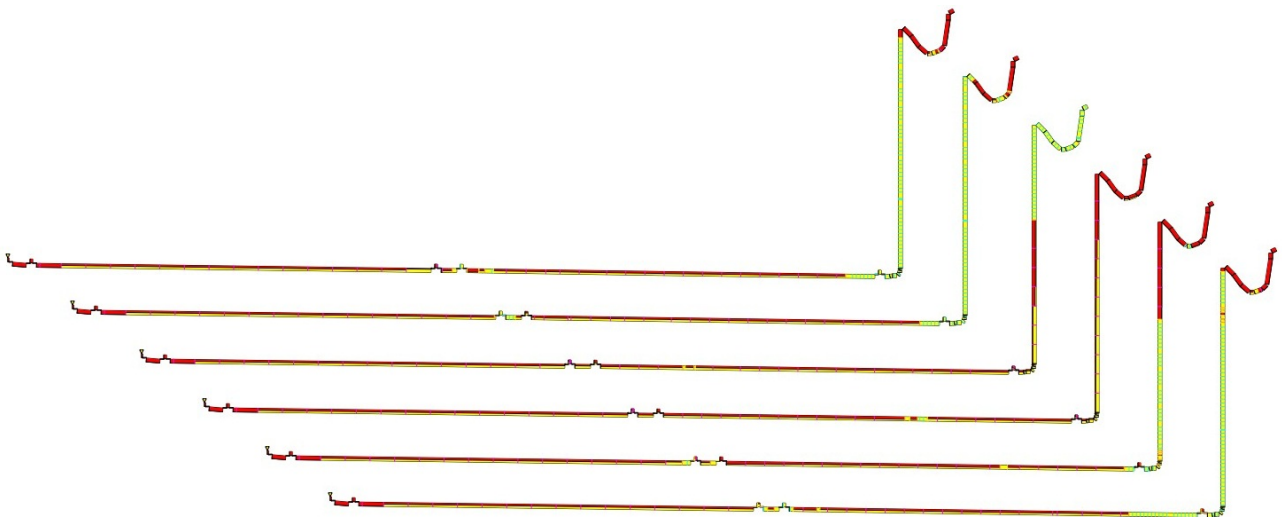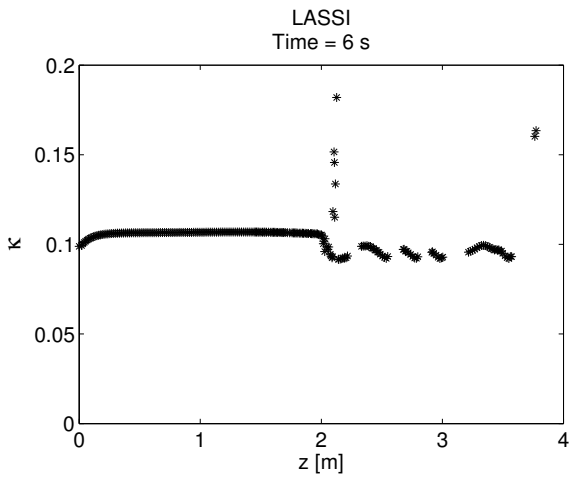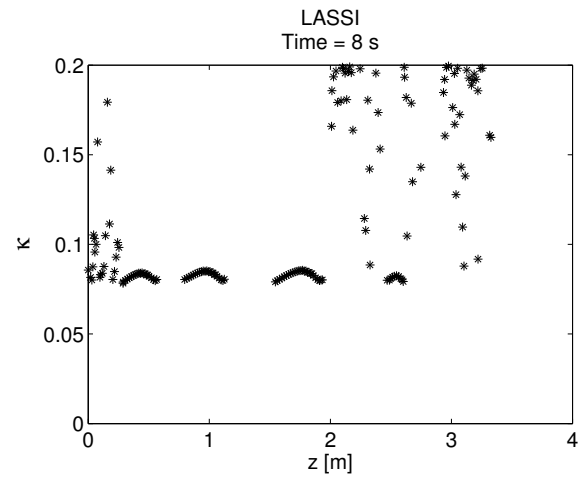

Figure B.3: Terrain slugging type I (severe slugging) – see Section 7.2. The snapshots are taken at times (top to bottom) $t \in \{5\,180\,\text{s},\ 5\,330\,\text{s},\ 5\,920\,\text{s},\ 6\,050\,\text{s},\ 6\,160\,\text{s},\ 7\,030\,\text{s}\}$. Notice the speed of blow out.
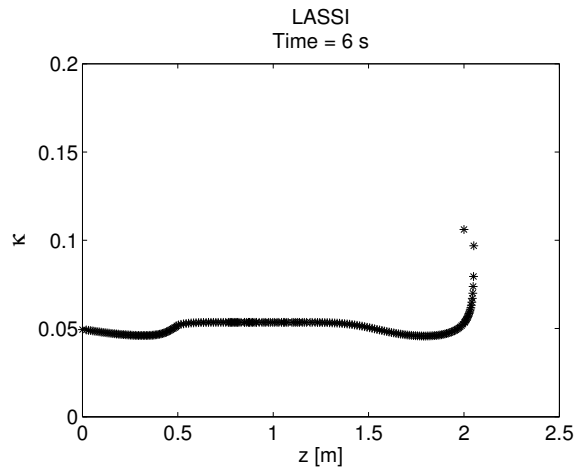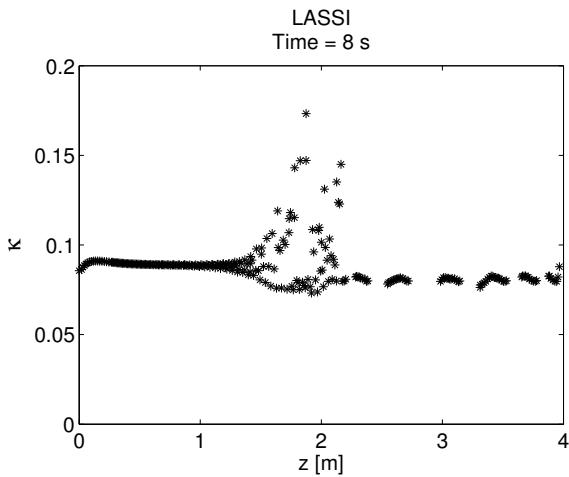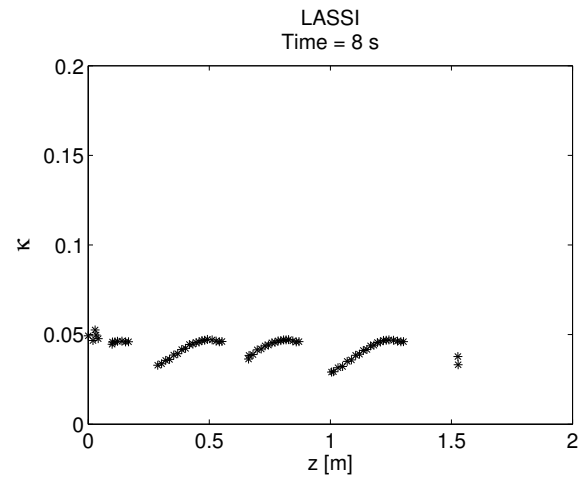
(a) $\phi = 0°$, $t_{mid} = 5.80$ s, $t_{out} = 13.30$ s

(b) $\phi = \mp 30°$, $t_{mid} = 1.50$ s, $t_{out} = 6.35$ s

(c) $\phi = \pm 30°$, $t_{mid} = 5.40$ s, $t_{out} = 7.35$ s

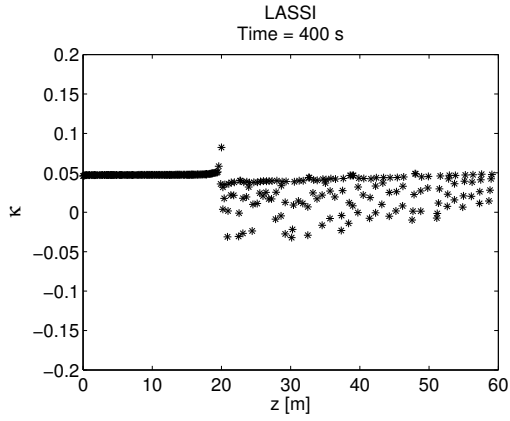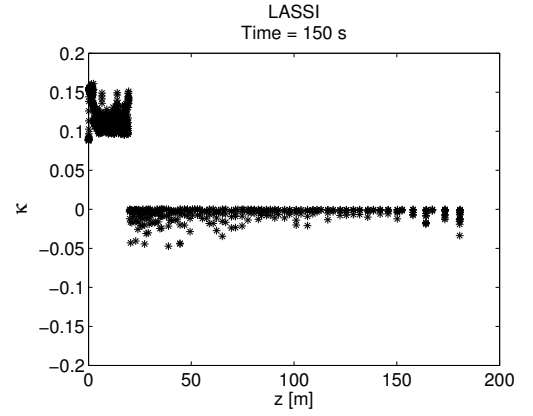(d) $\phi = \mp 60°$, $t_{mid} = 1.15$ s, $t_{out} = 4.80$ s

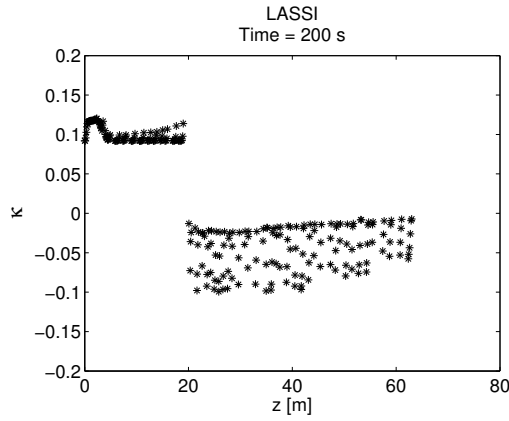(e) $\phi = \pm 60°$, $t_{mid} = 9.30$ s, $t_{out} = 10.50$ s

Figure B.4: κ as in (4.28), LASSI. V-section configuration, as in Figure 5.1. ($\delta t = 0.01$, $D = 0.012$, $\alpha_{l,i} = 0.5$). Generated during the mass conservation testing of Section 5.2
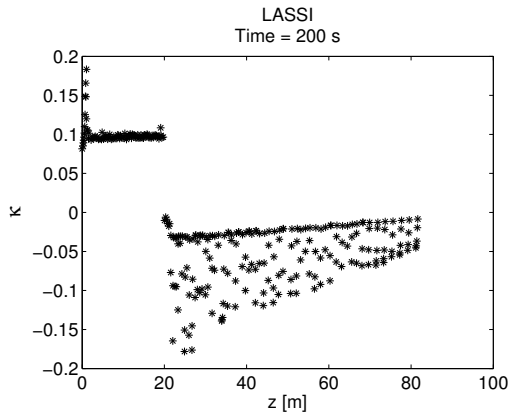
Figure B.5: κ as in (4.28), geometry as in Figure 5.4, LASSI. ($\delta t = 0.01$, $D = 0.012$, $U_{g,i}$, $\alpha_{l,i} = 0.5$). Generated during the mass conservation testing of Section 5.2

C   Productivity Index inlet

The productivity indec boundary conditions is formulated as [12]:

$$U_{1,i}^{S,ST} = K(P_{well} - p_i)/A \qquad \text{(C.1)}$$

where K is the productivity index – a empirically determined well parameter. It is often given in the units $[Sm^3/(bar \cdot day)]$. Water cut wc and Gas-Oil-Ratio GOR are input parameters used to compute the inlet water and oil superficial velocities, as in OLGA [12, p. 46]:

$$U_{\text{oil},i}^{S,ST} = U_{1,i}^{S,ST}(1 - wc) \qquad \text{(C.2a)}$$

$$U_{\text{H}_2\text{O},i}^{S,ST} = U_{1,i}^{S,ST} wc \qquad \text{(C.2b)}$$

$$U_{\text{g},i}^{S,ST} = U_{\text{oil},i}^{S,ST} GOR \qquad \text{(C.2c)}$$

Here, S denote 'superficial', $i.e.$ $U_\kappa^S = \alpha_\kappa U_\kappa$. ST indicate that the fluid is at standard conditions. The same standard conditions are used as those implemented in OLGA, which are representative for those widely used in the oil industry [12, p. 136]: $P^{ST} = 1\,\text{atm} = 1.01325\,\text{Pa}$, $T^{ST} = 15.56\,°\text{C} = 288.71\,\text{K}$.

As the well relation (C.1) apply to the state variables as standard conditions, a transformation to the local state is required at the inlet. In the present work, the ideal gas law is used for the PVT states for simplicity (despite the large system pressures). The phase velocities are found by regarding (C.1) as an expression for the mass flux and assuming this flux remain unchanged across the variation of pressures found at the inlet

$$\frac{\partial \dot{M}_{k,i}}{\partial \rho} = 0 \ \Rightarrow \ A\rho_g U_g = A\rho_g^{ST} U_g^{ST} \ \Rightarrow \ \frac{U_{\text{g},i}}{U_{\text{g},i}^{ST}} = \frac{\rho_g^{ST}}{\rho_{\text{g},i}}$$

additionally assuming isothermal flow

$$\frac{U_{\text{g},i}}{U_{\text{g},i}^{ST}} = \frac{P^{ST}}{p_i} \qquad \text{(C.3)}$$

or alternatively found by linearising around the standard conditions.[30]

Correction   In section 7.2 and 7.3, is was seen that this implementation introduces large errors in high-pressure cases because the GOR is apparently defined as the gas-oil separation that $would$ take place at standard conditions, not the separation $actually$ found at the inlet. Consequently, phase transition affects the mass rate and therefore $\dot{M}_{k,i} \neq \dot{M}_k^{st}$. PVT-support is thereby required for accurate implementation of a productivity index boundary condition.

D   Titbits of **MATLAB**® code

Some useful segments of code is shown here. The code is intended to be simple and illustrative. Optimisation has not been a main focus and loops have been used, contrary to the previous work [1].

Listing 1: General input data load

```
1  path = [main_dir, folder,'\',filename];
2  if load_data;
3      file_id = fopen(path,'r');
4      assert(file_id ~= -1, 'input data not found' );
5
6      data = textscan(file_id,['%f32 %f32 %f32 %f32 %f32 %f32 %f32',...
7          '%d %f32 %f32 %f32 %f32 %f32 %f32 %f32 %f32 %f32 %f32 %f32',...
8          '%f32 %f32 %f32 %f32'],'Delimiter',',');
```

---

[30]linearising around the specific volume produce (C.3) straight away as $\frac{\partial U_g}{\partial(1/\rho_g)} = \frac{U_g}{\rho_g}$ and all higher derivatives are identically zero, while linearising about ρ would produce $\frac{U_g}{U_g^{ST}} = \sum_{\zeta=0}^{\infty} \left(\frac{\rho_g^{ST} - \rho_g}{\rho_g^{ST}}\right)^\zeta$

```
9      if isempty(data{1}) % Data begins at second line of input file
10         data = textscan(file_id,['%f32 %f32 %f32 %f32 %f32 %f32 %f32',...
11            '%d %f32 %f32 %f32 %f32 %f32 %f32 %f32 %f32 %f32 %f32 %f322',...
12            '%f32 %f3 %f32 %f32'],'Delimiter',',','HeaderLines',1);
13      end
14      fclose(file_id);
15  end
```

Listing 2: Sorting data in single-time cells

```
1   var_names.SLUGGIT = {
2       'Time'          %1
3       'z'             %2
4       'Length'        %3
5       'u_b'           %4
6       'id'            %5
7       'Hold-up'       %6
8       'Pressure'      %7
9       'Pipe number'   %8
10      'u_l'           %9
11      'u_g'           %10
12      };
13  len_dat = length(data{1});
14  i_last = find(data{1}(2:len_dat),data{1}(1:len_dat-1)>0);
15  times = [data{1}(i_last);data{1}(len_dat)];
16  len_time = length(times);
17  prop = cell(len_time,1);
18  prop{1} = data{prop_index}(1:i_last(1));
19  for i = 2:len_time-1
20      prop{i} = data{prop_index}(i_last(i-1)+1:i_last(i));
21  end
22  prop{len_time} = data{prop_index}(i_last(i)+1:len_dat);
```

Listing 3: Creating mass rate - pressure phase portraits

```
1   % times defined in Listing 2
2   jt_start = find(times >= t_start,1,'first');
3   dotM_out = zeros(len_time-1-jt_start,1);
4   p_in = dotM_out;
5   count = 0;
6   for jt = jt_start:len_time-1
7       count = count+1;
8       % z, u, p and holdup generated from "prop" in Listing 2
9       jstart = find(z{jt}>z_inlet_p,1,'first');
10      jend = find(z{jt}<z_outlet,1,'last')-1;
11      dotM_out(count) = area*rhol*holdup{jt}(jend)*u{jt}(jend);
12      p_in(count) = p{jt}(jstart);
13  end
14  dotM_out_mean = mean(dotM_out);
15  p_in_mean = mean(p_in);
16  Mmark = (dotM_out - dotM_out_mean)/dotM_out_mean;
17  pmark = (p_in - p_in_mean)/p_in_mean;
```

Listing 4: Total liquid riser fraction - pressure phase portrait

```matlab
1  jt_start = find(times >= t_start,1,'first');
2  phi = zeros(len_time-1-jt_start,1);
3  p_in = phi;
4  count = 0;
5  for jt = jt_start:len_time
6      count = count+1;
7      % z, sec_len, p and holdup generated from "prop" in Listing 2
8      jinlet = find(z{jt}>z_inlet_p,1,'first');
9      jstart = find(z{jt}>=z_riser_inlet,1,'first');
10     jend = find(z{jt}<=z_riser_inlet+H,1,'last');
11
12     %Interpolate sections at riser inlet/outlet
13     dz_in = z{jt}(jstart)-z_riser_inlet;
14     dz_out = (z_riser_inlet+H)-z{jt}(jend);
15     weight_in = dz_in/sec_len{jt}(jstart-1);
16     weight_out = dz_out/sec_len{jt}(jend);
17
18     p_in(count) = p{jt}(jinlet);
19     phi(count) = ( weight_in*holdup{jt}(jstart-1).*sec_len{jt}(jstart-1) ...
20         + weight_out*holdup{jt}(jend).*sec_len{jt}(jend) ...
21         + sum(holdup{jt}(jstart:jend-1).*sec_len{jt}(jstart:jend-1)))/H;
22  end
23  phi_mean = mean(phi);
24  p_in_mean = mean(p_in);
25  phimark = (phi - phi_mean)/phi_mean;
26  pmark = (p_in - p_in_mean)/p_in_mean;
```

Listing 5: Integrating liquid fraction in riser through time

```matlab
1  % In this code, the liquid fraction any everty time step is
2  % projected down to an average riser length H with section
3  % length dz (= 1). Interpolation is used as data borders do
4  % not coinside with "mean riser" borders.
5  dz = 1;
6  dt = times(2)-times(1); %dt const in output file
7  x = 0:dz:H;
8  z_riser = length_horizontal:dz:length_horizontal+H;
9  holdup_profile_sum = zeros(1,length(z_riser));
10 includecount = 0;
11 notincludedcount = 0;
12
13 for jt = round(t_start/dt):lt
14     % z and holdup generated from "prop" in Listing 2
15     z_riser = z{jt}-length_horizontal;
16     j = 1;
17     for i = find(z_riser <= x(1),1,'last'):length(z_riser)-1
18         jnext = find(x >= z_riser(i+1),1,'first');
19         if isempty(jnext), break; end
20         holdup_profile_sum(j:jnext-2) = holdup_profile_sum(j:jnext-2)+holdup(i);
21         j = jnext;
22         holdup_profile_sum(j-1) = holdup_profile_sum(j-1) + ...
23             ((z_riser(i+1)-x(j-1))*holdup(i)+(x(j)-z_riser(i+1))*holdup(i+1))/dz;
24     end
```

```
25        holdup_profile_sum(j:end) = holdup_profile_sum(j:end) + holdup(i+1);
26        includecount = includecount+1;
27   end
28   alpha_profile = 1 - holdup_profile_sum/includecount;
```

Listing 6: IKH/well posedness criteria at time *t* across pipeline

```
1  % z, Ul, Ug, sec_len, p and holdup generated from "prop" in Listing 2
2  % see same listing for def. of 'times'
3  t_index = find(times > t, 1,'first');
4  % remove slugsection
5  H = holdup{t_index};
6   stratified = H<1;
7   H_strat = H(stratified);
8  z = z{t_index}(strat);
9  L = sec_len{t_index}(strat);
10 rhog = p{t_index}(strat)/(R*T);
11 ul = Ul{t_index}(strat);
12 ug = Ug{t_index}(strat);
13
14 [pipezs, angles] = getphi(); % function holding geometry data in array
15 phi = zeros(length(H_strat),1);
16 for k = 1:length(H_strat)
17     for j = 1:length(pipezs)
18         if z(k) < pipezs(j)
19             phi(k) = angles(j);
20             break
21         end
22     end
23 end
24  cosphi = cosd(phi);
25
26 % interphase angle through series expansion:
27 gamma = pi*H_strat+((3*pi/2)^(1/3))*...
28     ( 1-2*H_strat+H_strat.^(1/3)-(1-H_strat).^(1/3) );
29 % or through interative procedure:
30 % for j = 1:length(H_strat)
31 %     f_theta = @(gamma) (2*pi)\(gamma - sin(gamma)) - H_strat(j);
32 %      theta = fzero(f_theta, pi/2);
33 % end
34
35 dAldhl = 2*r*sin(gamma);
36  uglsq = (ug-ul).^2;
37 % IKH
38  RHS = (rhol*(1-H_strat)+rhog.*H_strat).*...
39     ( (rhol-rhog)./(rhol.*rhog))*G.*cosphi*area./dAldhl;
40 % well_posed
41 %RHS = (rhol-rhog).*G.*(H/rhol + (1-H)./rhog   ).*cosphi*area./dAldhl;
```

Listing 7: Numeric riser void fraction model

```
1  function [mean_alpha,z] = alpha_film_numeric_mixture(Mdotg,  Mdotl)
2
3  global H area R T G Po Uv rho_l
```

```
4
5   N = 5*H;
6   dz = H/N;
7   z = -dz:-dz:-H;
8   Gz = G*dz;
9   mean_alpha = zeros(N,1);
10  rho_g = zeros(N,1);
11
12  Uc1 = Mdotg*R*T/area;
13  Uc2 = Uv+1.2* Mdotl/(area *rho_l);
14  for j = 1:N
15      p = Po + Gz*( sum(mean_alpha(1:j-1).*(rhog(1:j-1) - rho_l)) + rho_l*(j-1) );
16      rho_g(j) = p/(R*T);
17      mean_alpha(j) = Uc1/(Uc2*p + Uc1);
18  end
19  end
```

Listing 8: Analytic riser void fraction model

```
1   function [mean_alpha,z] = alpha_film_numeric_mixture(Mdotg, Mdotl)
2
3   global H area R T G Po Uv rho_l
4
5   N = 5*H;
6   dz = H/N;
7   z = -dz:-dz:-H;
8   Gz = G*dz;
9   mean_alpha = zeros(N,1);
10  rho_g = zeros(N,1);
11
12  Uc1 = Mdotg*R*T/area;
13  Uc2 = Uv+1.2* Mdotl/(area *rho_l);
14  for j = 1:N
15      p = Po + Gz*( sum(mean_alpha(1:j-1).*(rhog(1:j-1) - rho_l)) + rho_l*(j-1) );
16      rho_g(j) = p/(R*T);
17      mean_alpha(j) = Uc1/(Uc2*p + Uc1);
18  end
19  end
```

Annexes

E   The Kelvin-Helmholtz stability criteria

Figure E.1 shows a photo of the onset of Kelvin-Helmholtz instability of stratified shear flow. The main physical mechanism behind the phenomenon is the Bernoulli suction which appears in the gas cross section as the gas is accelerated past a small perturbation of the smooth liquid surface. If the conditions are such that this suction is sufficient to amplify the perturbation, the flow conditions are unstable.

Figure E.1: Kelvin-Helmholtz instability of stratified shear flow. Source: [44].
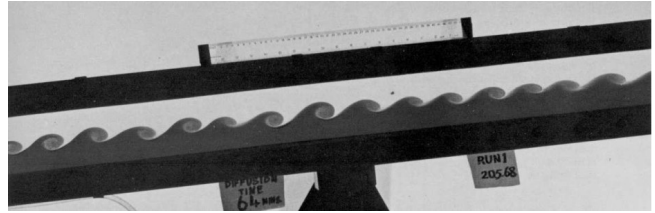
Barnea and Taitel presented in 1993 a linear stability analysis of the two-fluid model [3, 37]. As all models discussed in this work rely on the fundamental equations of this model, its stability domain is of interest.

The two-fluid model consists of two pairs of mass and momentum conservation equations, one for each fluid phase (4.26). A small disturbance in the stratified flow regime is considered. This disturbance is presented as a small perturbation in the state variables from their equilibrium states. This perturbation can be expressed as a Fourier sum of modes

$$\chi(t,z) = \overline{\chi} + \sum_{\zeta=0}^{\infty} \widetilde{\chi}_\zeta \, \exp\left\{i\left(\omega_\zeta t - k_\zeta z\right)\right\} ; \qquad \chi \in \{u_g, \ u_l, \ \alpha_g, \ \alpha_l, \ h_l, \ p\}$$

where χ is representative of the state variables. k_ζ and ω_ζ are respectively the mode wavenumber and its corresponding pulsation. It is clear from this expression that if there exists a wavenumber k with a corresponding pulsation ω whose imaginary part is negative, then this imaginary pulsation part will cause an amplification of this mode over time, resulting in instability. To find whether such a wavenumber exists, all frequencies of the disturbance may be considered individually. Therefore, the analysis proceeds by inserting a single Fourier mode and allow its wavenumber k to take on any value form zero to infinity. If the state equilibrium variables $\overline{\chi}$ are such that there exists a wavenumber k whose corresponding pulsation ω consists of a negative imaginary part. Accordingly, one proceeds by eliminating the pressure term in the two-fluid model (4.26) by combining the two momentum equations, inserting the mode

$$\chi(t,z) = \overline{\chi} + \widetilde{\chi} \, \exp\left\{i\left(\omega t - kz\right)\right\} ; \qquad \chi \in \{u_g, \ u_l, \ \alpha_g, \ \alpha_l, \ h_l, \ p\}$$

for the state variables, and deduct the equilibrium part. After linearising around the resulting volumetric force F_V on the liquid phase (see Equation (4.29),) the following *dispersion equation* for the pulsation ω is obtained

$$\omega^2 - 2[ak - ib]\omega + ck^2 - dk^4 - iek = 0 \tag{E.1}$$

where a, b, c and e are combinations of the equilibrium state variables using the original notation of Barnea and

Taitel [3].

$$\rho^* = \frac{\rho_l}{\alpha_l} + \frac{\rho_g}{\alpha_g}$$

$$a = \frac{1}{\rho^*}\left(\frac{\rho_l \overline{u_l}}{\alpha_l} + \frac{\rho_g \overline{u_g}}{\alpha_g}\right)$$

$$b = \frac{1}{2\rho^*}\left[\left(\frac{\partial F_V}{\partial u_l^S}\right)_{\alpha_l, u_g^S} - \left(\frac{\partial F_V}{\partial u_g^S}\right)_{\alpha_g, u_l^S}\right]$$

$$c = \frac{1}{\rho^*}\left[\frac{\rho_l \overline{u_l}^2}{\alpha_l} + \frac{\rho_g \overline{u_g}^2}{\alpha_g} - \left(\rho_l - \rho_g\right)g\cos\phi\overline{\left(\frac{\mathrm{d}\alpha_l}{\mathrm{d}h_l}\right)}^{-1}\right]$$

$$d = \frac{\sigma}{\rho^*}\left(\frac{\mathrm{d}\alpha_l}{\mathrm{d}h_l}\right)^{-1}$$

$$e = -\frac{1}{\rho^*}\left(\frac{\partial F_V}{\partial \alpha_l}\right)_{\alpha_l, u_g^S}$$

adopting the liquid volumetric force F_V from (4.29) and σ is the surface tension. Since the neutral stability limit occurs where the imaginary part of the pulsation ω turns from a positive to a negative value, the critical states will have $\Im\{\omega\} = 0$. In the following then, ω can be considered a purely real value.

Solving (E.1) for its imaginary parts yields a criterion critical wave velocity ω/k

$$\frac{\omega}{k} = \frac{e}{2b}$$

and solving for the real part of (E.1), using this critical wave velocity, yields a stability criterion:

$$\text{stable} \iff \text{For } \forall k : \left(\frac{e}{2b} - a\right)^2 + \left(c - a^2\right) - dk^2 < 0$$

The last LHS term is the only term involving surface tension, and is also the only term which is a multiple of the wavenumber. Consequently, surface tension is only important for large wavenumbers (short waves). Obviously, since d is always positive, $k \to 0$ is the determining wavenumber, producing the final viscous Kelvin-Helmholtz (VKH) criterion:

$$\text{stable} \iff \left(\frac{e}{2b} - a\right)^2 + \left(c - a^2\right) < 0 \tag{E.2}$$

The inviscid Kelvin-Holmholtz criterion (IKH) is easily found inserting the equilibrium state variables into (E.2), and neglecting the viscous and surface tension terms. The result is a simple imbalance where the hydrostatic forces must outweigh the Bernoulli suction for stability [3, 13]:

$$\text{stable} \iff (u_g - u_l)^2 < (\alpha_g \rho_l + \alpha_l \rho_g)\frac{\rho_l - \rho_g}{\rho_l \rho_g}g\cos\phi\left(\frac{\mathrm{d}\alpha_l}{\mathrm{d}h_l}\right)^{-1} \tag{E.3}$$

In the viscous Kelvin-Helmholtz criterion (VKH), the RHS of (E.3) is multiplied with a viscosity-dependant factor less than unity, which constitutes a smaller model stability domain. Rewriting slightly reveals the similarity to the well-posedness criterion (4.30):

$$\text{stable} \iff (u_g - u_l)^2 < (\rho_l - \rho_g)g\left[\frac{\alpha_g}{\rho_l} + \frac{\alpha_l}{\rho_g}\right]\left(\frac{\mathrm{d}\alpha_l}{\mathrm{d}h_l}\right)^{-1}\cos\phi$$

F Simplified models of void in riser

Preceding the riser void model of Section A, a model was made in which the liquid film around Taylor bubbles was neglected altogether. It was found that this approximation was good for cases in which the gas flow rate was low relative to the liquid flow rate (see *e.g.* Figure 5.11), but gave poor predictions otherwise. Since it was already documented, and because its character gives some insight to the liquid film influence, it has not been removed completely from this text.

The Assumptions D from Appendix A are retained while including an assumption on the bubble liquid film:

Assumptions E. *Simplified riser steady state void model*

E.1 Assumptions D still holds.

E.2 The local slug liquid velocity can be approximated by the local average liquid velocity (*i.e.* the influence of the velocity difference of the bubble liquid film is neglected)

Assumption D.1 gives:

$$\dot{M}_\kappa = A(\rho u \langle \alpha \rangle)_\kappa = const \tag{F.1}$$

and Assumption D.4 allows for $u_g = v_{b,n}$ where $v_{b,n}$ is the bubble nose velocity from Section 4.8. To compute it, the Bendiksen model from Section 4.8 is used, assuming no backflow and a 90° inclination, along with (F.1) for the liquid phase to approximate $u_{s,m}$ (Assumption E.2)

$$u_g = 1.2 \frac{\dot{M}_l}{A\rho_l(1 - \langle \alpha_g \rangle)} - U_\nu \tag{F.2}$$

where $U_\nu = 0.35\sqrt{gd}$ was the empirically determined bubble nose velocity in vertical pipes in still liquid.

As before, both a numerical and an analytical approximation is found.

F.1 Numerical calculation

As before, the riser is discretised $j \in \{0, N\}$ from outlet to inlet as in scetch A.1. Equation (F.1) gives, when inserting the ideal gas law, (F.2) for the gas velocity and (F.1) for the liquid velocity:

$$\dot{M}_g = A\langle \alpha_g \rangle_j \left(\frac{p_j}{RT} \right) \left(1.2 \frac{\dot{M}_l}{(1 - \langle \alpha_g \rangle_j)\rho_l A} + U_\nu \right)$$

After some rearranging, this yields an expression for $\langle \alpha_g \rangle$

$$\langle \alpha_g \rangle_j = \frac{a_j \pm \sqrt{a_j^2 - 4b_j}}{2} \tag{F.3}$$

where

$$a(p_j) = 1 + \frac{1.2 \cdot \dot{M}_l}{\rho_l A U_\nu} + \frac{\dot{M}_g}{p_j A U_\nu}$$

$$b(p_j) = \frac{\dot{M}_g}{p_j A U_\nu}$$

and $(\pm \Rightarrow -)$ is the only physical solution.[31] Pressure p_j and total average riser void fraction $\langle \Phi_g \rangle$ can then be obtained the same way as in Appendix A.1. Void fraction profiles of this procedure can be found in Figures A.4, 5.11 and 5.6.

As a final note, the special case of $\dot{M}_l \to 0$ requires some special attention. Figure A.4a shows that the numerical solution to the void fraction approaches unity as $\dot{M}_l \to 0$. The reason is that the the liquid velocity is intrinsically a part of this model so that u_l and therefore u_g increases proportionally. For cases where $\dot{M}_l = 0$ and $\dot{M}_g > 0.5292$, other states being the same, will give a gas volume at the outlet larger than can be accompanied in the pipe section at velocity $u_g = U_\nu$ (*i.e.* $b > 1$), for which the model is not defined (violating Assumption D.5.)The elementary solution $\langle \alpha_g \rangle = 1 \; \forall z$ is then found. Figure F.1 show the development of the gas volume fraction $\langle \alpha_g(z) \rangle$ with no liquid flow as the gas mass flux increases towards where it is ill-defined. The void fractions are respectively 0.085, 0.184, 0.303, 0.461, 0.750, 1.000 for increasing gas flux, where the last is not a valid solution.
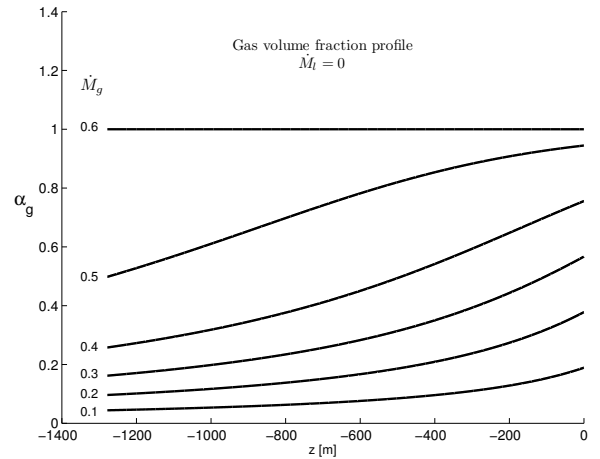

Figure F.1: Gas volume fraction $\langle \alpha_g \rangle$ profiles with no liquid flow

---

[31]In the case were $\dot{M}_l$ is exactly zero and $\dot{M}_g$ is larger than about 0.5 kg/s, the root becomes $\sqrt{(1-b)^2}$ with $b > 1$ and so $(\pm \Rightarrow +)$ is the hydrostatic solution, but gives an ill-defined $\alpha_g > 1$

F.2 Analytical approximation

Simplified expressions may also be developed using only inlet and outlet properties. Using the superficial gas velocities $u_b^S = u_b \langle \alpha_g \rangle$ and (F.1) yields:

$$\frac{\partial \dot{M}_g}{\partial z} = 0 \iff \frac{1}{u_b^S} \frac{\partial u_b^S}{\partial z} = \frac{1}{\rho_g} \frac{\partial \rho_g}{\partial z} = \frac{1}{RT\rho_g} \frac{\partial p}{\partial z} \quad \text{(F.4)}$$

To compute the bubble nose velocities $u_b = v_{b,n}$, the Bendiksen model from Section 4.8 is used, assuming no backflow and a 90° inclination, along with (F.1) for the liquid phase to approximate $u_{s,m}$ (Assumption E.2)

$$u_b = 1.2 \frac{\dot{M}_l}{A\rho_l(1 - \alpha_g)} - U_v \quad \text{(F.5)}$$

where $U_v = 0.35\sqrt{gd}$ was the empirically determined bubble nose velocity in vertical pipes in still liquid.

To simplify matters, z is defined positive upstream, along the gravitational force (see Figure A.1). Accordingly, the pressure gradient becomes:

$$\frac{\partial p}{\partial z} = g\rho_l(1 - \langle \alpha_g \rangle) \quad \text{(F.6)}$$

Using (F.1) for ρ_g and (F.6) for $\partial_z p$, (F.4) can be written

$$\frac{1}{v^S} \frac{\partial u_b^S}{\partial z} = -\frac{(Au_b)\alpha_g(1 - \langle \alpha_g \rangle)G\rho_l}{RT\dot{M}_g}$$

which can be rearranged and integrated to give the lift gas volume in the riser

$$V_g = \langle \Phi_g \rangle AH = \int_0^H \langle \alpha_g \rangle A \, dz = -\frac{RT\dot{M}_g}{g\rho_l} \int_0^H \frac{\frac{\partial u_b^S}{\partial z} \, dz}{v^S u_b(1 - \langle \alpha_g \rangle)} = \frac{RT\dot{M}_g}{g\rho_l} \int_{u_b^S(0)}^{v^S(H)} \frac{du_b^S}{(v^S)^2 \left(1 - \frac{1}{\langle \alpha_g \rangle}\right)} \quad \text{(F.7)}$$

The final integral in (F.7) is not trivial to solve analytically. To simplify matters, the gas fraction α_g is substituted with a frozen mean approximation value

$$\langle \alpha_g(z) \rangle \approx \overline{\langle \alpha_g \rangle} = \frac{1}{2} \left[\langle \alpha_g(H) \rangle + \langle \alpha_g(0) \rangle \right] \quad \text{(F.8)}$$

which gives

$$\langle \Phi_g \rangle AH \approx \frac{RT\dot{M}_g}{g\rho_l} \frac{\overline{\langle \alpha_g \rangle}}{1 - \overline{\langle \alpha_g \rangle}} \int_{u_b^S(0)}^{u_b^S(H)} \frac{du_b^S}{(v^S)^2} = \frac{RT\dot{M}_g}{g\rho_l} \frac{\overline{\alpha_g}}{1 - \overline{\alpha_g}} \left[\frac{1}{u_b^S(H)} - \frac{1}{u_b^S(0)} \right] \quad \text{(F.9)}$$

This is not a valid assumption when the gas volume fraction approaches unity! Further, (F.1) gives an implicit expressions for $\alpha_g(0)$ and $\alpha_g(H)$ with respect to the outlet pressure p_o when substituting with the ideal gas law:

$$\langle \alpha_g(0) \rangle = \frac{\dot{M}_g RT}{Ap_o} \frac{1}{u_b(0)} \quad \text{(F.10a)}$$

$$\langle \alpha_g(H) \rangle = \frac{\dot{M}_g RT}{A} \frac{1}{p(H)} \frac{1}{u_b(0)} \quad \text{(F.10b)}$$

The riser gas volume fraction V_g from (F.9) is also an implicit expression in terms of the riser inlet pressure $p(H)$, which, for simplicity, is approximated by neglecting the gas mas

$$p(H) \approx p_o + \int_0^H \rho_g g(1 - \langle \alpha_g \rangle) \, dz$$
$$= p_o + \rho_l g H \left(1 - \langle \Phi_g \rangle\right) \quad \text{(F.11)}$$

An iterative solving procedure can then be used in which (F.5) is solved for both phases. The riser inlet pressure $p(H)$ is found using (F.11), which is in turn used in finding the gas fractions $\langle \alpha_g \rangle$ from (F.10). From here, the mean fraction $\overline{\langle \alpha_g \rangle}$ can be computed from (F.8), and the riser gas volume (from the gas lift) V_g from (F.9). About ten iterations seems to be sufficient to reach an accuracy for $|\Delta\langle \Phi_g \rangle^i / \langle \Phi_g \rangle^i| < 10^{-6}$

For inlet liquid mass flow rates less than $10\,\text{kg/s}$ ($\dot{M}_g = 0.658\ kg/s$), or gas mas flow rate grater than $1.8\,\text{kg/s}$ ($\dot{M}_l = 33.69\,\text{kg/s}$), the iteration procedure with, more or less, arbitrary initial values begin to diverge. This probably has to do with the fact that the gas volume fraction modelled by $\dot{M}_g RT/(Apu_b)$ becomes larger than one at the outlet as the liquid velocity

approaches zero. Also, the mean gas volume fraction $\overline{\langle\alpha_g\rangle}$ simplification may influence the result.

As an ending note, for steady liquid, $u_b = U_\nu = 0.35\sqrt{gd}$ and $\partial_z u_b = 0$ giving a system on the form

$$\langle\Phi_g\rangle = \frac{\dot{M}_g RT}{AHU_\nu g\rho_l}\ln\frac{\langle\alpha_g(0)\rangle\langle\alpha_l(H)\rangle}{\langle\alpha_g(H)\rangle\langle\alpha_l(0)\rangle} \qquad (F.12)$$

which need no simplification as in (F.9). The logarithm arise as keeping ν constant produce a void integral on the form $\int\frac{d\langle\alpha_g\rangle}{\langle\alpha_g\rangle(1-\langle\alpha_g\rangle)}$ which can easily be solved by substituting $d\alpha_g$ with $d\left(1/\langle\alpha_g\rangle - 1\right)$...